

The Petrology, Geochemistry, and Origin of the East Australian Potassic Suite: Bulk Chemistry and Genesis

Anthony W. Lanati, Joshua J. Shea, Stephen F. Foley, Marthe Klöcking,
Arno Rohrbach, and Stephan Klemme

Author affiliation, contact details, and ORCID information are on Page 2.

This is a non-peer reviewed preprint submitted to EarthArXiv.

Version 1 of this preprint has been submitted to [Journal of Petrology](#) for peer review.

Version: 1

Date: 27.03.2025

*This is the first version of a manuscript submitted to Journal of Petrology that **has not yet undergone the peer review process.***

We advise that it is a near certainty that the eventual published version will differ (potentially significantly) from the one presented here.

Once accepted the preprint information will be updated to link to the published version of record.

All authors have agreed to this preprint being made available.

The Petrology, Geochemistry, and Origin of the East Australian Potassic Suite: Bulk Chemistry and Genesis

Anthony W. Lanati^{1,2*}, Joshua J. Shea³, Stephen F. Foley^{2,4},
Marthe Klöcking¹, Arno Rohrbach¹ and Stephan Klemme¹

¹Institut für Mineralogie, Universität Münster, Corrensstrasse 24, 48149 Münster, Germany, ²School of Natural Sciences, Wallumattagal Campus, Macquarie University, Sydney, NSW, Australia, ³Department of Earth Sciences, University of Cambridge, Cambridge, UK and ⁴Research School of Earth Sciences, Australian National University, 2601 Acton, ACT, Australia

*Corresponding author. a.lanati@uni-muenster.de

Abstract

The Eastern Australian Potassic Suite (EAPS) is an alkaline volcanic province made up of over 20 widely dispersed outcrops that extend almost 700 km, forming the southern portion of the world's longest continental hotspot track, the Cosgrove track. In contrast to the large basaltic volcanic complexes to the east and north, the EAPS occurs exclusively as mafic potassium-rich occurrences with inferred low-volume expressions on the order of hundreds of metres to a few kilometres. These localities are mostly on lithosphere thicker than 120 km suggesting that the lithosphere–asthenosphere boundary may have a strong influence on their depth of generation. The primary felsic mineral in these rocks is leucite, which has seen the EAPS defined as leucitites in constantly evolving classifications of exotic, but potentially economically significant alkaline melts. However, this classification does not reflect their chemical or genetic affinity. In this study, we undertake a systematic re-evaluation of these occurrences with the aim of understanding their source enrichment processes and melting conditions. Newly acquired major, trace, and volatile element whole-rock data shows that the EAPS is chemically variable, but exceptionally enriched in potassium, with high K_2O/Na_2O and MgO (Av.: K_2O 4.98 wt%; K_2O/Na_2O 3.23; MgO 12.14 wt%). We report the only complete volatile element data for the EAPS which show the lavas are similarly enriched in nitrogen to lamproites, while being more CO_2 -rich despite being partially degassed (N: 44–350 ppm; CO_2 : 1129–10274 ppm). Trace element patterns most closely resemble orogenic lamproites, and the mineralogy, major element and trace element concentrations closely match the classification criteria for lamproites. Trace element ratios of these near-primary mantle melts have a primitive signature generated from a highly enriched source that has previously undergone a degree of mixed silicate–carbonatite metasomatism. The most likely source for these rocks based on these new data is a hydrous phlogopite-bearing and olivine-poor assemblage that originates in the garnet stability field (i.e. phlogopite–garnet–pyroxenite). The inherited titanian affinity and elevated phosphorus contents of these magmas suggest apatite and oxide minerals were also present in the source. This new data helps inform interpretations of regional variations in melt generation and mantle source mineralogy in the highly heterogeneous metasomatised mantle beneath eastern Australia. We further suggest that the mechanisms that generated the EAPS likely include a combination of edge-driven convection and shear-driven upwelling as well as channelised melt flow which contributed to metasomatic depletion and refertilisation cycles. These cycles are synonymous with the initial stages of continental destabilisation that could develop toward rifting.

Key words: leucite, lamproite, pyroxenite, potassic magmatism, intraplate volcanism, mantle metasomatism, , Australia, Eastern Australian Volcanic Province

Introduction

Volcanism in Eastern Australia is dominated by large-volume basaltic eruptive centres ranging in age from late Mesozoic times to near present day. This activity has recently been shown to have been generated from a chemically similar mantle source, forming a 2,000 km long volcanic province, the Eastern Australian Volcanic Province (EAVP; Shea et al., 2022). However, potassic and ultrapotassic magmatism of a similar age is also common, spanning over 25 volcanic expressions spread over approximately 700 km (Figure 1a,b), and provides a unique insight into the geodynamic processes occurring beneath the Australian continental lithosphere. Potassium-rich magmas are comparatively rare globally, yet they are important in our understanding of melting and recycling processes in the mantle, including processes linked to the concentration of critical metals (Müller et al., 1992; Müller and Groves, 1993; Wang et al., 2006, 2022). Despite their relative scarcity when compared with tholeiites, alkaline magmas, and more specifically potassic magmas, are present in almost all tectonic settings and are believed to represent some of the first melts generated in magmatic provinces. They tend to be more enriched in volatile and moderately volatile elements such as water, carbon, nitrogen, sulfur and fluorine (Pe-Piper and Piper, 1992; Pe-Piper et al., 2014; Prelević et al., 2004, 2005; Foley et al., 2022; Foley and Ezad, 2024; Ezad and Foley, 2022; Edgar et al., 1994; Foley et al., 1987). Thus, they prove a useful tool to examine mass transfer processes such as metasomatism and incipient or partial melting in the mantle. However, due to the preferential mobility of alkali elements in low-temperature fluids, potassic volcanic rocks are susceptible to mineral-scale alteration and rapid breakdown of potassic minerals leading to a preservation bias (Roux and Hamilton, 1976; Prelević et al., 2004; Putnis et al., 2007). Alkaline volcanic fields such as those in western North America and Europe are often used as natural laboratories for understanding metasomatic processes and the interdependencies between melting, metasomatism and tectonic and geodynamic conditions including cratonic, orogenic, and active subduction environments (Farmer et al., 2002; Elkins-Tanton and Grove, 2003; Lee et al., 2006; Prelević et al., 2007; Prelević and Foley, 2007; Prelević et al., 2008b, 2005, 2013a, 2012). The Eastern Australian alkaline occurrences are similarly young (< 35 Ma) and have yet to undergo significant alteration, representing a unique tectonic setting with elements of recent subduction, orogenic and cratonisation processes. These rocks, however, are poorly known beyond the Australian geoscientific community and offer a unique opportunity to study these processes in an intraplate setting that exhibits a number of poorly understood phenomena.

In eastern Australia, volcanism was geographically expansive during the Cenozoic (Figure 1) while eruptions continued until roughly 5,000 years ago within the Newer Volcanic Province of Victoria in the south, and Kinrara in North Queensland (Cohen et al., 2017; Blackburn et al., 1982; Smith and Prescott, 1987). The Newer Volcanic

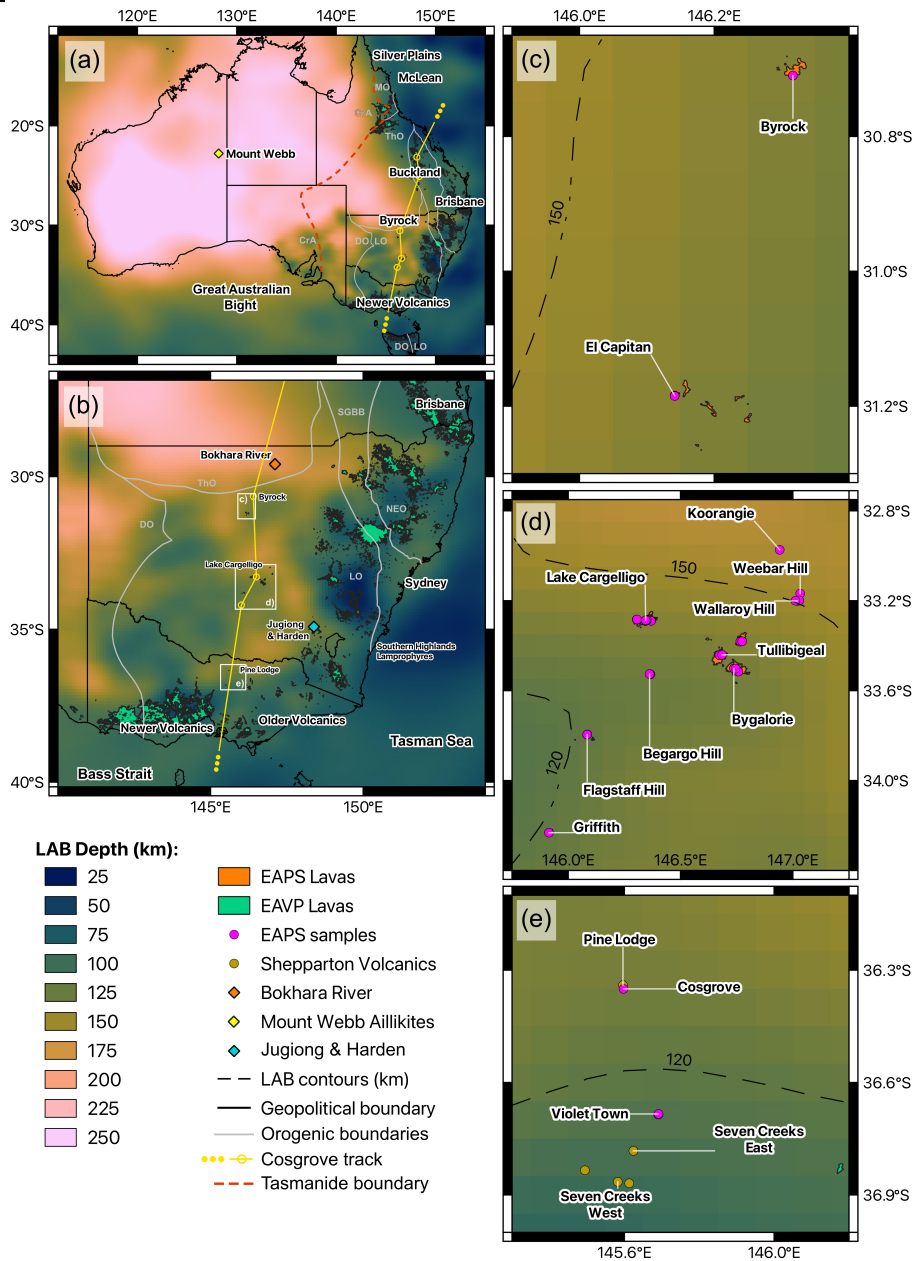


Fig. 1: (Caption next page.)

31 Province and the Cenozoic volcanism are both generally thought to be associated with plume activity due to
 32 a north–south age–progressive trend displayed in some of the volcanic regions (Sutherland, 1983; Wellman and
 33 McDougall, 1974; McDougall and Wellman, 1976; Cundari et al., 1978; Cohen et al., 2008, 2013; Davies et al.,
 34 2015). The alkaline magmas comprise a suite of leucite-bearing potassium-rich rocks known within the regional

Fig. 1: (a) Distribution of the EAVP (green) and EAPS (orange) outcrops as defined in Shea et al. (2022) and this contribution, respectively. Map coloured by depth of the lithosphere-asthenosphere boundary (LAB) from Rawlinson et al. (2017). Orogenic blocks (grey lines) and the inferred Tasmanide boundary (red dashed line) between cratonic Australia to the west and orogenic Australia to the east from Glen et al. (2016); note mismatch to LAB depth. Yellow line = the interpreted path of the Cosgrove plume (Davies et al., 2015) with inferred offshore progression of the plume (dotted line); open circles along the path mark the approximate locations of the outcrops with preferred ages as described in Cohen et al. (2008). (b) Zoom of Eastern Australia that also shows the location of the basanitic diatremes from Bokhara River (orange diamond) (Shea et al., 2024), and sample locations (white boxes). Panels (c), (d), and (e) show the north, central and southern field areas and samples locations (pink circles) of this study. Dashed black lines = LAB contours at 120 and 150 km. These depths are commonly inferred to represent the depth of melting for the source assemblages of the leucite-bearing EAPS lavas. The volcanic fields around Shepparton from Paul et al. (2005) are included in (e), while the Mount Webb aillikites of Sudholz et al. (2023) are shown in (a); the chemistry of these lavas are compared with the EAPS lavas in text. Abbreviations: Cratonic Australia (CrA); Delamarian orogen (DO); Lachlan orogen (LO); Mossman orogen (MO); New England orogen (NEO); Sydney–Gunnedah–Bowen basin (SGBB); and Thomson orogen (ThO).

literature as the "New South Wales Leucitites", named for the state within which most of the rocks erupted 35
(Figure 1b Cundari, 1973; Davies et al., 2015; McQueen et al., 2007). While the vast majority of previous work 36
centres on the basaltic volcanoes with compositions spanning tholeiitic through alkali basalt, information about 37
the potassic fields is relatively sparse. 38

Within these potassic rocks, which we define here as the Eastern Australian Potassic Suite (EAPS), the 39
presence of leucite as well as other potassic phases such as the amphibole K-richterite, sanidine, and most 40
commonly phlogopite mica, gives rise to primitive melt compositions that are extremely enriched in K compared 41
to basalts. Much like the basalts, these potassic lavas have been explained as plume-derived magmatism due to 42
an apparent age progression when corrected for suspected erroneous ages (Wellman and McDougall, 1974; Cohen 43
et al., 2008, 2013). Plume related genesis for the EAVP remains an open point of scientific interest with numerous 44
recent geophysical studies investigating the mechanisms of magma generation, and a mechanism involving plume 45
activity has not been excluded (Sutherland, 1983; Rawlinson et al., 2017; Davies et al., 2015). 46

The Cosgrove Track, as it is commonly known, spans over 2000 km of the Australian continent from Airlie 47
Beach in far-north Queensland through central-western New South Wales and Victoria, and is the longest 48
continental hotspot track currently recognised (Sutherland, 1983; Davies et al., 2015). It comprises predominantly 49
sub-aerial effusive volcanism of basaltic to basanitic composition within the volcanic fields of Hillsborough 50
through to Buckland in Queensland followed by a gap in volcanism of roughly 700 km until the next eruptive 51
centre at Byrock at the northern end of the EAPS (Figure 1a Shea et al., 2022). The EAPS centres traverse 52
the remainder of New South Wales and have been interpreted previously to extend into northern Victoria before 53
a transition in both composition and eruptive style that straddles the geographic margin of the Older and 54

Newer Volcanic Provinces (Shea et al., 2022; Heath et al., 2020). Geodynamically, this north–south sequence of volcanism has been used to link lithospheric architecture to compositional differences within the magmas as a function of plume–lithosphere interactions and mechanical processes such as edge–driven convection (EDC) and shear–driven upwelling (SDU) (Davies et al., 2015; Rawlinson et al., 2016, 2017; Duvernay et al., 2022, 2021; Manassero et al., 2024). The recent focus on geophysical interpretations has decoupled discussions of the EAPS genesis from the petrology of the magmatic sources and concentrated them on lithospheric architecture and mantle flow control. This is best exemplified by the observation that the northern– and southern–most portions of the Cosgrove track are on thin lithosphere of roughly 50 km thickness and erupt relatively normal basaltic compositions in contrast to the EAPS which erupts through much thicker lithosphere that exceeds 120 km and is in some cases up to 150 km (Glen, 2005; Shea and Foley, 2019; Shea et al., 2022). Previous work in subduction–related magmatic arcs has correlated elevated K contents to an increased melting depth (Dickinson, 1975). However, this correlation was shown to be highly dependent on arc type and is likely more sensitive to source composition than depth of melting (Dickinson, 1975). To our knowledge, there is currently no published petrological explanation to demonstrate why leucite–bearing magmas would preferentially erupt through thicker lithosphere in an intraplate setting.

The last detailed appraisals of the EAPS were in the 1970s and 80s, and did not consider all of the mapped occurrences (Birch, 1976, 1978, 1980; Cundari, 1973; Cundari and Ferguson, 1982; Cundari and Salviulo, 1989). As such, there are a number of gaps in our understanding of the EAPS, their chemistry, and genesis. In this contribution we present the most complete set of modern whole–rock chemical analyses for the EAPS. We provide an updated classification of these rocks in line with the current understanding of alkaline rocks. Using this new data, we present a number of likely mechanisms for the formation of the EAPS, identify source assemblages, and isolate the most likely metasomatic agents.

Leucite–bearing Lavas in Eastern Australia

The vast majority of the leucite–bearing rocks in Eastern Australia occur as part of the “NSW leucite suite” shown in [Figure 1c and d](#). However, there are a number of other occurrences which are reported to contain leucite including at Harden and Jugiong (Harvey and Joplin, 1940), within a lamprophyre near Wollongong (Southern Highlands), and in far–north Queensland within the McLean Volcanic field ([Figure 1a,b](#)).

The first leucite–bearing volcanic occurrences in Australia were described by Judd and Curran in separate papers in 1887 focusing on the Byrock and El Capitan volcanoes ([Figure 1c](#); Judd, 1887; Curran, 1888; David and Anderson, 1889). Both papers described the outcrops as leucite–basalts, and Curran noted that to his

knowledge this was the first leucite–basalt described outside of the Wyoming and Roman Leucitite fields. Further occurrences of leucite–bearing volcanics to the south of Byrock and El Capitan were identified in the Lake Cargelligo, Tullibigeal, and Condobolin areas (Figure 1d) and were classified as leucite–basalts, following the then established terminology (David and Anderson, 1889; Browne, 1933; Stonier, 1893). Curran (1891) was the first to undertake any microscopic assessment of the leucite–basalts, but it was not until Harvey and Joplin (1940) that detailed petrography and geochemical analyses were carried out. This work involved a summary of the mineralogy of a sample each from Byrock, El Capitan and Lake Cargelligo as well as descriptions and comparison of the whole rock major elements as determined by wet chemistry for these three samples with 17 others from around the world. These chemical analyses were the first analyses of EAPS rocks and, coupled with the comparison to other leucite and mica bearing volcanic rocks worldwide, led Harvey and Joplin to suggest that the NSW occurrences be called mica–leucite–basalts or, more generally, lamproites (Harvey and Joplin, 1940). In particular, the comparison was made to recently described lamproites of the West Kimberley in Western Australia by Prider and Wade (Prider, 1939; Wade and Prider, 1940) noting similar K_2O and MgO enrichment, but also similarly low SiO_2 and Na_2O shared between the EAPS and the West Kimberley lamproites (Harvey and Joplin, 1940). Furthermore, Harvey and Joplin (1940) noticed that K_2O/Na_2O of the EAPS was considerably higher than the average analysis of other leucite–basalts globally which, when coupled with the higher MgO and TiO_2 and the distinct mineralogy of the EAPS samples (i.e. abundant titanian poikilitic phlogopite) led to the conclusion that the NSW leucitites should be removed from the leucite–basalt grouping on both mineralogical and chemical basis.

The next examination of these samples saw the application of the name “olivine leucitite” to these rocks (Wellman et al., 1970), effectively ignoring the work and classification of Harvey and Joplin despite citing the paper. The samples were then classified by Aldo Cundari as melanocratic leucitites in a series of papers that examined the field, petrological, and geochemical characteristics of both the whole-rock and mineral compositions, including geochronological work that yielded ages of ~14 Ma for Begargo Hill (Figure 1d; Cundari, 1973; Cundari et al., 1978; Cundari and Ferguson, 1982; Cundari and Salviulo, 1989). The most complete petrological and field description of the EAPS to date is given by Cundari (1973) and includes modal mineralogy, whole–rock, and selected mineral analyses by electron microprobe. Ewart et al. (1988) referred to the EAPS lavas as either “high–potassium mafic regions”, or leucitites; confirming the classification given by Wellman and McDougall (1974) that has been used since. Ewart et al. (1988) also included the Pine Lodge basalt in northern Victoria as part of the series, based on the observation of leucite in the outcrop and the geochemical assessment by Birch (1976, 1978, (Figure 1b and e)). Birch (1978) suggested that leucite–bearing basalts may extend south from Pine Lodge

116 toward Euroa and into the Newer Volcanic Province (Birch, 1978). The observation by Paul et al. (2005) of 5%
117 leucite in basalt occurrences to the south of Pine Lodge–Cosgrove at Seven Creeks East, to the south of Euroa,
118 extended the known occurrences of leucite in Eastern Australian basaltic rocks even further south, well into the
119 Newer Volcanic Province of Victoria (Figure 1b,e). Significantly, the area around Euroa includes a number of
120 volcanic outcrops that display mixed chemistry, indicating links in magmatic origin to the eastern edge of the
121 Newer Volcanic Province (Figure 1b and e; Paul et al., 2005; Heath et al., 2018, 2020).

122 Although leucite is known to be present in other volcanic rocks in Eastern Australia, such as the McLean
123 volcanic field in far-north Queensland, in lamprophyres near Wollongong, and in a "monchiquitic basalt" at
124 Harden, these outcrops vary drastically in age, chemistry, and interpreted geodynamic setting. Harvey and Joplin
125 (1940) also interpreted the Harden basalts to be lamprophyric, specifically leucite monchiquites. Chemically,
126 when compared to the EAPS, this corresponds to lower SiO₂ (39–41 wt%), much higher Al₂O₃ (10–15 wt%) and
127 Na₂O (3–5 wt%), and significantly lower K₂O (1–2 wt%). The Hoskings Peak outcrop within the McLean field
128 is yet to be studied in its entirety, largely due to its limited exposure and geographically isolated location. Given
129 the age and genetic association of other outcrops to the south with the Cosgrove hotspot track (i.e. Buckland
130 Figure 1a); Shea and Foley, 2019), it is possible that the McLean field is an additional expression of volcanism
131 synonymous with the EAPS (Barron et al., 1996).

132 Methods

133 A comprehensive description of methods can be found in the supplement with an abridged version presented
134 here. Aliquots of each sample were inspected for alteration features and the most representative portions were
135 disaggregated and powdered. Aliquots were taken from areas free from iddingsite, xenocrysts, and xenoliths.
136 Powders were produced by cutting and drying a small block close to the location of the thin section block, then
137 partially disaggregated using a rock crusher. Rock fragments from the disaggregated samples were collected and
138 only fragments in the size range of 5–15 mm were used to ensure a clean powder. Fragments were powdered in a
139 TEMA agate puck mill for between 2 and 10 minutes. Agate mills were cleaned between samples by milling silica
140 sand for around 5 minutes, rinsed with tap-water, then washed with milli-Q water, and cleaned with ethanol.

141 X-Ray Fluorescence Spectroscopy & Loss on Ignition

142 Fused disc XRF was undertaken using a lithium metaborate: lithium tetraborate (LiM:LiT) flux in a 12:22 ratio.
143 Sample powders were weighed into clean Pt crucibles in 1 g aliquots recorded to four decimal places and combined
144 with 10 g of pre-dried LiT:LiM flux (sample:flux=1:10). Homogenised sample-flux mixtures were then melted

at 1050 °C for 20 minutes in a rocking furnace at the Macquarie GeoAnalytical (MQGA) Facility within the School of Natural Sciences, Macquarie University. NH₄I tablets, reacted for 3 minutes, were used as a releasing agent to increase surface tension before the mixture was poured into a Pt mould and cooled under air to room temperature. Analyses were carried out using a PANalytical Axios 1kW WDXRF, with the USGS Hawaiian Basalt BHVO-2, BCR-2, and OKUM reference materials, along with an in-house standard PB-SS (alkaline basalt from Prospect, NSW) used to monitor accuracy and precision. Multiple analyses of BHVO-2 or BCR-2 from each measurement batch returned values ranging from 0.05–8% from the GeoReM preferred values (Jochum et al., 2005), with only Al₂O₃ (1.19%) and P₂O₅ (8.01%) deviating by more than 1% for BHVO-2. Uncertainties on BHVO-2 measurements were also calculated with only P₂O₅ and Cr₂O₃ exceeding 1% standard error (2.23 and 2.33%, respectively). Values for all other reference materials showed similar accuracy and precision to those reported above for BHVO-2. Loss on Ignition (LOI) was undertaken by weighing ~1.4 g of sample (recorded to four decimal places) into pre-dried alumina crucibles. Samples were then fired in an 1100°C furnace overnight (minimum 10 hours), and reweighed with absolute loss determined numerically before conversion to percent loss.

Trace Element Geochemistry

Trace elements were determined using solution ICP–MS at MQGA. Digestions were undertaken on a sub-set of sample powders selected after XRF analyses were complete to reduce the total number of digestions and limit replicates on sub-samples from the same localities. A 100mg aliquot of sample powder (recorded to four decimal places) was added to clean savillex Teflon 15mL beakers and digested via sequential fluxing under concentrated HF (Merck, Suprapur grade), concentrated HNO₃ (Merck, Analar grade), perchloric (HClO₄; Merck Suprapur), and HCl acids. Care was taken to ensure residual fluorides and chlorides from acids were not present following each step and additional method steps were undertaken to digest spinels present in the sample. Final sample solutions were diluted to 100mL with 2% HNO₃ and 0.25% HF in a 1:1000 sample solution. A 5mL aliquot of the diluted sample solution was separated and prepared for ICP–MS analysis with the addition of 0.02mL of a multi-element internal standard spike containing ⁶Li, As, Rh, In, Tm and Bi to correct for instrument drift. Spiked samples were run on an Agilent 7500cs ICP–MS for the masses of ⁷Li, ⁹Be, ⁴⁵Sc, ⁴⁷Ti, ⁵¹V, ⁵³Cr, ⁵⁵Mn, ⁵⁹Co, ⁶⁰Ni, ⁶⁵Cu, ⁶⁶Zn, ⁷¹Ga, ⁸⁵Rb, ⁸⁸Sr, ⁸⁹Y, ⁹¹Zr, ⁹³Nb, ⁹⁵Mo, ¹¹⁴Cd, ¹²¹Sb, ¹³³Cs, ¹³⁷Ba, ¹³⁹La, ¹⁴⁰Ce, ¹⁴¹Pr, ¹⁴⁶Nd, ¹⁴⁷Sm, ¹⁵³Eu, ¹⁵⁷Gd, ¹⁵⁹Tb, ¹⁶⁰Gd, ¹⁶³Dy, ¹⁶⁵Ho, ¹⁶⁷Er, ¹⁶⁹Tm, ¹⁷³Yb, ¹⁷⁵Lu, ¹⁷⁸Hf, ¹⁸¹Ta, ¹⁸⁴W, ²⁰⁸Pb, ²³²Th, ²³⁸U. Method and acid blanks were carried out at the beginning and end of each run, as well as after 10 analyses in each run. Internationally recognised standards BCR-2, BHVO-2, and BIR-1 in 1:1000, 1:2000 and 1:5000 spiked solutions were analysed throughout the run to monitor accuracy and precision.

175 The calibration standard used was BCR-2 and additional analyses of BCR-2 were used as a secondary standard.
176 Measurements of BHVO-2 fell within 1.03–30.66% of the GeoReM preferred values, with the majority of elements
177 within 10% of the reference value. Only Li, Be, Cr, Cu and Cd were above 15% (17.18, 30.66, 26.28, 28.23 and
178 65.38%). However all of these elements were within 15% of either BCR-2 or BIR-1, both of which are closer
179 to the average concentration of the unknown samples analysed. All measurements of BHVO-2 fell within a 3%
180 standard error for all elements except Mo, which had a standard error of 8.06%.

181 Volatile Element Analysis

182 Carbon, Hydrogen, Nitrogen, and Sulfur were determined using a Elementar vario EL cube elemental analyser
183 (Elementar, Langensfeld, Germany) at MQGA following the methods of Alard et al. (2022) and Ananuer and
184 Alard (in prep.). Whole rock sample powders were weighed into pre-formed Sn-foils in either 50 or 100mg aliquots
185 added to a flux of WO_3 (tungsten oxide, Elementar Langensfeld, Germany) in a ratio of 1:1.1 (i.e. sample /
186 $\text{WO}_3 \approx 1.1$) prior to drying in a vacuum oven (ca. 0.1 bar) for around 24 hours at 105°C flushed with Ar-gas.
187 Sample filled Sn-foil packets were then compressed by hand into pellets. Pellets were weighed pre- and post-
188 packing to ensure no ruptures or loss of sample from packets. Sample pellets were then loaded into the analyser
189 and ignited in an oxygen-He gas atmosphere furnace at a temperature of 1150°C. Prior to ignition the system
190 was purged with He to wash out atmospheric nitrogen. A blank was run before each sample to reduce possible
191 contamination from previous sample(s). Ignition under O_2 atmosphere causes the complete decomposition of
192 the sample powder releasing H_2O and CO_2 as well as NO_x and SO_x which are reduced through reaction with
193 Cu-chips in the reduction chamber to NO_2 and SO_2 respectively. Halogens are removed prior to reduction in
194 order to prevent reaction with the Cu-chips by a silver wool trap placed at the top of the combustion chamber.

195 Volatile gases emitted after ignition were isolated by gas chromatographic separation and measured using
196 a thermal conductivity detector (TCD), or infrared detector (IR; S-only). The TCD has an intrinsic LLD of
197 roughly 40 ppm for all elements, while IR has a theoretical LLD ca. 1 ppm. However, long-term (≈ 5 years) blank
198 measurements indicate that LLD is ca. 100 ppm for N, 32 ppm for C, 150 ppm for H, and 40 and 5 ppm for
199 S by TCD and IR, respectively Alard et al. (2022). Measurements obtained on 7 procedural blanks (Sn foils +
200 100 mg of WO_3) obtained during this study are in-line with the long-term performances of the elemental analyser.
201 Precision and accuracy were assessed by repeated analyses of the Geo-Reference Materials BCR-2, BE-N, DR-N,
202 OKUM, PM-S, and WS-E. Measured values were within 15% of the reported value for all elements; procedural
203 blanks and standard analyses are provided in the supplementary materials. A major limitation of this technique

is the lack of reliable reference values for the standard reference materials, especially for the elements N and C, but also H; this is remedied in part by the work of Ananuer and Alard (in prep.).

204

205

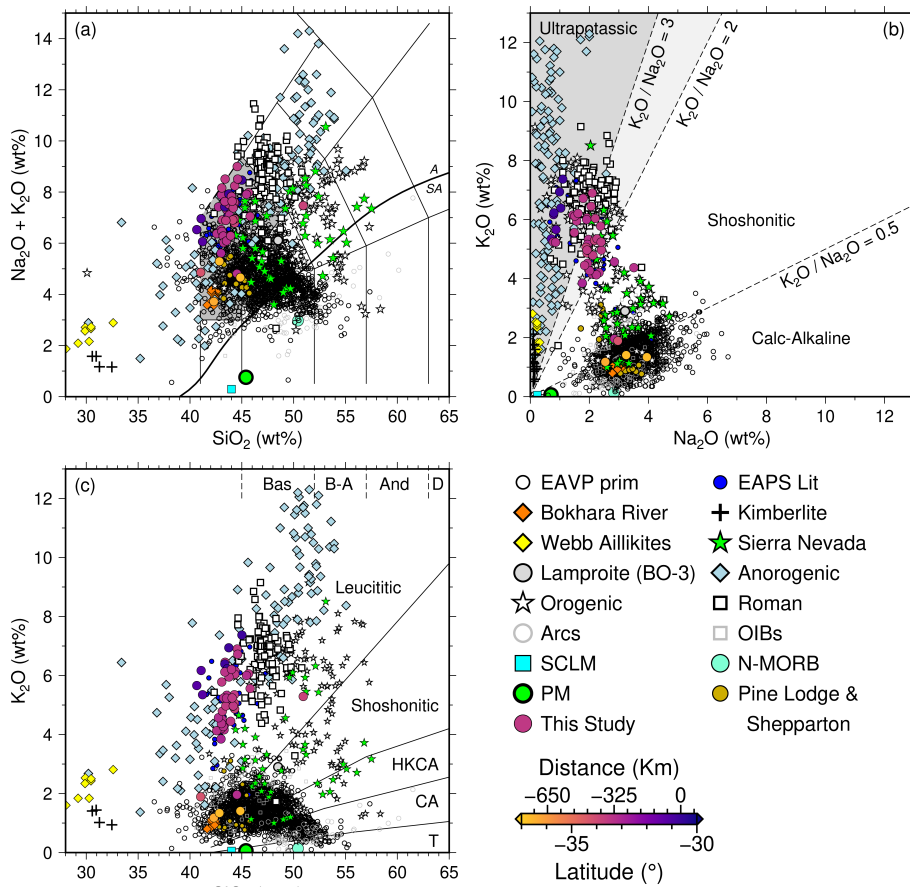


Fig. 2: Major element discrimination diagrams showing data from this study in (a) total-alkali versus silica (TAS), (b) K_2O vs. Na_2O , and (c) K_2O vs. SiO_2 space. EAPS symbols (large circles) coloured by latitude in (a)–(c). Data sources: Shea et al. (2022) (EAVP and EAPS Lit); Shea et al. (2024) (Bokhara River); Sudholz et al. (2023) (Webb Aillikites); Paul et al. (2005) (Pine Lodge and Shepparton); Casalini et al. (2022) (orogenic, anorogenic, and BO-3 lamproites); Farmer et al. (2002) (Sierra Nevada leucitites); Tappe et al. (2017) (Kimberlites); Plank (2005) (Arcs); Willbold and Stracke (2006) (OIBs); Palme and O'Neill (2013) (primitive mantle (PM)); McDonough (1990) (sub-continent lithospheric mantle (SCLM)); Gale et al. (2013) (N-MORB). Roman province compiled from GEOROC database (<https://georoc.eu/>; version 2023-12-01).

Table 1. Whole rock analyses collected on the EAPS samples by this study. (this is a place holder. Please see xlsx sheet)

Results

Major and Minor Element Geochemistry

The samples presented here are silica-undersaturated and for the most part enriched in potassium (**Table 1**) (Lanati and Shea, 2022). All but one plot within the foidite field of the TAS diagram and contain SiO₂ 40–45 wt% (**Figure 2a, c**), with the vast majority of samples containing >4 wt% K₂O, placing them within the leucititic and potassic to ultrapotassic fields (**Figure 2b, c**). On a molar basis they have K₂O/Na₂O of 0.22–5.15, and are moderately peralkaline and perpotassic ([molar(K₂O+Na₂O)/Al₂O₃ = 0.22–0.70] and [molar K₂O/Al₂O₃ = 0.13–0.93]) (**Table 1**). When plotted against MgO, which along with K₂O is the only element to vary significantly, all other elements show minor variations representing some of the most enriched compositions for TiO₂, P₂O₅, Cr, Ni, and Cu globally when compared with other basaltic melts (**Figure 3b,e and 4d–f**). The EAPS samples also exhibit lower Al₂O₃ and FeO_T than the primitive basalts of the EAVP (*plotted as EAVP Prim*; Shea et al., 2022), while CaO, MnO, and Na₂O overlap with the basalts (**Figure 3f and 4b–c**). EAPS samples can be geographically discriminated in terms of K₂O versus Na₂O with more enriched compositions in the northern volcanoes at Byrock and El Capitan than in the central exposures centred around Tullibigeal and Lake Cargelligo (**Figure 2b**). The southern exposures have consistently lower K₂O/Na₂O at ≤0.5. In order to compare the new analyses with primitive melts globally, published data was filtered for Mg number ≥ 55, FeO_T ≥ 6 wt%, MgO ≥ 4 wt%, and SiO₂ <60 wt% to remove fractionated and evolved melts based on filters similar to Prelević et al. (2008b) and Shea et al. (2022). When compared with leucitites from the Sierra Nevada volcanics (Farmer et al., 2002) and the Roman province (compiled from GEOROC database (<https://georoc.eu/>; version 2023-12-01) the EAPS lavas are enriched in TiO₂ and FeO_T, while SiO₂ is generally lower. In **Figures 2, 3, and 4** the EAPS lavas are also compared to lamproites using the compilation from Casalini et al. (2022) indicating a considerable overlap with anorogenic lamproites in most chemical spaces. Orogenic lamproites are more enriched in Al₂O₃ and Na₂O, but with lower TiO₂ and FeO than the anorogenic and EAPS lavas (**Figures 2b, 3b–d, and 4b**). However, anorogenic lamproites are clearly delineated by lower CaO than the EAPS, which overlap with orogenic lamproites and Sierra Nevada leucitites as well as intraplate basalts from the broader EAVP (**Figures 4c and 5a,b,d**). Orogenic lamproites also show significant spread in K₂O versus SiO₂ and K₂O versus Na₂O space traversing the calc-alkaline to leucititic fields, and shoshonitic to ultrapotassic fields in **Figure 2b, c**. In contrast, anorogenic lamproites are much more restricted in both K₂O versus SiO₂ and K₂O versus Na₂O space, exclusively plotting within the leucititic and ultrapotassic fields (**Figure 2b, c**). Other Australian alkaline rocks are included for comparison, specifically the Mount Webb aillikites that erupt through thick lithosphere in Central Australia (Sudholz et al., 2023) and the basanitic Bokhara River diatremes (Shea et al., 2024, **Figure**

1a, b). The Bokhara River locality was inferred to be part of the same volcanic event as the EAPS (Cohen et al., 2008; Jaques, 2002) until a recent investigation showed these diatremes to be Jurassic in age (Shea et al., 2024). The Webb Aillikites show greatest affinity to kimberlites from Tikiusaaq in western Greenland and less frequently with the anorogenic lamproites, but share almost no major or minor element characteristics with the EAPS (Figures 2a–c, 3, and 4a–d). Bokhara River, however, does share some chemical similarity with the less enriched expressions of the EAPS, most notably Wallaroi Hill and the southern localities at Pine Lodge, Shepparton, and Griffith (Figures 1b, d, e and 2a–c).

Trace Element Geochemistry

The EAPS rocks display a flat enrichment in the HFSE and LILE with approximately $100\times$ N–MORB and up to $1000\times$ primitive mantle (PM) values for Ba (Figure 6a). Regardless of the normalising system chosen, Ti exhibits a slight negative anomaly and Eu is unaffected by feldspar fractionation, whereas a minor negative PM–normalised Pb signature is observed for the central and southern EAPS outcrops. In contrast, the northernmost outcrops, Byrock and El Capitan (Figure 1a–c), exhibit no Pb anomaly (Figure 6a). Potassium values for all samples shown in Figure 6 are calculated from the conversion from K_2O to K. Similarly, where values for Ti were not reported for published data, whole–rock TiO_2 values were converted to elemental Ti. Ce/Pb does not exhibit significant evidence of subduction input, while the strong convex upward up shape of the pattern results in high La/Yb and Sm/Yb values that suggest significant garnet in the mantle source (Figure 6a). Patterns are steep, illustrating decreasing enrichment from north to south (Figure 6a). Values for Ba vary the most dramatically, from 6940 ppm for the El Capitan volcano (sample 0803) to 573 ppm for sample 1603 within the Tullibigeal fields. Rb and Sr are also most enriched within the El Capitan volcano, with Rb = 366 ppm and Sr = 2824 ppm for samples 0803 and 0801 respectively. The Griffith sample (1801) exhibits the lowest concentrations of both Rb and Sr (41 and 940 ppm), while also having Cs contents of 0.97 ppm which is significantly below the average of all samples (1.44 ppm) and only higher than the southernmost samples from Violet Town (Figure 1e), which also exhibits a strong negative K anomaly (yellow lines; Figure 6a). The Pine Lodge outcrop near Cosgrove (sample 2001) was not analysed for trace elements in this study but was previously analysed by Paul et al. (2005) whose data also show lower–than–average concentrations of fluid–mobile elements such as Cs, Rb, Ba, Th, U, K, and Sr (gold circles; Figure 6b). Interestingly, HREEs heavier than Dy cross the N–MORB values which is a common feature of anorogenic lamproites, and is seen along the entire 725 km sampling area.

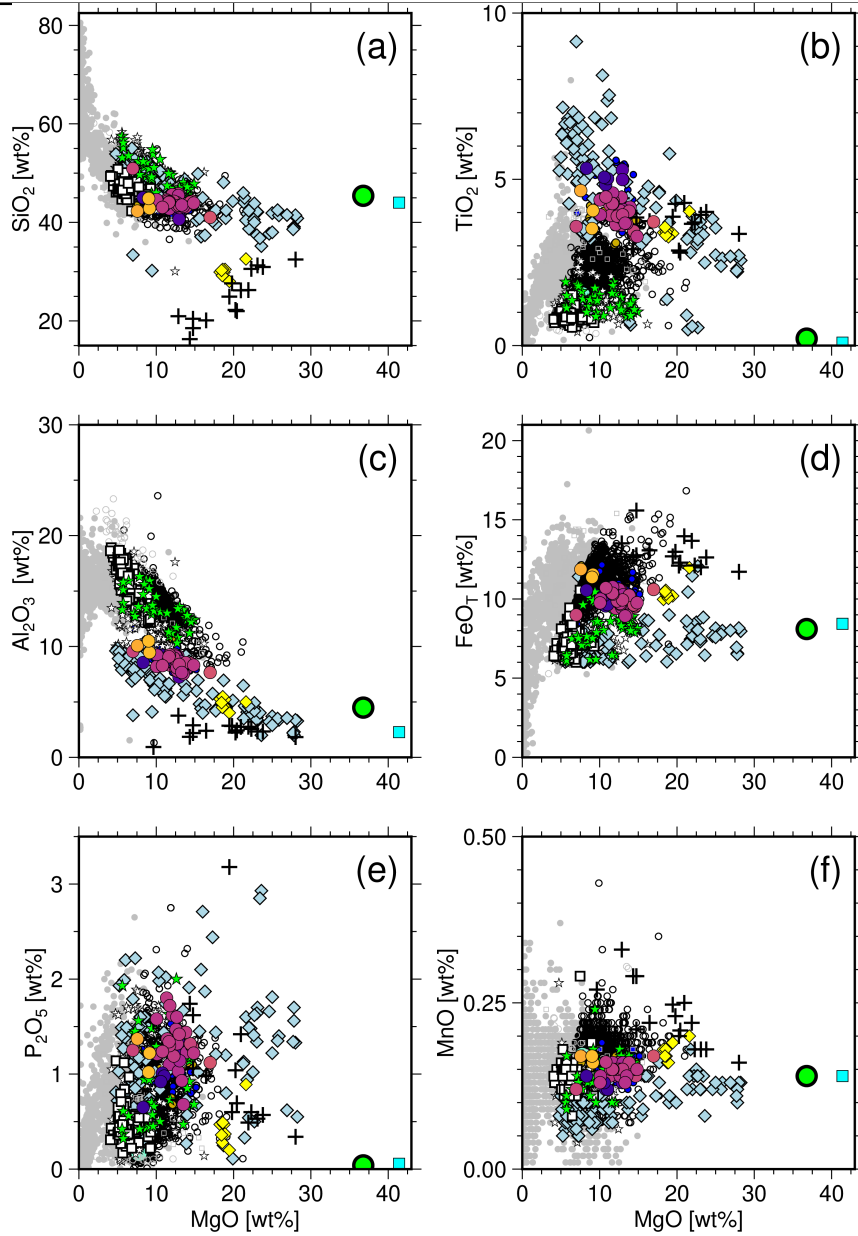


Fig. 3: Major element variation diagrams displaying all major and selected minor elements against MgO wt% with EAPS lavas plotted together with published data. Solid grey dots are samples from the EAVP as compiled by Shea et al. (2022) which do not pass the primitive melt filter described in text. Other symbols and data sources as in Figure 2.

265 Volatile Element Geochemistry

266 CHNS analyses reveal that the northern exposures of Byrock and El Capitan are the most sulfur-enriched of all
 267 the EAPS lavas with up to 330 ppm S, which is a roughly six times higher than the remainder of the localities

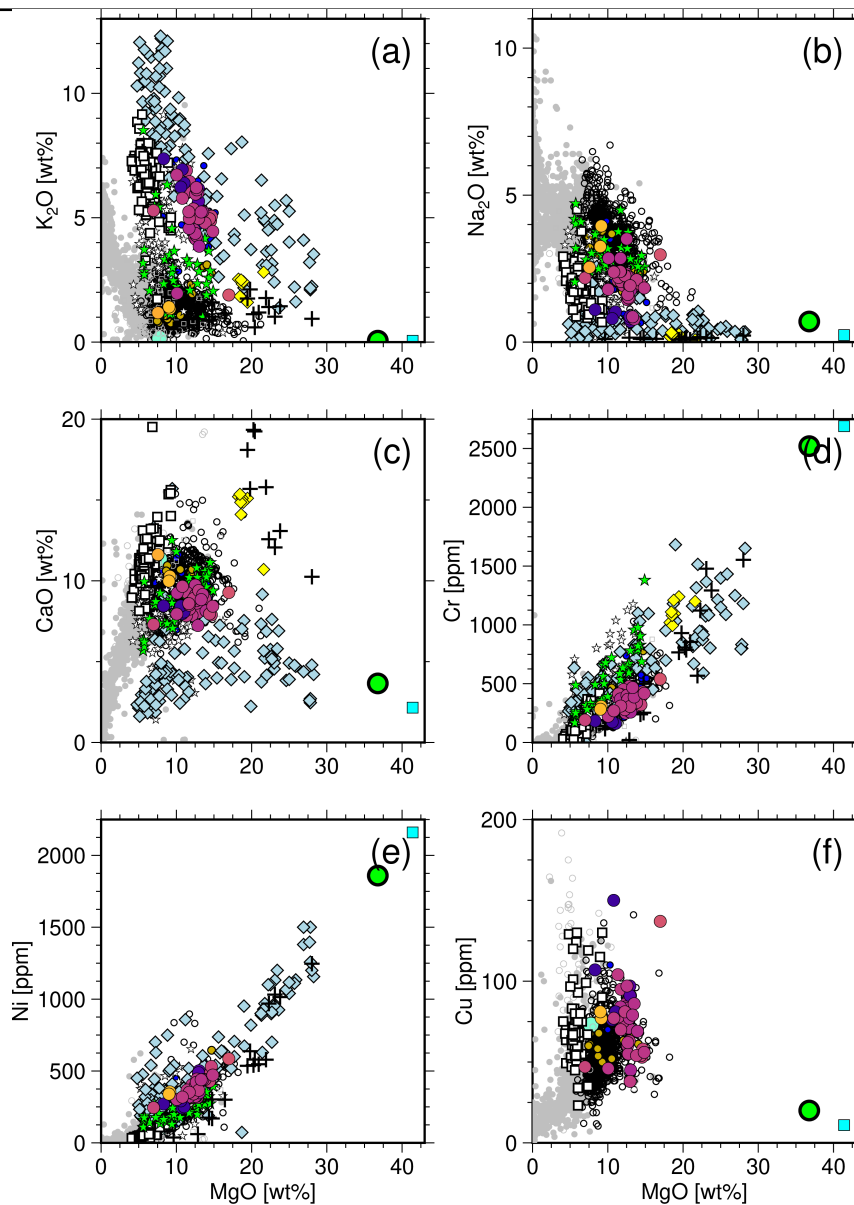


Fig. 4: Alkaline major element variation diagrams and select trace elements against MgO wt% for EAPS lavas and published data. Symbols and data sources as in [Figure 2 and 3](#).

included here that contain in the order of 50 ppm or less ([Figure 7c](#)). Carbon contents range between 839 and 268
 2459 ppm for the northern localities, and over a similarly large range for the the central exposures (308–2804 269
 ppm; as $\text{CO}_2 = 1129\text{--}10274$ ppm; [Figure 7d](#)). Nitrogen is the only element where measurements fall below the 270
 long-term detection limits established by Halimulati and Alard, (2025; in prep), but all values are above the 271
 intrinsic detection limits of the technique. Given the scarcity of published measurements for N we report all 272

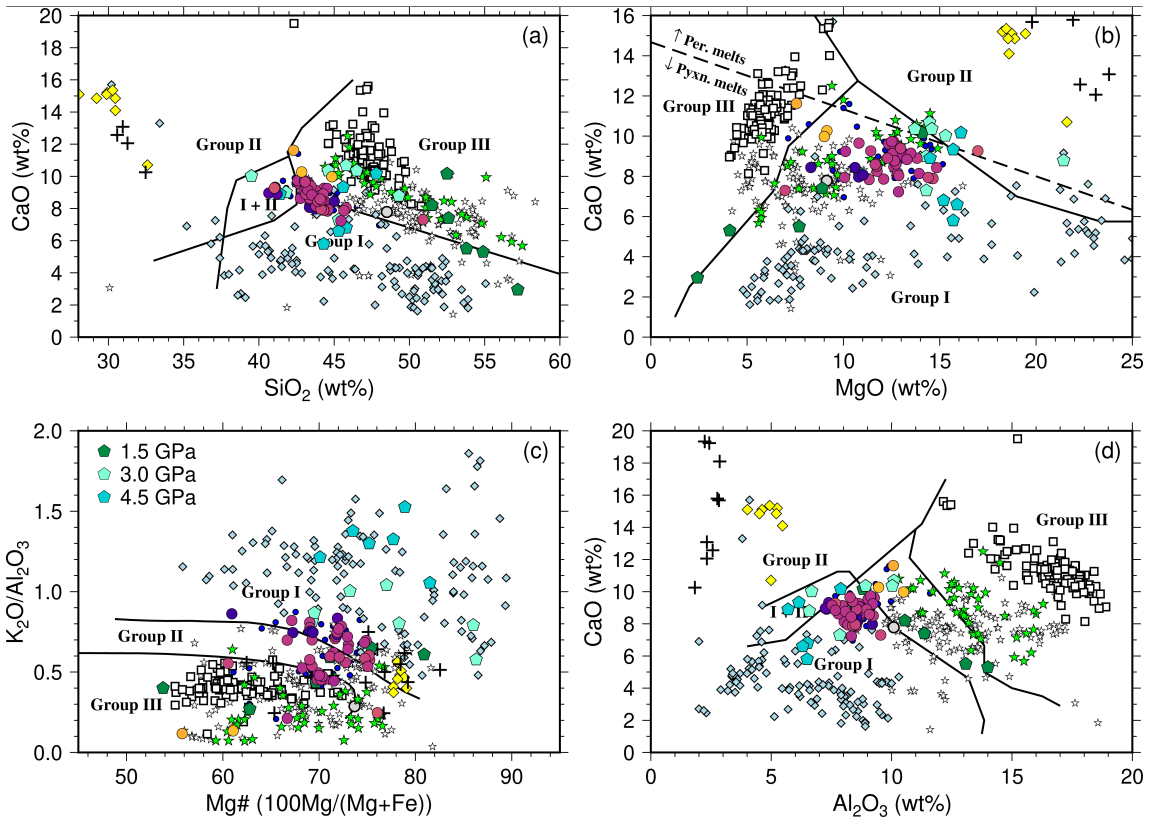


Fig. 5: Lamproite discrimination diagrams as defined by Foley et al. (1987), showing the EAPS lavas analysed in this study compared to values for other alkaline lavas. Group I, II, and III refer to I – lamproites, II – kamaufugites, III – leucitites. Coloured pentagons correspond to high-pressure hydrous pyroxenite experiments from Shu et al. (2024). Note the EAPS lavas south of Griffith (34°S; yellow and orange circles) are not ultrapotassic. Pyroxenite and peridotite partial melt divide is plotted in (b) as shown in Herzberg (2011) and Herzberg and Asimow (2008). Symbols as in Figure 2.

273 values measured for this study, however analyses below 150 ppm should be treated with caution (Figure 7b).
 274 N concentrations are highest in the central area but also exhibit the most variation (44–350 ppm), while the
 275 northern lavas cluster around 162–213 ppm N (Figure 7b). Hydrogen varies between 410–3559 ppm, which is
 276 equivalent to 0.73–6.36 wt% H₂O, across the entire EAPS and displays no clear trend or clustering between
 277 eruptive centres (Figure 7a). The southern centres of Shepparton and Pine Lodge show moderate variation and
 278 are generally more enriched in H and N, and slightly enriched in C compared to the remaining localities measured
 279 in the central and northern areas, while S contents are within error of the average. Shepparton is more enriched
 280 in C, H, and N (1562, 3185, and 324 ppm respectively), but slightly depleted in S (55 ppm) in comparison to
 281 Pine Lodge (C= 1186, H= 2431, N= 249, S= 92 ppm).

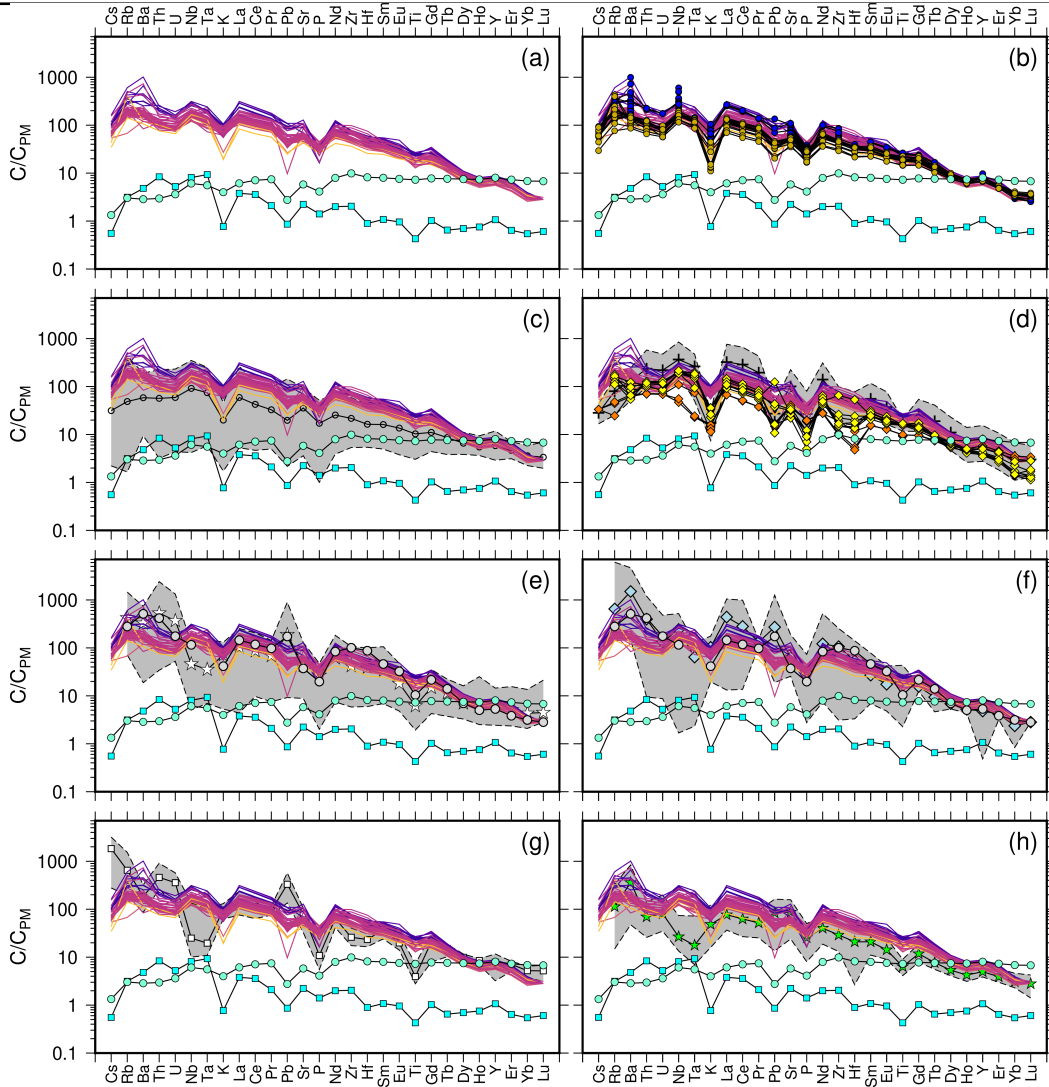


Fig. 6: Trace element variation diagrams with measured trace elements normalised to primitive mantle (PM) values from Palme and O'Neill (2013). New analyses from this study are coloured by latitude; N-MORB values from Gale et al. (2013) and SCLM values from McDonough (1990) included for reference (symbols as in Figure 2). Panel (b) shows the EAPS with SCLM and N-MORB compared to the EAPS literature values (note variability in the number of points per element) and the Shepparton lavas analysed by Paul et al. (2005). The grey bands in panels (c)–(h) represent the absolute range for the published dataset represented by the symbol plotted within the band, which also marks the average pattern for those samples. Bokhara River and Mount Webb (orange and yellow diamonds, respectively) in (d) are plotted over the West Greenland kimberlites (black crosses and grey band; Tappe et al., 2017). The orogenic lamproite BO-3 from Prelević et al. (2005) is included in both (e) and (f) for comparison given its similar mineralogy to the EAPS samples. Symbols for published data as in Figure 2.

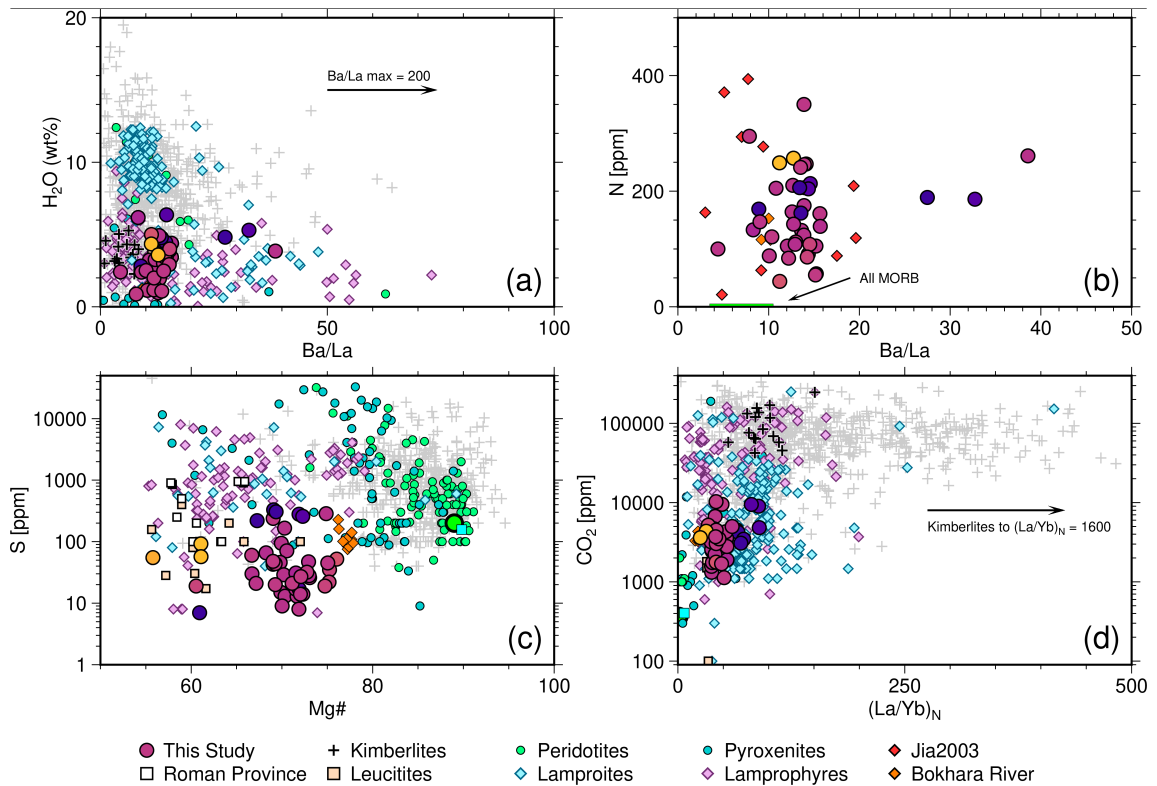


Fig. 7: Volatile element results plotted against relevant trace element ratios or Mg#. H₂O (a) and N (b) are plotted against Ba/La based on similar behaviour and likely source (sediments). Sulfur (c) shows a degree of degassing with samples from the same outcrops showing both high and low-S for similar Mg#. CO₂ (d) also exhibits degassing, but still overlaps with global lamproites, lamprophyres, and some kimberlites. Colours for EAPS (this study) follow Figure 2. Published values are screened for Mg# ≥ 55 and represent converted total abundances for all species of that element reported. Data sources: “All MORB” in (b) from Johnson and Goldblatt (2015) and Gale et al. (2013); GEOROC precompiled files (kimberlites, peridotites, pyroxenites, lamproites, lamprophyres, and leucitites); kimberlites from Tappe et al. (2017) highlighted in black; Jia2003 (N-only; lamproites and lamprophyres; Jia et al. (2003))

282 Compared to published values the EAPS analyses show similarity with lamproites, lamprophyres and leucitites
 283 with respect to H₂O and S contents, but are most similar to lamproite CO₂ contents (Figure 7a, c, d). H₂O
 284 contents also overlap with some kimberlites, specifically those from west Greenland (Tappe et al., 2017). However,
 285 kimberlites as a group span a large range of values for H₂O, S, and CO₂ (Figure 7a, c). Sulfur contents of the
 286 EAPS also resemble those of the Roman leucitites and other leucitites globally, but the EAPS are more magnesian
 287 overall (Figure 7c). Published literature that combines analysis of both trace elements and volatile elements is
 288 scarce i.e. Tappe et al., 2017. Further, volatile elements are rarely measured by dedicated methods like we have
 289 employed here. Nitrogen is perhaps the best example of this with the available published data being severely
 290 limited (Figure 7b), however the reliability of published S analyses is also questionable given most data are

determined via XRF. While there are occasional instances where the EAPS samples exhibit elevated volatile element concentrations that are replicated in whole rock trace element ratios or non-volatile elements (i.e. S vs. Cu; S vs. Ni; S vs. Pb; H₂O vs. La/Yb; C vs. (La/Yb)_N) these are not consistent across the dataset (Figure 7d). Therefore, unlike the general enrichment trends in major and trace elements (Figures 2-6, and 8), we observe no systematic spatial trend in volatile element geochemistry, nor do we see any clear correlation when plotted against any of the common whole rock trace element ratios for volatile-bearing or influenced sources. This suggests the volatile analyses are likely modified by degassing upon ascent and eruption which is not unexpected for potassic and ultrapotassic melts that are considered relatively volatile-laden (Prelević et al., 2004). We tested CO₂/Ba for our samples to investigate if degassing has occurred and, if so, to what degree. Observed ratios between 0.5–13 suggest significant degassing has taken place compared to ratios of around 140 exhibited in undegassed basalts and melt inclusions (Hauri et al., 2018; Matthews et al., 2017, 2021). Degassing, in the case of the EAPS, is most obviously exemplified by the clear separation of values for S from the same outcrops (i.e. Byrock) in Figure 7c, where degassed samples exhibit S \sim ≤100 ppm. Given the majority of samples sit at or below this threshold, we suggest that the values reported here represent minimum values and are probably decoupled from the source volatile contents.

Discussion

Classification of the EAPS Rocks

Lamproites as a group of rocks have been considered enigmatic for much of the time since they were first described, and the same can be said for leucitites and leucite-bearing rocks that have been variably described and named around the world. In most cases the name assigned to a rock or outcrop is inconsequential except to give the reader a general idea of the mineralogy or approximate chemical range within which it sits. Lamproites and leucitites are not easily identified in hand specimen with few obvious markers to isolate what the rock is, perhaps with the exception of phenocrystic phlogopite or leucite in lamproites and leucitites respectively. All naming schemes for highly-alkaline rocks require modal mineralogy and mineral chemistry analyses or microbeam imaging techniques (Woolley et al., 1996; Mitchell and Bergman, 1991; Mitchell, 2021; Le Bas, 1989; Le Bas and Streckeisen, 1991; Le Maitre et al., 2002; Tappe et al., 2005). This is further complicated by the wide range of textures present in this type of rock and the prevalence of heteromorphism. Recent contributions have worked to identify chemical and mineralogical markers of tectonic or geodynamic setting for both of these melt types, leading to the general (*yet imperfect*) association of leucitites with subduction-related melts (Innocenzi et al., 2024; Lustrino et al., 2019; Lustrino and Wilson, 2007), and lamproites with orogenic or anorogenic (i.e. intraplate/cratonic) melting

321 processes (Prelević et al., 2008a, 2010, 2013b, 2012). This paper seeks to re-evaluate the EAPS in light of this
322 more general association of melts with specific melting and mass transfer processes in well understood geodynamic
323 settings.

324 The primary distinguishing feature between leucitites and lamproites is the presence of phlogopite mica in
325 lamproites and its absence in leucitites (Mitchell, 2020; Mitchell and Bergman, 1991; Rock, 1991; Woolley et al.,
326 1996; Bergman, 1987). While the presence of other minerals such as leucite, olivine, and sanidine are shared
327 between both rock types, the diversity and modal abundance of other mineral species occurring in lamproites
328 is in itself characteristic. The EAPS exhibits a similar diversity of minerals present in the rock to the range of
329 minerals expected in lamproites, as well as poikilitic and phenocrystic phlogopite mica which are also expected
330 in lamproites and not in leucitites (*detailed petrography presented in Lanati et al. (in prep.)*). The major barrier
331 to the entire EAPS being reclassified as lamproites are the outcrops including and south from Griffith, i.e. from
332 34°S and southward (**Figure 1d**) (Lanati et al., in prep.). These outcrops have all undergone some degree of
333 alteration. In these samples analcime is more common than leucite and only olivine cores are preserved, with the
334 remainder of the olivine having partially or fully transformed to iddingsite (Lanati et al., in prep.). This includes
335 the outcrop at Pine Lodge, in which no leucite is preserved (**Figure 1b, e**; previously known as Cosgrove, for
336 which the hotspot track is named). The observation of pseudoleucite or analcime should be treated with caution
337 especially given the work of Prelević et al. (2004) who undertook analyses on a similar set of rocks to those
338 analysed in this paper. Their work showed that transformation of leucite to analcime in a natural geological
339 setting leads to falsification of K_2O/Na_2O and enrichment in some LILE and HFSE's during the transformation
340 (e.g. Cs, Th, U), while also exhibiting depletion in others (e.g. K and Rb) (Prelević et al., 2004).

341 On a geochemical basis the EAPS rocks meet most of the discriminators to be lamproites as described by
342 several studies (Foley et al., 1987; Bergman, 1987; Woolley et al., 1996; Prelević et al., 2008b). The whole rock
343 geochemistry (**Figures 2, 3, 5**) displays significant overlap with other lamproites globally (**Figure 5**). However,
344 there are no whole-rock end-member compositions in the EAPS and samples 1402 (Wallaroy Hill), 1703 (Flagstaff
345 Hill), and 0901a from the Byrock outcrop (**Figure 1b-d**) are less lamproitic (i.e. variable $MgO < 9 \text{ wt\%}$ or > 15
346 wt\% ; $Mg\# < 65$; or $SiO_2 > 46$) compared to the other sub-samples from these outcrops (**Figures 2, 3, 5, 8**).
347 This can be explained by the tendency for these samples to include significant olivine cargo, assumed to be
348 xenocrystic, or by inclusion of altered xenoliths where olivine appears to have been replaced by near pure SiO_2
349 (*xenoliths of the EAPS are the basis of a forthcoming manuscript*). Similar to the mineralogical criteria, the
350 outcrops south of 34°S that include Griffith, Pine Lodge, and Violet Town (**Figure 1**) deviate significantly from
351 the broader grouping in most major element spaces (**Figures 2, 3, 5**). Most notably, the K contents of these

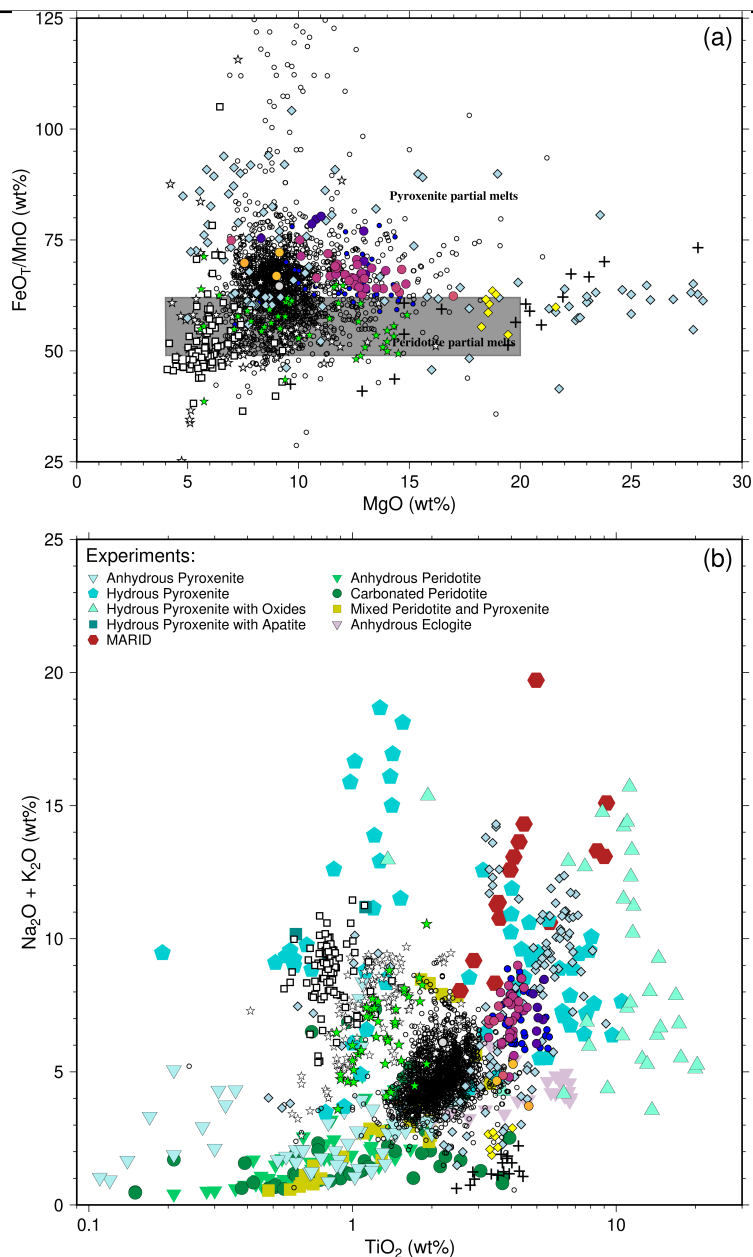


Fig. 8: Source component discrimination diagrams. (a) FeO_T/MnO vs. MgO with grey box showing the range of values for partial melts from an anhydrous peridotite source defined by Herzberg (2011). (b) The range of mantle source lithologies in (log-scale) TiO_2 versus total alkali ($Na_2O + K_2O$) from experimental studies; compilation after Shea et al. (2022). Symbols not shown in panel (b) plot legend are for the EAPS and published data representing natural samples and are the same as in Figure 2.

samples (Figure 2b, c, and 3h) range from 1.18–1.41 wt% which is significantly lower than almost all of the other samples presented here. These samples also exhibit $K_2O/Na_2O < 0.5$ while containing Na_2O of 2.54–3.95

352

353

354 wt% (Figure 2b and 4b), meaning they are not ultrapotassic. This is another hallmark of analcimitisation as
355 described by Prelević et al. (2004).

356 Taken together, these characteristics show that the majority of the EAPS lavas are best characterised as
357 lamproites. The whole-rock chemistry shows an overlap between the EAPS and both orogenic and anorogenic
358 lamproites, but there appears to be a stronger affinity towards the anorogenic grouping in the global lamproite
359 dataset (Figures 2a, c, 3b, c, e, f, 4a, d,e, and 5; Casalini et al., 2022). Globally, lamproites occur alongside a range
360 of magmatic compositions within the same broader field area (Mitchell, 2020), which means that the presence
361 of analcime in the southern exposures should not impact viewing the EAPS as a suite of mostly lamproites.
362 Furthermore, given their high-K affinity, these rocks are particularly susceptible to weathering and alteration
363 by hydrous fluids (Roux and Hamilton, 1976; Gupta and Fyfe, 1975; Roux and Hamilton, 1976; Prelević et al.,
364 2004). This does mean, however, that the outcrops south of 34°S included in this study cannot be classified
365 on a petrographic or primary geochemical basis. Chemically they exhibit depletion in K and enrichment in Na
366 (Figure 2b, c, and 4a, b), reflecting the analcimitisation of leucite. From the major elements, they cannot be
367 definitively reclassified as lamproitic magmas, although the more incompatible whole-rock trace elements from
368 Eu–Lu give some suggestion that they are chemically similar to the remainder of the EAPS (Figure 6). Previous
369 Nd, Pb, and Sr isotopic work on the Pine Lodge sample provides evidence that this outcrop is more chemically
370 linked to the Victorian Newer Volcanic Province (NVP) basalts than the leucitites, in agreement with previous
371 petrological studies (Birch, 1978; Nelson et al., 1986). Our recommendation is that samples from Griffith (1801),
372 Pine Lodge (2001), and Shepparton (Violet Town Quarry; 2101 – 2022) should not be considered lamproites
373 or leucitites and that they should be treated with caution as they no longer possess the magmatic composition
374 at the time of eruption. This is particularly relevant for Pine Lodge that sits between the EAPS and the NVP
375 in chemical and petrological space. However, further work that includes modern isotopic analyses is needed to
376 understand the genesis of the southern samples.

377 The holistic view of the EAPS data presented here reveals, based on trace element patterns and ratios, a
378 clear demarcation between the northernmost outcrops at Byrock and El Capitan, and the fields further south at
379 Tullibigeal, Lake Cargelligo, and Begargo Hill (Figures 1b–d, 6a, 10a–d, and 11a,b,d). The separation between the
380 trace element ratios of these samples (Figures 6a, 10b,d, and 11a,b,d) suggests that a more extreme enrichment
381 process was at play beneath the northernmost volcanoes. Furthermore, the northernmost samples consistently
382 overlap with anorogenic lamproites more frequently than any other group of lavas (Figure 10a,b and 11a,b,d).
383 Therefore, we suggest that Byrock and El Capitan be considered as a separate volcanic field to the remainder of
384 the EAPS. In the grouping proposed here, we term the northern outcrops the *Tindarey lamproites*, the central

outcrops the *Tullibigeal lamproites*, both after the local geographic centre of the fields, while the southern outcrops of Griffith, Pine Lodge, and Violet Town remain unchanged.

Magma Sources and Geodynamic Environments of Eastern Australia

The generally accepted model for the formation, stabilisation and growth of the Australian continent begins with the formation of three Precambrian cratonic blocks in the Archean and Proterozoic, the West Australian Craton, South Australian Craton, and North Australian Craton (Fergusson and Henderson, 2015). Progressive accretion of orogenic belts then followed to form part of the Gondwana supercontinent through the Phanerozoic, which extended the continent eastward beginning with the accretion of the Delamarian and Thomson orogens in the Middle Cambrian to Ordovician (Fergusson and Henderson, 2015; Glen, 2005). The accretion of the Delamarian and Thomson orogens overlaps with the formation of Lachlan orogen in the southeast which began in the Cambrian before accretion in the Middle Ordovician. The final stages of orogeny resulted in the accretion of the Mossman orogen on the northeast tip of Australia, on to modern day cratonic Australia (Figure 1a) during the Silurian and Devonian which occurred roughly syngenetically with the collision of the New England orogen in the Late Devonian to Early Carboniferous with the Thomson and Lachlan orogens in the central to southeast (Fergusson and Henderson, 2015; Glen, 2005). These five orogenic blocks are referred to collectively as the Tasmanides and make up modern-day eastern Australia (Figure 1a,b). They are all characterised by large-scale deformation and plutonic intrusion events as well as arc volcanism, which is best characterised by the heavily mineralised Macquarie Arc within the Lachlan Orogen (Fergusson and Henderson, 2015; Glen, 2005). Parts of the Tasmanides are also known to have undergone various rifting events most notably during the Cambrian (back-arc rifting) and then through the Mesozoic including the Permian and Triassic Sydney-Gunnedah-Bowen Basin system (Glen, 2005).

Once the consolidation of orogenic eastern Australia was complete intraplate volcanism became widespread, especially during the Cenozoic with some Oligocene but more commonly Neogene volcanism continuing into the Holocene making up the EAVP and the EAPS (Wellman and McDougall, 1974; Cohen et al., 2008, 2013, 2017; Blackburn et al., 1982; Smith and Prescott, 1987). The source and mechanism that induced melting to generate these intraplate volcanics have been linked to several processes including mantle plumes (Sutherland, 1983; Wellman and McDougall, 1974; McDougall and Wellman, 1976; Cundari et al., 1978; Cohen et al., 2008; Davies et al., 2015), edge-drive convection (EDC; Davies et al., 2015; Rawlinson et al., 2016, 2017), and more recently shear-driven upwelling (SDU; Duvernay et al., 2022; Manassero et al., 2024). The major difference between these processes is that for both EDC and SDU the primary control on melting and subsequent magmatism is the

architecture of the lithospheric base. In contrast, for a hypothesis invoking plumes, melting and magmatism were assumed to be controlled by a large temperature difference between the plume and surrounding mantle, with the plume producing large volumes of melt below the LAB. Plate motion plays a significant role in all scenarios but the contribution to melt generation is inversely proportional. In the case of SDU and EDC, faster plate motions would result in greater volumes of mantle material being moved to higher levels and therefore induces larger degrees of melting. On the other hand, faster plate movement would reduce the time during which the plume head is in contact with the base of the lithosphere, making it more likely that melt production will be lower in any one place, hindering melt extraction.

Temperatures Under Eastern Australia

Some of the primary lines of evidence for plume-derived origins of age-progressive volcanism in Eastern Australia include elevated temperatures calculated by various methods. Most recently, Ball et al. (2021) used REE inverse modelling techniques to calculate temperatures of 1350 °C and melting depths of 50 km, or about 1.5 GPa, for the more abundant basalts of the EAVP. This model, however, explicitly excluded the EAPS lavas due to their enriched potassic composition. The temperatures modelled are elevated compared to the ambient mantle (~1250 °C) and cannot be explained by normal adiabatic melting from the South Eastern Australian Geotherm (SEAG) as defined from xenoliths by O'Reilly and Griffin (1985) and reproduced by Griffin et al. (1987) (Figure 9b). All currently available whole-rock thermometers and barometers, regardless of the calculation method, are based on experiments on four-phase peridotites, or on basaltic glasses such as those erupted from shield volcanoes like Mauna Loa and Mauna Kea (Putirka, 2008). These compositions represent the bulk composition of the modern day mantle and include variations of four-phase peridotite to encompass compositions ranging from enriched to heavily depleted. Hydrous and non-peridotitic sources, as well as primitive heterogeneous mantle sources, present a significant challenge for these approaches in calculating an accurate melting temperature and depth. Anhydrous peridotites, for example, underpin the assumptions and model calibration used for thermometry by inverse REE modelling. In contrast to hydrous or metasomatised sources, anhydrous peridotites have significantly higher solidi (Figure 9b) (Green, 2015) meaning the comparatively lower solidus of hydrous sources may result in overestimates of melting temperatures (e.g. Katz et al., 2003).

This is significant given that all of the samples in this study, despite having compositions within the calibrated chemical ranges for many thermometers and barometers, are derived from heavily metasomatised and heterogeneous mantle sources (Shea and Foley, 2019; Shea et al., 2022; Frey and Green, 1974; Frey et al., 1978), making it difficult to determine the temperatures and pressure for the EAPS lavas.

While many geothermobarometers exist, the most applicable of the available whole-rock thermometers and barometers for the EAPS are those calibrated on natural basaltic glass compositions or peridotite compositions from high-pressure and temperature experiments (Putirka, 2008; Lee et al., 2009). Putirka (2008) used Hawaiian basaltic glasses to derive both pressure-independent and pressure-dependent (Eq. 14 and 15 in Putirka 2008, respectively) thermometers. In contrast, Lee et al. (2009) used an approach including hydrous and anhydrous experimentally determined basaltic compositions, from mostly peridotite-like starting assemblages, to calibrate a combined thermometer and barometer for volcanic compositions. Of these two options, the experimentally calibrated thermometer is believed to be the most robust, however use on metasomatised sources like those expected for alkali-rich melts is explicitly discouraged by the authors (Lee et al., 2009). In light of this, we apply the equations of Putirka (2008) to our samples, as it has the broadest compositional range of the available options. However, we first tested equations 14 and 15 by comparing calculated to experimental temperatures using the experimental melt compositions collated in [Figure 8b](#). Using both the pressure-independent and pressure-dependent thermometers there is good correlation between the calculated and experimental temperatures for melts derived from anhydrous peridotite, anhydrous pyroxenite, as well as carbonated peridotites, and mixed peridotite and pyroxenite sources which fall within the margin of error of the thermometer. However, for hydrous pyroxenite, anhydrous eclogites, and MARID sources the thermometer either over- or underestimates the calculated temperatures compared to the experimental temperatures. In the case of melts from experiments on anhydrous eclogite assemblages temperature estimates are lower by 200°C, while for hydrous pyroxenites the range of calculated temperatures is larger and usually results in an overestimation of around +120°C compared to the experimental temperature.

Applying this predicted temperature offset for hydrous pyroxenite melting to the EAPS samples the range of temperatures reduces from 1217–1490°C to 1097–1370 °C with an average of 1244 °C ([Figure 9a](#)), which is roughly equivalent to the ambient mantle value (O'Reilly and Griffin, 1985; Ball et al., 2021). This suggests that no thermal perturbation was required to initiate melting. The EAPS could have been generated by normal adiabatic melting of a metasomatised source and, as a consequence, the invocation of a plume or hotspot is not necessary.

Metasomatism and Magma Generation

Anhydrous peridotite that makes up the bulk of the Earth's mantle cannot produce highly alkaline primary magmas (e.g Falloon and Green, 1988; Green, 2015; Hirose and Kushiro, 1993; Novella and Frost, 2014; Robinson et al., 1998; Robinson and Wood, 1998; Takahashi, 1986). Fertile lherzolites produce basaltic melt compositions

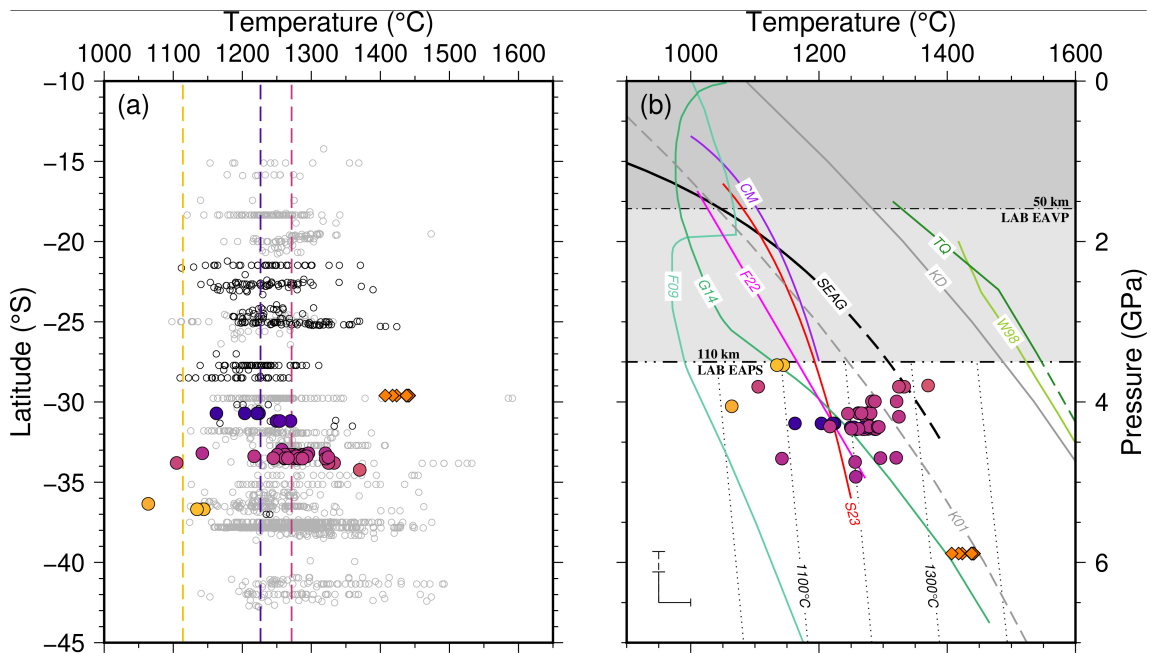


Fig. 9: Calculated temperatures vs latitude south (a) and depth (b) for the EAPS Lavas (coloured symbols for Bokhara and EAPS lavas follow Figure 2). Dashed coloured lines in (a) show averages for north, central, and south EAPS; open black and grey circles represent age-progressive (plume related) and non-age-progressive EAVP basalts, respectively. Grey fields in (b) are the LAB depths beneath eastern Australia, while coloured lines are experimentally determined solidi for mantle assemblages compared with the SEAG (black solid and dashed line) and mantle adiabats (dotted lines below 3.5 GPa). Reduced peridotite solidus below 2 GPa and dry pyroxenite (MIX1G) solidus roughly follow K01 and KD, respectively (Foley et al., 2009; Pintér et al., 2021; Kogiso et al., 2003). Dashed pressure error bar = EAPS, solid = EAVP (Rawlinson et al., 2017). Data sources: F09 = Foley et al. (2009) oxidised peridotite; G14 = Green et al. (2014) pyrolite +0.4 wt% H₂O; F22 = Foley et al. (2022) hydrous pyroxenite; S23 = Shu et al. (2024) phlogopite-websterite; CM = phlogopite lherzolite (Condamine and Médard, 2014; Condamine et al., 2016); K01 and KD = 0.1 wt% H₂O and dry lherzolite (Katz et al., 2003); TQ = Tinaquillo (depleted) lherzolite (Robinson et al., 1998; Robinson and Wood, 1998); W98 = KR43004 fertile lherzolite (Walter, 1998).

475 when melting occurs at high-pressure or low melt fractions, which, compared to the overall EAPS, are still
 476 depleted (i.e. Falloon et al., 1997; Walter, 1998). Even when volatile components such as water and carbon,
 477 usually as H₂O and CO₂, are added these mantle assemblages still cannot replicate the range of primary magmas
 478 with elevated alkali element contents (Foley and Pintér, 2018; Novella and Frost, 2014; Pintér et al., 2021; Green,
 479 2015; Hirose, 1997). Only melting of olivine-poor (*or free*) mantle rocks, such as pyroxenites, generates partial
 480 melts that are within the major element range of alkaline magmas (Foley et al., 2025; Hirschmann et al., 2003;
 481 Kogiso et al., 2003; Lambart et al., 2009, 2012, 2013; Pertermann and Hirschmann, 2003). The main challenges
 482 in producing alkaline melts from peridotite sources centre around generating sufficiently high K₂O, FeO_T, TiO₂,
 483 and Na₂O. Alkali deficiencies in experimental partial melts can only be addressed by increasing the alkali

contents, usually K_2O , of the starting mixtures to represent metasomatised mantle assemblages that reflect natural xenoliths, sediment input, or be based on inferred compositions (Conceição and Green, 2004; Pintér et al., 2021, 2022; Wang and Foley, 2018). Subduction-related metasomes and fluids are the most common process investigated in experimental studies as sediments are a suitable source of alkalis and volatiles (Chen et al., 2021, 2023; Förster et al., 2019, 2021; Wang et al., 2024, 2017, 2021). However, the source processes and exact type of metasomatic agents that can produce alkaline and potassic magmas in intraplate settings are not well constrained from experimental evidence.

Mantle metasomatism was proposed based on the observation of clear replacement textures in lherzolite nodules entrained in lavas of the West Eifel and South West Uganda (Lloyd and Bailey, 1975; Hough, 1972). These textures showed the “dissolution” of olivine, orthopyroxene and clinopyroxene within a spinel lherzolite that were replaced by mica and clinopyroxene (Lloyd and Bailey, 1975). Modern mantle metasomatism (hereafter ‘metasomatism’) represents a continuum of processes from fluid-rock through partial melting and melt-solid reactions (i.e. Dawson, 1984; Harte, 1983; O’Reilly and Griffin, 2013). Applying this to the EAPS lamproites it is, therefore, completely likely that the mantle beneath the EAPS has undergone several styles and generations of metasomatism to create a distinct mantle domain (metasome) that can produce such alkaline enriched melts. This notion is supported by multiple xenolith and xenocryst studies from across the EAVP that have observed evidence of metasomatism across major, minor and trace element, and multiple radiogenic isotope systems (Alard et al., 2000, 2002; Pearson et al., 2006; Powell et al., 2004; Powell and O’Reilly, 2007; Yaxley et al., 1997, 1991; Andersen et al., 1984; O’Reilly and Griffin, 2000; O’Reilly, 1987; O’Reilly and Griffin, 1984; O’Reilly et al., 2008; Irving, 1974; Wass and Rogers, 1980; Wass et al., 1980; Wass, 1979b,a; Irving and Frey, 1984; Menzies and Wass, 1983; Barron et al., 1996; Robertson et al., 1985; Wilkinson, 1975; Wilkinson and Hensel, 1991; Zhang and O’Reilly, 1997; Zhang et al., 1999, 2001; Griffin et al., 1984; Gaul et al., 2000, 2003).

It has been argued that alkaline melts could be products of either magmatic fractionation or that their composition has been altered due to crustal assimilation. This implies that while these melts can be primary relative to their source, they would not be considered as parental or primitive. We outline below that the EAPS melts are primitive in nature, match mantle values across many element systems, and thus are primary mantle melts (Figure 10a,b,d, and 11c). Nb/U shows clearly that the EAPS plots completely within the mantle array and as Nb/U is especially sensitive to crustal inputs compared to other systems like Ce/Pb ((EAPS = 17–35 \approx mantle array) Hofmann et al., 1986), arguing strongly against the presence of any crustal component in the EAPS melts. Coupled P_2O_5/TiO_2 values ranging from 0.12–0.45, and Ti/Eu of roughly 4000–6500 (Figure 11a) trending toward primitive mantle values of 0.19 and 7600 respectively, also support a mantle origin. Furthermore,

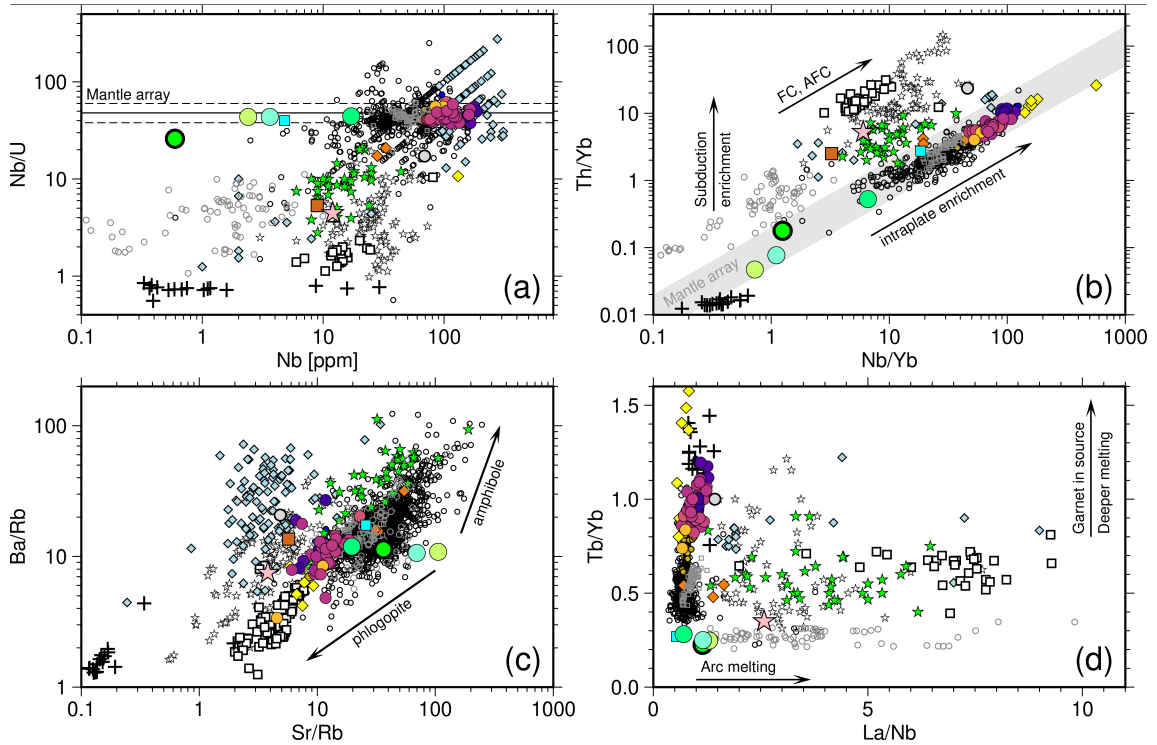


Fig. 10: Dominant mantle source trace element ratio discrimination plots of the EAPS showing (a) Nb vs. Nb/U indicating primitive-mantle derived magmas; Nb/U is sensitive to crustal contamination; mantle array from Hofmann et al. (1986). (b) Nb/Yb vs. Th/Yb showing mantle array and arrows illustrating subduction enrichment, assimilation and fractional crystallisation (FC, AFC), and intraplate enrichment after Pearce (1983); Ersoy et al. (2014). (c) Sr/Rb vs. Ba/Rb with phlogopite- and amphibole-bearing source compositional vectors (arrows). (d) La/Nb vs. Tb/Yb with garnet and inferred source melt depth arrows, after Wang et al. (2002). Symbols for standard compositions (MORB, UCC, and GLOSS) follow Figure 11 while remaining symbols as in Figure 2.

515 subduction-related processes such as arc-type melting, including contribution to the melt by slab-derived fluids,
 516 the melting of pelagic sediments, and fractionation can be ruled out using Th/Yb, La/Nb, Ba/La, Ba/Nb, and
 517 La concentrations (Figures 10b and 11b-d). This contrasts with some other lamproites globally; especially the
 518 orogenic lamproites that are the most likely to have elements added by interaction with slab fluids or melting of
 519 pelagic sediments (Figures 10b and 11b,c). Among the published data included for comparison, arc style melting
 520 is observed almost exclusively in the Sierra Nevada alkaline rocks and the Roman Province (Figures 10b,d
 521 and 11c). However, as observed from La-enrichment and Th/Yb against Nb/Yb, fractionation via fractional
 522 crystallisation is very important in the Roman Province (Figures 10b and 11d). While orogenic lamproites and
 523 the Sierra Nevada alkaline rocks also display enrichments in Th/Yb and Nb/Yb as well as La, the La contents

show a less dramatic enrichment and are thus less conclusively impacted by fractional crystallisation (Figures 10b and 11d).

524

525

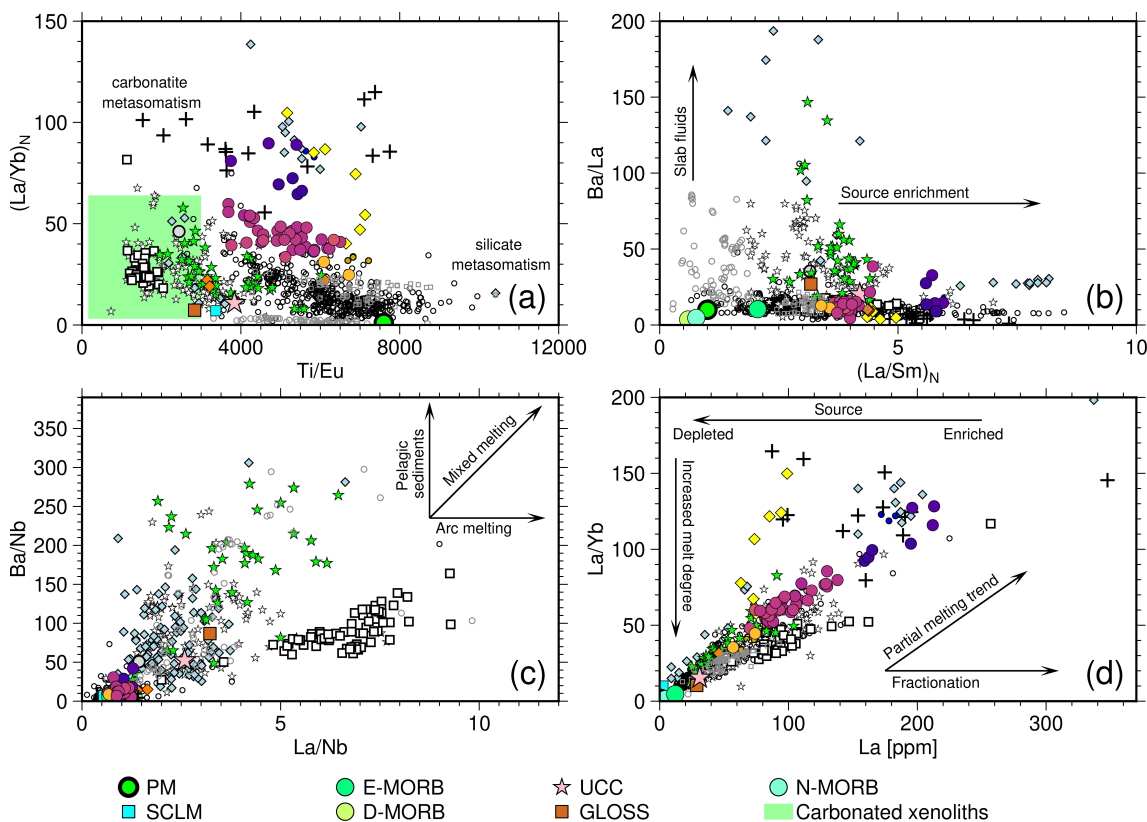


Fig. 11: Trace element ratio demarcation plots of the EAPS showing (a) Primitive mantle-normalised La/Yb vs. Ti/Eu displaying carbonatite and silicate metasomatism end-members compared to carbonatite metasomatised xenoliths (shaded green rectangle) from Yaxley et al. (1991); (after Coltorti et al. (1999); Rudnick et al. (1993); Klemme et al. (1995)). (b) Primitive mantle-normalised La/Sm , as an indicator of mantle source enrichment, versus Ba/La for identifying melts associated with subduction related slab fluids, after Elliott et al. (1997); Aldanmaz et al. (2000). (c) La/Nb vs. Ba/Nb plotted with arrows showing general trends expected for melting with pelagic sediments, melts derived from mixed source, and arc-style melting. (d) La vs. La/Yb showing source enrichment, partial melt/ melt degree, and fractionation trends. Published data: MORB (Gale et al., 2013); UCC (Rudnick and Gao, 2013); and GLOSS (Plank and Langmuir, 1998). Remaining symbols as in Figure 2.

Another objective is to isolate the style and type of metasomatism that could create the EAPS melts. While the EAPS rocks exhibit primitive signatures and are mantle-derived they also exhibit a significant degree of enrichment characteristic for intraplate settings (Figure 10b). This enrichment is assumed to reflect the mantle assemblage from which these rocks melted (Figure 11b,d), and has been both conceptually and numerically modelled in early works on the EAVP (Frey and Green, 1974; Frey et al., 1978). In opposition to this, however,

526

527

528

529

530

531 are the xenoliths sampled within Eastern Australia, including in rocks of the EAPS, that are relatively depleted
532 assemblages such as lherzolites, harzburgites, and dunites. A subset of these xenoliths provides clues to the
533 mechanism of enrichment. Hydrous silicate minerals, as well as apatite and occasional sulfide minerals, are
534 uncommon in the xenoliths of the EAVP; carbonates are never directly observed except as inclusions, although
535 geochemical evidence of their presence in the mantle beneath eastern Australia has been extensively studied
536 (Alard et al., 2000, 2002; Andersen et al., 1984; Barron et al., 1996; Irving, 1974; Irving and Frey, 1984; Menzies
537 and Wass, 1983; O'Reilly and Griffin, 1984, 2000; Powell et al., 2004; Powell and O'Reilly, 2007; Robertson et al.,
538 1985; Wass, 1979b,a; Wass and Rogers, 1980; Wass et al., 1980; Wilkinson, 1975; Wilkinson and Hensel, 1991;
539 Yaxley et al., 1991, 1997). Carbonated peridotites have been shown experimentally to melt at lower temperatures
540 than anhydrous peridotites (Figure 9b). At pressures equivalent to the LAB of the EAPS incipient melting in this
541 system can begin at around 1270°C and persist for over 300°C before major melting occurs regardless of if the
542 assemblage is enriched or not, especially if water is also present (Dasgupta et al., 2007; Pintér et al., 2021). This
543 makes melts derived from carbonated peridotites viable and potentially potent metasomatic agents that could
544 contribute to geochemical and mineralogical changes in the mantle source, especially with melting temperatures
545 at roughly ambient mantle. However, these are unlikely to be responsible for the enrichment in K, and reaction
546 experiments between lamproite melts and peridotites have demonstrated that the lamproitic character of the
547 primary melt is quickly lost on contact with the peridotite (Foley and Pertermann, 2021).

548 Similar to carbonates, hydrous phases such as phlogopite and amphibole can significantly reduce the solidus
549 of peridotites even if the modal abundance of these phases is low. If amphibole is the dominant hydrous phase in
550 the peridotite instead, melt compositions more closely resembling basanites and nephelinites (Condamine et al.,
551 2022; Dasgupta et al., 2007; Dasgupta and Hirschmann, 2006; Green, 2015; Pintér et al., 2021, 2022). Although
552 the melting of peridotites enriched with either carbonates or hydrous silicate phases acting as a transient silicate–
553 metasomatic agent could impart an enriched signature on an otherwise depleted lithospheric mantle, they alone
554 are not capable of producing lamproitic melts like the EAPS. Instead the melts from this type of peridotite shows
555 a spectrum of compositions that range from highly silica undersaturated to more silicic melts and illustrate the
556 enrichment of SiO₂ from carbonatite to basaltic magmatism (Dasgupta et al., 2007; Dasgupta and Hirschmann,
557 2006; Pintér et al., 2021, 2022; Condamine et al., 2022; Green, 2015).

558 In contrast to melt metasomatism, fluid metasomatism is another possibility. This is likely to result in a
559 highly transient geochemical signature due to the extremely reactive nature of immiscible fluids where only
560 minor, if any, precipitates may remain as witness to any solid–liquid interaction (O'Reilly, 1987; O'Reilly and
561 Griffin, 2013). Evidence for both fluid and melt–derived metasomatism has been reported in Eastern Australia

(Frey and Green, 1974; Frey et al., 1978; Andersen et al., 1984; O'Reilly and Griffin, 2000, 1984; O'Reilly, 1987), as has carbonatite metasomatism (Frey and Green, 1974; Yaxley et al., 1997; Shea and Foley, 2019; Liu et al., 2021). Primitive mantle normalised La/Yb coupled with Ti/Eu is used as a discriminator of silicate versus carbonatite metasomatism (Figure 11a), the EAPS and in particular the northern Tindarey lamproites plot above the broader EAVP including the fields shown to have carbonatite signatures (Coltorti et al., 1999; Klemme et al., 1995; Zinngrebe and Foley, 1995; Rudnick et al., 1993; Shea and Foley, 2019; Liu et al., 2021). They show similar enrichment in $(La/Yb)_N$ to other highly alkaline rocks like some anorogenic lamproites, and aillikites (ultramafic lamprophyres) with silica contents 28–33 wt% (Sudholz et al., 2023). Compared to carbonated xenoliths from the southern portion of the EAVP, the EAPS lamproites span a similarly wide range of values but are more enriched in $(La/Yb)_N$ (Figure 11a). The Ti/Eu for the EAPS is not as low as in the carbonated xenoliths, or lavas from the Roman province, Sierra Nevada, and orogenic lamproites, which may be explained by the variability of Ti/Eu fractionation in carbonatites (Figure 11a; Foley et al., 2009). Low Ti/Eu has also been observed, coupled with high Ca/Sc, in eclogite xenoliths from the Kimberley region where the metasomatic agent was determined to be an alkali-rich silicate melt (Rehfeldt et al., 2008; Jacob et al., 2009). Experimental work on clinopyroxene partitioning between peridotite and carbonatite melt has shown that, assuming the residue of melting includes clinopyroxene, a low Ti/Eu signature is a valid indicator for carbonatite metasomatism (Klemme et al., 1995). Importantly, in systems where clinopyroxene is the dominant anhydrous phase, clinopyroxene both enters the melt and occurs in the residue (Edgar and Mitchell, 1997; Foley et al., 2022; Foley and Ezad, 2024; Foley et al., 2025; Funk and Luth, 2013; Konzett, 1997; Konzett et al., 1997; Lloyd et al., 1985; Luth, 1997; Shu et al., 2024, in revision; Sweeney et al., 1993). This would mean that when an assemblage with abundant clinopyroxene melts, and Ti is no longer held back, it would still initially enter the melt and result in higher Ti/Eu giving a signature similar to silicate metasomatism even if a carbonatite was involved in the melt reaction.

The final open question to determine the source of the EAPS lamproites is, if not a four-phase peridotite then what could generate these melts and what components are needed? As stated above, olivine-poor assemblages have been shown to be capable of generating alkaline melts (Figure 8b). However many of these assemblages fail to impart sufficiently high K contents on the melt to explain lamproite genesis. The primary K-bearing minerals within the upper mantle are micas and amphiboles. Phlogopite and phengite micas will both persist at pressures up to ~ 10 GPa, but more commonly 7–8 GPa (Foley, 1991; Sudo and Tatsumi, 1990; Domanik and Holloway, 2000; Harlow, 2003; Luth, 1997; Schmidt, 1996; Harlow and Davies, 2004). Amphibole occurring at shallower depths is calcic amphibole, and peridotitic xenoliths contain only pargasite. Calcic amphiboles do not contain significant K ($K_2O/Na_2O < 1$) and are not stable above 2.5–4 GPa (Berkési et al., 2019; Dawson and

Smith, 1973; Aoki and Shiba, 1973; Ishimaru and Arai, 2008; Ghent et al., 2019; Ito, 1986; Winterburn et al.,
1990). Deeper in the mantle, K-richterite is the primary amphibole and its stability in the deep mantle has
been recorded by xenolith occurrences in kimberlites and lamproites, and through experiments, which suggests
K-richterite may be a viable source for some K-rich alkaline melts (Erlank et al., 1987; Foley, 1991; Harlow
and Davies, 2004; Mitchell, 1995; Mitchell and Bergman, 1991; Bergman, 1987; Konzett and Fei, 2000; Konzett
and Ulmer, 1999; Konzett et al., 1997; Konzett, 1997). Both K-richterite and phlogopite are stable on cold
subduction geotherms, where K-richterite can outlast phlogopite well into the transition zone (up to 15 GPa)
(Trønnes, 2002). Along warmer geotherms and at pressures greater than 6 GPa K-richterite, the high-pressure
variant of K-richterite with an M₄ site containing K, Ca, or Na capable of hosting up to ~12 wt% K₂O in its
structure and almost no Na₂O, becomes stable and becomes more potassic as pressure increases (Harlow, 2003;
Luth, 1997; Konzett and Fei, 2000; Konzett and Ulmer, 1999; Konzett et al., 1997; Konzett, 1997; Mandler and
Grove, 2016). The enrichment of K₂O in lamproites, however, can simply be achieved through the melting of
phlogopite in the source that can also explain the high modal abundance of phlogopite in these rocks (Condamine
and Médard, 2014; Foley, 1989, 1992a; Foley and Peccerillo, 1992; Foley, 1993; Fritschle et al., 2013; Mallik et al.,
2015; Putirka et al., 2012; Wang et al., 2017). This is best illustrated in Figure 10c where Ba/Rb is sensitive to
amphibole and phlogopite given that Ba will preferentially partition into amphibole but is incompatible during
melting, assuming both phlogopite and amphibole are in the source. Ba concentrations from amphibole then
naturally contribute more strongly to the melt than the Rb from the phlogopite will, acting as a proxy for the
amount of amphibole in the source as it will melt more readily and has a more restricted stability field (Foley
et al., 2022; Ezad and Foley, 2022; Ezad et al., 2024; Foley and Ezad, 2024). Similarly, phlogopite has insignificant
concentrations of Ca, unlike amphibole, with calcic minerals known to display higher contents of Sr, thus pushing
melts from calcic sources toward higher Sr/Rb (Figure 10c). In this sense amphibole-bearing sources should plot
above phlogopite-bearing sources in both Ba/Rb and Sr/Rb space. Additionally given the incompatibility of
both K and Na in the main peridotite minerals, with K being the more incompatible, the K₂O/Na₂O of the melt
must reflect the collective K₂O/Na₂O of the alkali minerals in the source. The only amphibole observed in the
EAPS is K-richterite, which commonly has a K₂O/Na₂O ≈ 1, whereas the EAPS rocks range up to K₂O/Na₂O
≈ 8 (Figure 2b; Lanati et al., in prep.). Integrating the geochemical evidence with geophysical interpretations
of the approximate LAB depth beneath the EAPS from seismic tomography, all of the EAPS samples reported
were probably generated between 113–158 km, or roughly 3.5–4.9 GPa (Figure 9b; Rawlinson et al., 2017). Both
K-richterite and phlogopite would be stable, meaning all potassium and almost all water would be held by these
phases but only melting of phlogopite could produce the K₂O/Na₂O observed in the EAPS.

Given the LAB depth beneath the EAPS it is almost certain that garnet, which becomes stable at pressures roughly above 2 GPa if sufficient Al_2O_3 is present, must have a place in the mantle source assemblage for the EAPS. Geochemical indicators for garnet mostly utilise the heavy rare earth elements (HREEs) like Yb, Tb, and Dy that range, in order, from strongly to marginally compatible. This behaviour, makes high $(\text{La}/\text{Yb})_N$, Dy/Yb and Tb/Yb effective indicators of a garnet-bearing source, producing a steeply sloping trace element pattern towards the HREEs (Figure 6a), that when combined indicate the relative proportion of garnet (Figures 10d, and 11a,d). Low Dy/Yb (i.e. <2 ; EAPS 3.47–4.66) indicates a spinel-bearing source (Yang et al., 2007). Tb/Yb, in particular, is sensitive to garnet-bearing source assemblages because, unlike La/Yb that is influenced by degree of melting due to La incompatibility, both elements are compatible, allowing Tb/Yb to be used for both the proportion of residual garnet in the source and melting depth (Stracke and Bourdon, 2009; Turner et al., 2003; Wang et al., 2002). High Tb/Yb reflects melting at greater depths — a relationship we observe in the EAPS lavas with samples erupting through the thickest lithosphere displaying the highest Tb/Yb (Figure 10d; Wang et al., 2002).

FeO_T/MnO ratios show that the EAPS rocks have signatures consistent with a pyroxenite mantle source (Figure 8a). This is grounded in the principle that Mn is held back in the source by garnet, regardless of whether a peridotite or pyroxenite is the dominant assemblage. The lower solidus of a pyroxenite-dominated source compared to a similarly anhydrous peridotite requires significantly high melt fractions in order for garnet to actively melt (Herzberg, 2011). Iron will be readily liberated from the melting of clinopyroxene in this assemblage resulting in high FeO_T/MnO ratios (Herzberg, 2011). High CaO is a common feature of peridotite-derived melts due to the high solidus temperatures that result in clinopyroxene being the least stable phase in the assemblage (Herzberg and Asimow, 2008; Herzberg, 2011). Pyroxenite assemblages on the other hand are more likely to include clinopyroxene in the residue, leading to lower overall Ca contents in low-degree melts (Herzberg and Asimow, 2008; Herzberg, 2011). The discrimination line in CaO versus MgO space is shown in Figure 5b along with the EAPS samples, of which all but one sit within the pyroxenite-derived melts field. It should be noted there are a number of high-Ca pyroxenites that would plot above this line as detailed by Herzberg (2011), but in their system none of the peridotite partial melts will cross into the pyroxenite field, thereby making this a good discriminant for pyroxenite melting. Orthopyroxene is also likely to play a role in the source for the EAPS and is a good candidate to aid the high-MgO affinity within the suite while buffering the SiO_2 contents (Lee et al., 2009; Mallik et al., 2016). In order to generate the range of melt chemistry exhibited by the EAPS the source would need to have little or no olivine, significant pyroxene, and some garnet (Figures 5b and 8a,b). Additionally, the high-Ti and potassic character of these melts necessitates the inclusion of phlogopite and a

titanium-rich phase like rutile or ilmenite (Figure 8b). As noted in Figure 3i the phosphorus content in the EAPS is elevated, suggesting apatite in the source. The presence of carbonate inclusions and carbonated glasses in the samples (Lanati et al., in prep.) illustrates that the source is also carbonated, although whether this carbonation is a remnant of the metasomatic agent, inherent in the source, or acquired during ascent cannot be determined. Therefore the most likely source for the EAPS based on the chemistry presented here is a phlogopite-garnet-websterite with apatite \pm Ti-oxides. Recent experiments by Shu et al. (2024, in revision) support our preferred source and align with the evidence from major and trace element indicators used in this study. In their work Shu et al. (2024, in revision) show that the melting of an olivine-free phlogopite-garnet-websterite assemblage similar to the one we propose here results in a melt with increased MgO and SiO₂. However before orthopyroxene contributes to the melt both MgO and SiO₂ contents remain buffered in a range similar to the EAPS analyses, showing good agreement in the lamproite discrimination diagrams (Figure 5; Shu et al., 2024, in revision). Importantly, the experimental melts most applicable to the EAPS lavas occur at pressures of 3 and 4.5 GPa, and in the range of 1200–1300°C for most major elements, except TiO₂ which mimics the EAPS from temperatures of 1350 °C (Shu et al., 2024, in revision). These conditions match the estimates of LAB depth as extracted from seismic tomography of roughly 3.5–4.9 GPa (113–158 km), as well as the temperature calculated here of 1244 °C (av; 1097–1370 °C) and ambient mantle beneath Eastern Australia (Figure 9).

671 Geodynamic Environment of Eastern Australia through time

672 Geochemistry and petrology alone cannot resolve the difference between hotspot volcanism and other geodynamic
673 processes; however, they can elucidate processes of mantle source generation and magma production to reinforce
674 arguments for a set of prevailing geodynamic conditions. Chemical and petrological discriminators can discern
675 between processes such as various forms of partial melting, fractional crystallisation, or metasomatic processes
676 such as fluid or melt infiltration. These processes are predominantly controlled by temperature and source
677 composition, but may allow inferences to be drawn about the geodynamic environment.

678 **Plume origin:** The EAPS is commonly associated with the inferred Cosgrove hotspot track due to radiometric
679 age progression data consistent with plate motion (Sutherland, 1983; Wellman and McDougall, 1974; Cohen et al.,
680 2008, 2013; Davies et al., 2015). This association is not without controversy as the initial interpretations of age-
681 progressive volcanism in the EAVP assigned different volcanic expressions to the plume track, creating a degree
682 of inconsistency. The EAPS were among the fields variably included or excluded by studies tracking the motion
683 of the Australian plate, with the evolving understanding of the Eastern Australian hotspot changing rapidly
684 based on the authors' interpretation of age and spreading-rate vector projections (Sutherland, 1983). Further,

no associated modern plume, in the form of a definitively recognisable thermal anomaly extending deeper than 110 km depth, has been observed in regional or global seismic tomographic models (Davies et al., 2015; Rawlinson et al., 2016, 2017). The Cosgrove plume head is currently believed to be situated beneath the Bass Strait between mainland Australia and Tasmania (Figure 1a,b), as determined by the projection of plate motion since the last related eruption (de Laat et al., 2023). Yet, only a small low-velocity zone beneath the Bass Strait off the south coast of Victoria is visible in global tomographic models between 80–110 km which has been suggested to be remnant melt from the now waned plume or a plume that has been captured by an existing edge-driven convection (EDC) cell (Figure 12a; Davies et al., 2015; Rawlinson et al., 2016, 2017; de Laat et al., 2023).

This is consistent with petrological evidence from magmatic flux estimates that potentially indicate a waning plume (Tapu et al., 2023). An investigation of slab-plume interactions between Australia and New Zealand using whole-mantle seismic tomography reports a “subslab hot upwelling”, interpreted to be a connected whole mantle structure concentrating heat in the transition zone beneath the Bass Strait and the Newer Volcanic Province (Figure 1a, b; Toyokuni and Zhao, 2024). However, this upwelling deflects southward which is in contrast to the northward plate motion that would likely drag hot material to the north (Toyokuni and Zhao, 2024). The lack of a large-scale seismic anomaly consistent with plate motion, and therefore the inferred age-progressive volcanism, means that there is no consistent evidence for a singular deep mantle plume traversing to crustal levels and persisting today. Instead, seismic tomographic models are more consistent with smaller scale plume-like structures, or localised melts generated through another process like EDC or shear driven upwelling which are primarily controlled by lithospheric architecture.

Importantly, even smaller scale plume-like structures (i.e. plumelets) require non-adiabatic temperature profiles and still mandate that an elevated temperature, relative to ambient mantle of 1250–1315°C must be recorded to some degree in the final melt (Ball et al., 2021; O’Reilly and Griffin, 1985; Griffin et al., 1987). However, the average best-estimate temperature of 1244°C we have calculated above is consistent with ambient mantle temperatures, and the generation of these melts therefore does not necessitate a plume or plumelet as a direct heat source.

Lateral mantle flow: An alternative geodynamic mechanism is melting induced by lateral flow of material from a plume that is offset from the volcanism. For Eastern Australia, the most likely source would be the Tasmantid plume which has been imaged as a larger scale seismic velocity anomaly in the Tasman Sea (south)east of the EAPS. However, several aspects make this scenario unlikely for melting in Eastern Australia. Firstly, the Tasmantid plume is roughly 1000 km to the east of the volcanoes sampled here yet the inferred buoyancy flux of the plume is too small to sustain lateral flow over these distances (Crossingham et al., 2017; Seton et al., 2019).

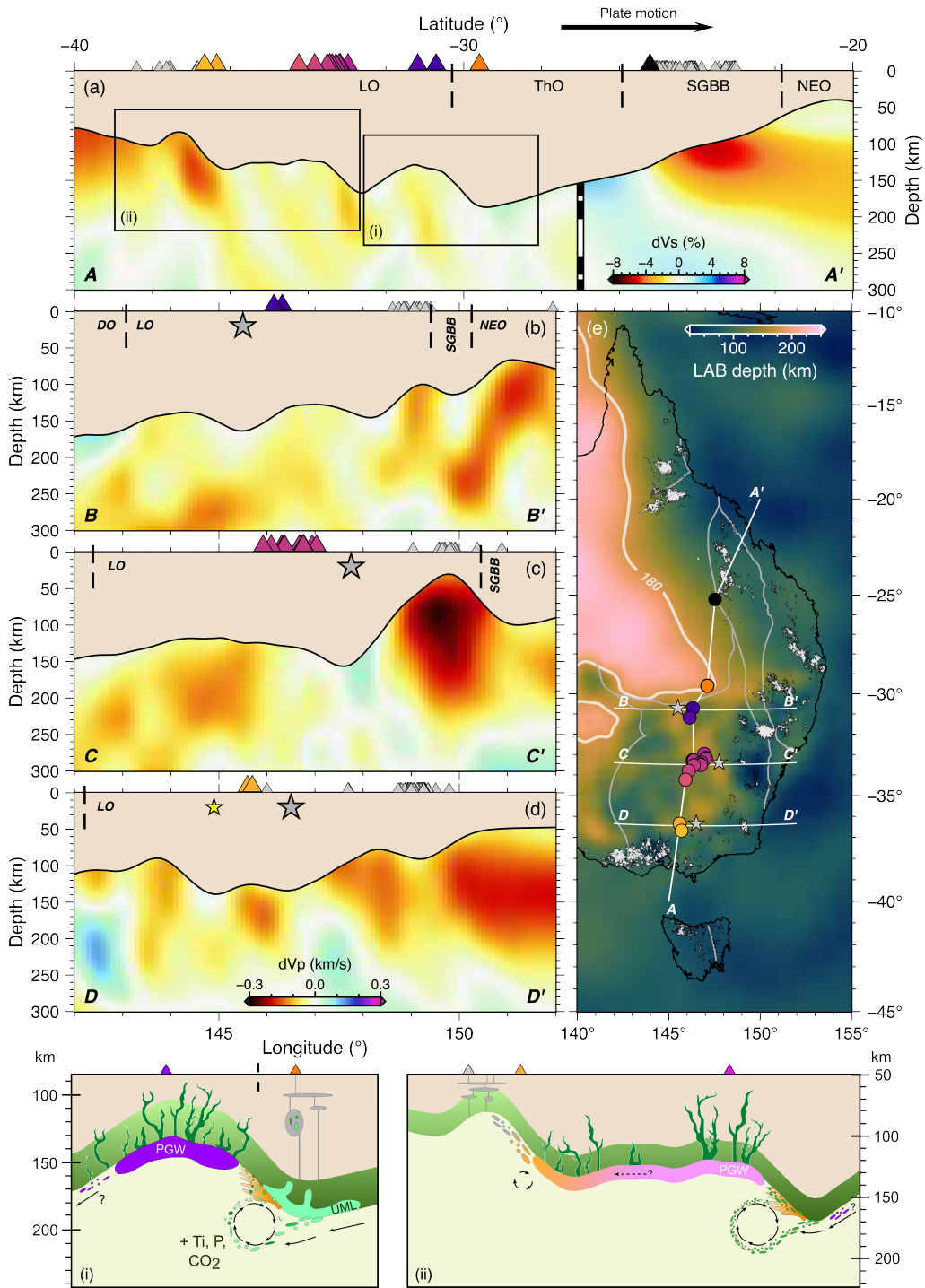


Fig. 12: (Caption next page.)

Fig. 12: LAB depth and seismic tomography profiles (a) along the Cosgrove track, (b) Byrock latitude, (c) through Lake Cargelligo and Tullibigeal, and (d) at Pine lodge with volcano locations projected on each transect. Transect location and direction are indicated in (e) along with the orogenic boundaries, volcanic fields of the EAVP (Shea et al., 2022), and 180 km LAB depth contour that roughly indicates the edge of cratonic Australia (Hoggard et al., 2020). Grey stars (b)–(e) show deepest LAB ridge position under each field noting the position relative to the volcano at the surface; yellow star in (d) shows isolated LAB ridge creating a melt channel beneath Pine Lodge. Insets show a schematic representation of the petro-geodynamic environment under Byrock (i), and Tullibigeal to Pine Lodge (ii). UML = ultra-mafic lamprophyre; PGW = phlogopite-garnet websterite; green gradient above LAB represents degree of metasomatism with cross-cutting veins providing a conduit for melt extraction; black arrows show direction of mantle flow relative to plate motion, and EDC cells. Plumbing systems (grey ellipses) beneath Bokhara River with xenoliths (i) and the Newer Volcanic Province (ii). In (a)–(d) the warm colours represent slow regions while cool colours show fast regions. Tomography sections beneath the EAPS in (a)–(d) come from high-resolution regional data by Rawlinson et al. (2017), while the section in (a) from -27° – -20° is lower resolution global data from de Laat et al. (2023). Volcano colours follow Figure 2, with the exception of Buckland (black) and the broader EAVP basalt (grey) volcanoes.

Secondly, plate motion for the Australian plate is generally northward, which would cause the plume head and any associated lateral mantle flow to be pushed northward, leading to a decoupling of ages between the Tasmantid chain and the broader EAVP and EAPS, which is not the case (Cohen et al., 2013; Crossingham et al., 2017; Mather et al., 2020; McDougall and Wellman, 1976; Seton et al., 2019; Wellman and McDougall, 1974). Thirdly, the stepped nature of the east Australian LAB means that any lateral mantle flow would need to overcome a significant lithospheric keel of >50–100 km to reach the melt source region of the EAPS (Figure 12a–d). Only if the material displaced by a plume were to move significantly far enough westward and able to traverse either down and across the steps, or be caught in a channel within the lithosphere, then there would be a viable case for channelised melt flow style dynamics from the Tasmantid plume. A small remaining thermal anomaly would then be sufficient to trigger adiabatic or reactive melting of a previously metasomatised lithospheric mantle source of the EAPS, similar to EDC or SDU.

The primary lithosphere-asthenosphere boundary architecture in Eastern Australia not only steps progressively deeper east to west, but also steps progressively shallower north to south from roughly beneath the Byrock outcrop of the Tindarey lamproites to the Newer Volcanic province (Figures 1 and 12). In addition, seismic tomography reveals a N–S trending lithospheric ridge coinciding with the locations of the EAPS (grey stars, Figure 12b–d). This creates a unique mantle channel of relatively shallow LAB depths bounded by the thicker lithosphere of cratonic Australia to the west and this ridge to the east. Coupled with plate motion, this LAB morphology would force the upward movement of mantle material; promoting decompression melting directly below the EAPS (Duvernay et al., 2022, 2021). The mechanisms dominating this style of channelised melt flow have been the focus of several recent geodynamic studies (Davies et al., 2015; Rawlinson et al., 2016, 2017; Duvernay et al., 2022, 2021). Through these processes the turbidity created by the deepest portions of

the lithosphere passing over the underlying mantle sucks mantle material upward to fill the depressions behind these steps through shear driven upwelling (Figure 12i-ii). This then induces convecting cells at the edge of the lithospheric steps that couple with the shearing force of the material moving vertically to induce melting of the frozen metasomatised assemblages at the base of the lithosphere (Figure 12i-ii). Melts generated in this way can then either erupt directly or form chemically insulated veins within the lithosphere that aid later melt transport (Foley, 1992b). Another possibility is that these melts accumulate in pools that can fill the stepped depressions entirely or spill out and migrate further southward through the lithospheric channel to shallower steps acting as secondary metasomatic agents (Figure 12b-d). In this scenario, edge-driven convection and shear driven upwelling can explain both age-progressive and non-age progressive volcanism concurrently, while promoting the generation of melts at lower temperatures.

Melting due to subduction-related fluids and metasomatism: It has been suggested that some of the melts within the EAVP have isotopic signatures (i.e. $^{87}\text{Sr}/^{86}\text{Sr}$, ϵNd , Pb) commonly associated with subduction related fluids and melts (Nelson et al., 1986; Nelson, 1992). However, the most recent subduction, during the accretion of the Macquarie Arc in the Lachlan fold belt, ceased ~ 300 million years before the eruption of the EAPS (Fergusson and Henderson, 2015; Glen, 2005). Melting of carbonates accumulated in the transition zone has been suggested as a potential source of these signatures (Mather et al., 2020). As discussed above, our data suggests carbon is present in the source of the EAPS but isolating the source of that carbon is more challenging. Although some experimental work on subducted igneous crust has demonstrated that all carbon should be remobilised before reaching the transition zone (Thomson et al., 2016), this is an area of contention given much of the research has been done on mineralogically simple systems that create simplified melting reactions and phase stability fields. Drawing on the available experiments it is clear that this relationship will depend heavily on the assemblage and subduction geotherm. For example, experiments on a mix of ‘dirty limestone’ (i.e. natural limestone mixed with silicate sediment) show that carbonates infiltrated by chlorine-rich fluids can persist along colder geotherms and resist complete volatilisation (Chen et al., 2023). Even in the absence of significant chlorine, ‘dirty limestone’ assemblages can withstand melting at upper mantle conditions and may persist as a viable carbon reservoir in convergent margins (Chen et al., 2021). Similarly, higher pressure experiments indicate that the maximum upper stability limit for magnesite, and carbonates more broadly, is probably the very top of the lower mantle but would survive to the deep upper mantle (Thomson et al., 2014; Libon et al., 2024). Where hydrous-fluids are present several studies show the mobility of carbon increases, resulting in recycling rates that return only roughly one-third of subducted carbon to the surface (dependant on H_2O flux and depth) (Farsang et al., 2021; Schmidt and Poli, 2003; Van Keken et al., 2011). However, as shown in Figures 10b and 11b, c,

none of the widely used whole-rock geochemical trace element ratios utilising fluid mobile (i.e. Ba) or sediment sourced (i.e. Ba, Th) elements support a definitive subduction, or subduction related aqueous fluid signature in the melts of the EAPS and EAVP. While a strong negative Pb anomaly often associated with fluid loss during subduction-driven magmatism is present in the EAVP basalts (Figure 6c) (Zhang et al., 2001; Shea et al., 2022), this is more or less absent from the EAPS lavas (Figure 6a).

Certainly the EAPS melts require carbon in the source as recorded in $(La/Yb)_N$ vs. Ti/Eu and elevated CO_2 contents of the EAPS relative to other alkaline rocks (Figures 7d and 11a). A more likely source of carbon and subduction-like isotopic ratios than melting originating in the mantle transition zone could come from the melting and assimilation of orogenic accretionary lithologies within the lithosphere. While in the absence of a geologically contemporaneous carbon source, it becomes plausible that any carbon would have been introduced in metasomatic fluids or melts, produced by the melting of accreted lithospheric packages or frozen melts like lamprophyres. This could include modified or partially devolatilised stored sediments locked in the convergent margin before being remelted and reacting with a peridotite to create an ultramafic lamprophyre (Chen et al., 2021; Pintér et al., 2021; Foley et al., 2009). Carbon can exist within the mantle for geologically significant periods of time, evident from calculations of carbon recycling rates (i.e. Farsang et al. (2021)), even under cratonic areas and contributes to a range of processes (Foley, 2008; Foley and Fischer, 2017; Foley et al., 2024). Geochemical evidence from mantle xenoliths and megacrysts reinforces the notion of significant carbon storage in the eastern Australian lithospheric mantle, even in the absence of physical measurements of carbon (Yaxley et al., 1991; Wass and Rogers, 1980; Wass et al., 1980; O'Reilly and Griffin, 1988; Sutherland, 1996; Menzies and Wass, 1983; Robertson et al., 1985; Wass, 1979b), including limited diamond occurrences of unknown origin (*that mostly predate Cenozoic volcanism*) (Sutherland, 2003; Barron et al., 2005; Griffin et al., 1998; Davies et al., 2002). The relative abundance of volatile elements in the EAPS lavas limits the range of potential sources that could be mobilised to contribute to metasomatic change, and eventual melt generation to produce the chemistry observed (Figures 3e and 7a,d). This would be most readily achieved if carbon, water, and phosphorus were stored in ultramafic sinks like redox frozen kimberlitic or lamprophyritic metasomes where hydrous minerals, apatite and carbonates (or diamond) are common crystallites (Foley, 2011; Pintér et al., 2021, 2022; Foley et al., 2009; Rohrbach and Schmidt, 2011; Wass and Rogers, 1980; Wass et al., 1980; O'Reilly and Griffin, 1988; Menzies and Wass, 1983; Barron et al., 1996; Sutherland, 2003; Barron et al., 2005; Irving and Frey, 1984). The probability of either metasome being the host for carbon and other volatile elements is primarily dependent on increased depth, or more precisely pressure, where kimberlites would be more stable at much deeper levels and higher pressure at or in excess of 200 km (≈ 6 GPa) where diamond is likely to be stable (Veter et al., 2017; Jacob, 2004; Pintér

799 et al., 2022). In **Figure 11a** the EAPS are plotted alongside the Mount Webb aillikites (**Figure 1a**) from Sudholz
800 et al. (2023) and likewise occupy the space between pure carbonatite and silicate metasomatism end-members,
801 suggesting the metasomatic agent (or agents) may be intermediate between a silicic and carbonatitic character.
802 Ultramafic lamprophyres and kimberlites encompass this space well, however an ultramafic lamprophyre is more
803 viable as these agents tend to be more stable at shallower depths than kimberlites (Veter et al., 2017; Berkesi
804 et al., 2023). LAB depths in Eastern Australia seldom exceed 150 km (**Figure 1**) which is roughly the source depth
805 of the EAPS, and at these levels lamproitic compositions are suggested to be more sustainable than kimberlitic
806 or lamprophyric melts (Veter et al., 2017). The similarity between the EAPS and the aillikites from Mount Webb
807 as well as the elevated CO₂ contents of the EAPS relative to some lamproites and lamprophyres, despite having
808 undergone degassing, reinforces that an ultramafic lamprophyre is a reasonable metasomatic agent for the EAPS
809 source (**Figures 7d and 11a**).

810 **Architectural control and extension:** Incipient rifting has largely been neglected in the consideration
811 of the geodynamic processes at play within the EAVP, and EAPS more specifically, with very few studies
812 acknowledging the possibility of it having occurred (Sutherland and Barron, 2003; Nelson et al., 1986). Nelson
813 et al. (1986) and Nelson (1992) argue that the isotopic compositions of the EAPS are most similar to potassic
814 and ultrapotassic rocks of the Bufumbira volcanics within the East African Rift; implying a link between source
815 and process in the EAPS and EAR which may be linked to the age-progressive nature of both regions. During the
816 orogenic accretion of the Tasmanides there is evidence of extensional cycles taking place between the majority of
817 the major accretion events. The most well studied are the back-arc rifting observed in rocks from the Cambrian
818 through to the Permian–Triassic with the formation of the Sydney–Gunnedah–Bowen basin that culminated in
819 episodic shortening in the Mid-Permian (Glen, 2005; Fergusson and Henderson, 2015; Champion, 2016). In the
820 areas surrounding the EAPS eruptions dedicated structural geological studies are scarce primarily due to the
821 thick regolith of predominantly Cenozoic sediments that can exceed 700 m thick. Deep seismic lines have been
822 collected in the areas adjacent to Byrock, specifically the Eromanga basin and Nelyambo trough, and to the
823 south of Lake Cargelligo around Rankin Springs (Glen et al., 2013; Doublier et al., 2018; Kennett et al., 2013).
824 The seismic lines carried out near Rankin Springs show clear fault structures that are both shallow and steeply
825 dipping, and occasionally extend to the surface (Kennett et al., 2013). Several rift basins are visible from a range
826 of time periods. The clearest structures proximal to the EAPS are the horst and graben like features created
827 by the Mount Jack fault and the Olepoloko fault (50 km north of Byrock), and the flower structures of the
828 Cobar Rift basin, 160 km west of Byrock (Glen et al., 2013; Doublier et al., 2018). The Olepoloko fault is one of
829 the major faults in the region that extends from the surface to the Moho causing a 9 km offset in Moho depth

and marking the boundary between the Lachlan and Thompson orogens (Doublier et al., 2018). The Cobar Rift basin is interpreted to be Devonian in age while the Olepoloko fault is Late- to Post-Devonian (Doublier et al., 2018). Unless these structures were later reactivated, active extension in this area appears to have ceased in the Paleozoic, although it is noted by Glen et al. (2013) that the southern margin of the Thomson orogen appears to have remained a weak zone at least until the Triassic.

The alkaline mafic character seen in the EAPS and broader EAVP, encompassing both the highly-alkaline, potassic, and more moderately alkali signatures, is comparable to volcanic rocks in well-defined rift systems such as the Rio Grande Rift (RGR), Labrador Sea Rift, and the East African Rift (EAR) (Gibson et al., 1993; Veter et al., 2017). Age progression is another similar characteristic as for both the RGR and EAR the unzipping of the rift results in clear age progressive magmatism (Ebinger et al., 2000; Klöcking et al., 2018; Williams, 1982). Finally, both in the EAVP and the EAR, the melts on the thickest portion of the lithosphere are sourced from the most heavily metasomatised portion of the underlying mantle (Rosenthal et al., 2009; Veter et al., 2017). Linking these together it becomes clearer that the strong architectural control exhibited within rift systems is analogous to the way stepped lithosphere in eastern Australia has been interpreted to induce adiabatic melting of the deepest and most enriched parts of the lithosphere to generate highly alkaline melts. In the absence of active crustal scale tectonic activity though, a more reasonable explanation for these characteristics is post-collisional relaxation leading to localised extension that may in turn trigger intraplate melting. A similar model has been evaluated in detail for the Eastern Mediterranean that shares many of the same geochemical features as the lavas presented here, including a north to south age-progression (Prelević et al., 2010, 2013b, 2012). In their model Prelević et al. (2012) propose a multi-step formation sequence for the western Anatolian lamproites in the eastern Mediterranean that encompasses the ultra-depletion of the mantle before accretion to the lithosphere, then refertilisation by melting of sediments or crustal assemblages (i.e. orogenic delamination), and later upwelling of mantle through a tear in downgoing slabs to initiate melting of the overlying refertilised lithosphere. In the EAPS, several similarities can be drawn to this type of model with a few notable differences. The primary exception to the application of this model to Eastern Australia is the absence of any obvious slab remnant in the upper mantle. However, the lithospheric steps beneath Eastern Australia should essentially function in the same way by creating localised turbidity within the mantle allowing upwelling and decompression melting. Similarly to the Mediterranean occurrences, whole-rock HREE signatures of the EAPS suggest significant depletion is inherent in the source (Figure 6a). The EAPS melts also appear to have been enriched through interaction with a refertilised domain likely generated by the previous melting of an accretionary sequence to create a carbon-rich silicate melt similar to an ultra-mafic lamprophyre (Figures 10b and 11a,b,d).

Therefore, mild extensional stresses due to post-collisional extension could have triggered melting of heavily metasomatised lithosphere, generating channels and deepening the steps in the lithosphere beneath the EAPS. In an intraplate setting absent of active subduction, this would be best characterised as a proto-rift style of magmatism that exploits refertilised conduits containing assemblages rich in hydrous minerals (Figures 10c and 12i,ii), the occurrence of which beneath the EAPS is consistent with magnetotelluric modelling and the implementation of joint inversions of seismic and magnetotelluric data (Kirkby et al., 2020; Manassero et al., 2024). The heterogeneous and disparate nature of these hydrous zones, that likely contain modally high proportions of phlogopite, combined with expected low-volume melts would explain why volcanism is limited to a smaller population of volcanoes. Further, depletion of the source during melt extraction would make remelting more difficult and therefore limit the temporal scope of the volcanism, preventing the EAPS from advancing to a fractionated bimodal style which is present in the EAVP (Crossingham et al., 2018; Shea et al., 2022). The lack of modern and well-developed rift structures coupled with a cessation of volcanism suggests that the extension has stalled, potentially in part due to the freezing of melt conduits and depletion of the mantle source. Nonetheless, a rift could develop in future if existing faults and melt conduits are reactivated and continue eroding the lithosphere base.

In summary, while the precise geodynamic conditions beneath the EAPS are unknown the evidence presented here provides broad constraints. Significant magmatic input from previous subduction is unlikely and any extension has not progressed past a “proto-rift” stage, indicating that post-collisional relaxation has occurred. In the absence of strong evidence for elevated mantle potential temperatures, the most plausible of the remaining options is a combination of edge-driven convection and shear-driven upwelling enhancing channelised melt flow from north to south with no plume input.

Conclusions

We propose that the outcrops formerly known as the NSW Leucitites are lamproites on both a mineralogical and chemical basis (Figure 5). We group these rocks together into the Eastern Australian Potassic Suite (EAPS). The two northernmost exposures of Byrock and El Capitan (Tindarey lamproites) display considerable heteromorphism and are chemically distinct from the remainder of the EAPS due to more significant trace element enrichment (Figures 1b,c, 6a, 10a–d, and 11a,b,d). The central portion of the suite (the Tullibigeal lamproites) are chemically and mineralogically similar to one another. Although the Tullibigeal lamproites are less enriched than the Tindarey lamproites, they are still potassic to ultrapotassic and display the characteristics of lamproites (Figures 1b,d, 10b,d, and 11a,b,d). Based on the published criteria both the Tindarey and Tullibigeal lamproites

resemble cratonic or anorogenic lamproites more closely than orogenic lamproites. Weathering of outcrops south of 34°S has resulted in the alteration of leucite to create analcime, which masks or completely erases the potassic character of these rocks and we do not include them in the lamproite group at this time.

The source of the EAPS requires phlogopite with abundant pyroxene. Magmatic source depths in excess of 2 GPa are also necessary to ensure garnet is in the source, with the titanian affinity (TiO_2 : 3.28–5.33 wt%) of the magmas inherited from oxide minerals (most likely rutile or titanite). Phosphorus and carbon in the source are likely present as apatite and carbonate minerals like magnesite or calcite which are reflected in the mineralogy of the samples as inclusions within phlogopite plates and carbonated melt pools (Lanati et al., in prep.). We suggest that a phlogopite–garnet–websterite is the most likely source for the EAPS melting deeper than ~100 km. This source assemblage must have undergone metasomatism by a carbonatitic or ultramafic lamprophyric melt, likely prior to freezing and remelting, to impart a sufficiently phosphoric, carbonated and titanian mark on the final melt composition (P_2O_5 : 0.65–1.80 wt%; Ti/Eu: 3692–6737; $(\text{La}/\text{Yb})_N$: 24.88–89.66).

The temperatures recorded by our samples suggest low melting temperatures (av: 1244 °C) that are in line with ambient mantle beneath Eastern Australia (1250 °C); a geodynamic environment that lacks extreme heat anomalies (Figure 9). This negates a plume related genesis and reinforces a source prerequisite of a potassium-rich, likely hydrous or volatile bearing (i.e. carbonated/sulfidated), olivine-poor assemblage such as a mica-pyroxenite in the garnet stability field. This is further strengthened by the experiments of Shu et al. (2024, in revision) that generated EAPS-like melts from a similar assemblage. The geodynamic processes most likely to initiate melting in the lithospheric mantle beneath Eastern Australia are a combination of edge-driven convection and shear-driven upwelling with no plume input (Figure 12i–ii). The geodynamic conditions we propose for the generation of the EAPS lavas and their source are common in old stable continental regions with well-established architecture. The chemistry of the EAPS supports a genesis whereby metasomatic episodes of volatile rich fluids or melts have sequentially fertilised the subcontinental lithosphere and lithospheric mantle of Eastern Australia (Figure 12i–ii). These episodes of metasomatism have aided in the destabilisation of the lithospheric mantle to the degree that deep channels have formed and enabled highly-enriched potassic magmatism mimicking the initial stages of rift related magmatism.

Data Availability

All original data collected and presented in this manuscript is available in Lanati and Shea (2025) at the DIGIS Geochemical Data Repository hosted by GFZ Data Services. Literature datasets that underwent filtering to make them comparable to the EAPS lavas are available as compiled or reference values (i.e. primitive mantle etc.)

921 in the referenced papers or as precompiled files from the GEOROC database (<https://georoc.eu/>; versions
922 2023-12-01 or 2024-12-01).

923 Acknowledgments

924 The authors wish to acknowledge and pay our respects to the first nations people of Australia on whose lands
925 the fieldwork and sample collection took place, the Wiradjuri, Wongaibon, Wailwan, and Yorta Yorta peoples.
926 We would also like to thank the communities and landholders for hosting us and allowing us access to outcrops.
927 Peter Weiland is thanked for his assistance and training with whole-rock XRF and trace-element geochemistry.
928 Olivier Alard is thanked for assistance with the CHNS analyses, Luke Milan and the Lapidary laboratory at the
929 University of New England are thanked for their expert petrographic slide preparation. We are also incredibly
930 grateful to Maik Trogisch at the Institute für Mineralogie, University Münster, for his expert (and amazingly
931 quick!) preparation of additional petrographic sections. Andreas Stracke, Felix Genske, and Mischa Böhnke are
932 thanked for multiple constructive discussions around the robustness of metasomatised mantle source indicators
933 and chemical geodynamics more broadly. Colour scales used in this manuscript are from Crameri et al. (2020)
934 to prevent distortion of data and the exclusion of colour-vision impaired readers. The first author wishes to
935 additionally acknowledge the highly collaborative and engaging environment provided by colleagues at the now
936 defunct *Macquarie University Department of Earth and Planetary Sciences, and ARC Centre of Excellence for*
937 *Core to Crust Fluid Systems*; several ideas and themes presented here could not have been developed without
938 their influence and support.

939 Funding

940 Parts of this study were supported by a Geological Society of Australia – Victoria Division Postgraduate
941 Grant, as well as a Macquarie University Postgraduate Research Fund award to AWL. SFF and JJS, and
942 the broader study were supported by funding from an ARC Laureate Fellowship to SFF (FL180100134). JJS
943 acknowledges funding from UKRI NERC grants NE/T012455/1 and NE/V011383/1. MK is supported by the
944 German Research Foundation (DFG grant number KL3162/3-1; 503863705). AWL is funded by a Deutscher
945 Akademischer Austauschdienst (German Research Exchange Service) Research Grant (Grant No. 57507869),
946 and an Australian Government Research Training Program (RTP) Stipend and RTP Fee-Offset Scholarship
947 through Macquarie University (Allocation No. 2018177). This work forms part of the first author's PhD thesis.

Author Contributions

AWL and JJS designed the study in consultation with SFF. AWL, JJS, and SFF undertook fieldwork. AWL and JJS undertook the sample preparation, and powder processing together. AWL completed the petrography (*presented in a forthcoming manuscript*), the majority of the whole rock geochemistry and CHNS analyses, completed all data processing, produced the figures, and wrote the initial manuscript. JJS provided multiple edits to the manuscript and helped streamline discussion points, especially around consistency with the literature of East Australian Volcanism. MK assisted with data compilation, figure making and design, and provided significant input for the discussion. AR provided detailed feedback on figures and several parts of the discussion. SFF, SK, and AR edited the manuscript, acquired funding and supervised this project. This project is part of the broader Eastern Australian Volcanism project within the Earth Evolution group at Macquarie University led by SFF, of which the first authors PhD project is a part. All authors have read and contributed to the reviewing and editing of the final manuscript.

948
949
950
951
952
953
954
955
956
957
958
959

References

- 960 Alard, O., Griffin, W.L., Lorand, J.P., Jackson, S.E., O'Reilly, S.Y., 2000. Non-chondritic distribution of the highly
961 siderophile elements in mantle sulphides. *Nature* 407, 891–894. doi:10.1038/35038049.
- 962 Alard, O., Griffin, W.L., Pearson, N.J., Lorand, J.P., O'Reilly, S.Y., 2002. New insights into the Re-Os systematics of
963 sub-continental lithospheric mantle from in situ analysis of sulphides. *Earth and Planetary Science Letters* 203, 651–663.
964 doi:10.1016/S0012-821X(02)00799-9.
- 965 Alard, O., Halimulati, A., Gorojovsky, L., Wieland, P., 2022. Sulfur Mass Fractions in Thirty-Seven Geological Reference
966 Materials by Titration, XRF and Elemental Analyser . *Geostandards and Geoanalytical Research* , 1–20doi:10.1111/
967 *ggr*.12473.
- 968 Aldanmaz, E., Pearce, J.A., Thirlwall, M.F., Mitchell, J.G., 2000. Petrogenetic evolution of late Cenozoic, post-collision
969 volcanism in western Anatolia, Turkey. *Journal of Volcanology and Geothermal Research* 102, 67–95. doi:10.1016/
970 S0377-0273(00)00182-7.
- 971 Ananuer, H., Alard, O., in prep. C and h concentrations in 32 geo-reference materials measured by elemental and
972 simultaneous thermal analysers.
- 973 Andersen, T., O'Reilly, S.Y., Griffin, W.L., 1984. The trapped fluid phase in upper mantle xenoliths from Victoria,
974 Australia: implications for mantle metasomatism. *Contributions to Mineralogy and Petrology* 88, 72–85. doi:10.1007/
975 BF00371413.
- 976 Aoki, K.I., Shiba, I., 1973. Pargasites in lherzolite and websterite inclusions from itonome-gata, Japan. *The Journal of the*
977 *Japanese Association of Mineralogists, Petrologists and Economic Geologists* 68, 303–310. URL: [http://www.jstage.
978 jst.go.jp/article/ganko1941/68/10/68_10_303/_article](http://www.jstage.jst.go.jp/article/ganko1941/68/10/68_10_303/_article), doi:10.2465/ganko1941.68.303.
- 979 Ball, P.W., Czarnota, K., White, N.J., Klöcking, M., Davies, D.R., 2021. Thermal Structure of Eastern Australia's
980 Upper Mantle and Its Relationship to Cenozoic Volcanic Activity and Dynamic Topography. *Geochemistry, Geophysics,*
981 *Geosystems* 22, 1–31. doi:10.1029/2021gc009717.
- 982 Barron, B.J., Barron, L.M., Duncan, G., 2005. Eclogitic and ultrahigh-pressure crustal garnets and their relationship to
983 Phanerozoic subduction diamonds, Bingara Area, New England fold belt, Eastern Australia. *Economic Geology* 100,
984 1565–1582. doi:10.2113/gsecongeo.100.8.1565.
- 985 Barron, B.J., Sutherland, F.L., Robertson, A.D., 1996. Olivine 'leucites', their xenolith and megacryst suites, Hoskings
986 Peaks, north Queensland. *Australian Journal of Earth Sciences* 43, 231–244. URL: [http://www.tandfonline.com/doi/
987 abs/10.1080/08120099608728251](http://www.tandfonline.com/doi/abs/10.1080/08120099608728251), doi:10.1080/08120099608728251.
- 988 Bergman, S.C., 1987. Lamproites and other potassium-rich igneous rocks: A review of their occurrence, mineralogy and
989 geochemistry. *Geological Society Special Publication* 30, 103–190. doi:10.1144/GSL.SP.1987.030.01.08.
- 990 Berkesi, M., Czuppon, G., Szabó, C., Kovács, I., Ferrero, S., Boiron, M.C., Peiffert, C., 2019. Pargasite in fluid inclusions
991 of mantle xenoliths from northeast Australia (Mt. Quincan): evidence of interaction with asthenospheric fluid. *Chemical*
992 *Geology* 508, 182–196. doi:10.1016/j.chemgeo.2018.06.022.
- 993

- Berkési, M., Myovela, J.L., Yaxley, G.M., Guzmics, T., 2023. Carbonatite formation in continental settings via high pressure – high temperature liquid immiscibility. *Geochimica et Cosmochimica Acta* 349, 41–54. doi:10.1016/j.gca.2023.03.027.
- Birch, W.D., 1976. Mineralogical note the occurrence of a leucite-bearing lava at cosgrove, Victoria. *Journal of the Geological Society of Australia* 23, 435–437. doi:10.1080/00167617608728957.
- Birch, W.D., 1978. Mineralogy and geochemistry of the leucite at cosgrove, Victoria. *Journal of the Geological Society of Australia* 25, 369–385. doi:10.1080/00167617808729047.
- Birch, W.D., 1980. Mineralogy of vesicles in an olivine leucite at Cosgrove, Victoria, Australia. *Mineralogical Magazine* 43, 597–603. doi:10.1180/minmag.1980.043.329.06.
- Blackburn, G., Allison, G., Leaney, F., 1982. Further evidence on the age of tuff at Mt Gambier, South Australia. *Transactions of the Royal Society of South Australia* 106, 163–167.
- Browne, W.R., 1933. Presidential address. An account of post-Palaeozoic igneous activity in N.S.W. *Journal and proceedings of the Royal Society of New South Wales* 67, 1–95. URL: <https://www.biodiversitylibrary.org/part/360074>, doi:10.5962/p.360074.
- Casalini, M., Avanzinelli, R., Tommasini, S., Natali, C., Bianchini, G., Prelević, D., Mattei, M., Conticelli, S., 2022. Petrogenesis of Mediterranean lamproites and associated rocks: The role of overprinted metasomatic events in the post-collisional lithospheric upper mantle. *Geological Society Special Publication* 513, 271–296. doi:10.1144/SP513-2021-36.
- Champion, D., 2016. *Geodynamic Synthesis of the Phanerozoic of eastern Australia. Second Edition. Record 2016/007. 2009.* URL: <http://www.ga.gov.au/metadata-gateway/metadata/record/90096/>.
- Chen, C., Förster, M.W., Foley, S.F., Liu, Y., 2021. Massive carbon storage in convergent margins initiated by subduction of limestone. *Nature Communications* 12. URL: <http://dx.doi.org/10.1038/s41467-021-24750-0>, doi:10.1038/s41467-021-24750-0.
- Chen, C., Förster, M.W., Foley, S.F., Shcheka, S.S., 2023. Carbonate-rich crust subduction drives the deep carbon and chlorine cycles. *Nature* 620, 576–581. doi:10.1038/s41586-023-06211-4.
- Cohen, B.E., Knesel, K.M., Vasconcelos, P.M., Schellart, W.P., 2013. Tracking the Australian plate motion through the Cenozoic: Constraints from $^{40}\text{Ar}/^{39}\text{Ar}$ geochronology. *Tectonics* 32, 1371–1383. doi:10.1002/tect.20084.
- Cohen, B.E., Knesel, K.M., Vasconcelos, P.M., Thiede, D.S., Hergt, J.M., 2008. $^{40}\text{Ar}/^{39}\text{Ar}$ constraints on the timing and origin of Miocene leucite volcanism in southeastern Australia. *Australian Journal of Earth Sciences* 55, 407–418. doi:10.1080/08120090701769514.
- Cohen, B.E., Mark, D.F., Fallon, S.J., Stephenson, P.J., 2017. Holocene-Neogene volcanism in northeastern Australia: Chronology and eruption history. *Quaternary Geochronology* 39, 79–91. URL: <http://dx.doi.org/10.1016/j.quageo.2017.01.003>, doi:10.1016/j.quageo.2017.01.003.
- Coltorti, M., Bonadiman, C., Hinton, R.W., Siena, F., Upton, B.G., 1999. Carbonatite metasomatism of the oceanic upper mantle: Evidence from clinopyroxenes and glasses in ultramafic xenoliths of Grande Comore, Indian Ocean. *Journal of Petrology* 40, 133–165. doi:10.1093/petroj/40.1.133.
- Conceição, R.V., Green, D.H., 2004. Derivation of potassic (shoshonitic) magmas by decompression melting of phlogopite+pargasite lherzolite. *Lithos* 72, 209–229. doi:10.1016/j.lithos.2003.09.003.

- 1030 Condamine, P., Couzinié, S., Fabbrizio, A., Devidal, J.L., Médard, E., 2022. Trace element partitioning during incipient
1031 melting of phlogopite-peridotite in the spinel and garnet stability fields. *Geochimica et Cosmochimica Acta* 327, 53–78.
1032 doi:10.1016/j.gca.2022.04.011.
- 1033 Condamine, P., Médard, E., 2014. Experimental melting of phlogopite-bearing mantle at 1 GPa: Implications for potassic
1034 magmatism. *Earth and Planetary Science Letters* 397, 80–92. URL: <http://dx.doi.org/10.1016/j.epsl.2014.04.027>,
1035 doi:10.1016/j.epsl.2014.04.027.
- 1036 Condamine, P., Médard, E., Devidal, J.L., 2016. Experimental melting of phlogopite-peridotite in the garnet stability field.
1037 *Contributions to Mineralogy and Petrology* 171, 1–26. doi:10.1007/s00410-016-1306-0.
- 1038 Crameri, F., Shephard, G.E., Heron, P.J., 2020. The misuse of colour in science communication. *Nature Communications*
1039 11, 5444. URL: <https://doi.org/10.1038/s41467-020-19160-7>, doi:10.1038/s41467-020-19160-7.
- 1040 Crossingham, T.J., Ubide, T., Vasconcelos, P.M., Mallmann, G., 2018. Parallel plumbing systems feeding a pair of coeval
1041 volcanoes in Eastern Australia. *Journal of Petrology* 59, 1035–1066. doi:10.1093/petrology/egy054.
- 1042 Crossingham, T.J., Vasconcelos, P.M., Cunningham, T., Knesel, K.M., 2017. 40Ar/39Ar geochronology and volume
1043 estimates of the Tasmanid Seamounts: Support for a change in the motion of the Australian plate. *Journal of Volcanology*
1044 and *Geothermal Research* 343, 95–108. URL: <http://dx.doi.org/10.1016/j.jvolgeores.2017.06.014>, doi:10.1016/j.
1045 *jvolgeores.2017.06.014*.
- 1046 Cundari, A., 1973. Petrology of the leucite-bearing lavas in New South Wales. *Journal of the Geological Society*
1047 of Australia 20, 466–492. URL: <http://www.tandfonline.com/doi/abs/10.1080/00167617308728829>, doi:10.1080/
1048 00167617308728829.
- 1049 Cundari, A., Ferguson, A.K., 1982. Significance of the pyroxene chemistry from leucite-bearing and related assemblages.
1050 *TMPM Tschermaks Mineralogische und Petrographische Mitteilungen* 30, 189–204. doi:10.1007/BF01082329.
- 1051 Cundari, A., Renard, J.G., Gleadow, A.J., 1978. Uranium-Potassium relationship and apatite fission-track ages for a
1052 differentiated leucitite suite from New South Wales (Australia). *Chemical Geology* 22, 11–20. URL: [https://www.
1053 sciencedirect.com/science/article/pii/0009254178900177](https://www.sciencedirect.com/science/article/pii/0009254178900177), doi:10.1016/0009-2541(78)90017-7.
- 1054 Cundari, A., Salviulo, G., 1989. Ti solubility in diopsidic pyroxene from a suite of New South Wales leucitites
1055 (Australia). *Lithos* 22, 191–198. URL: <https://www.sciencedirect.com/science/article/pii/0024493789900558>,
1056 doi:10.1016/0024-4937(89)90055-8.
- 1057 Curran, J.M., 1888. Note on a leucite-basalt from central New South Wales. *Proceedings of the Linnean Society of New*
1058 *South Wales*. 2, 974–975. doi:10.5962/bhl.part.29220.
- 1059 Curran, J.M., 1891. A contribution to the microscopic structure of some Australian rocks. *Journal and proceedings*
1060 *of the Royal Society of New South Wales* 25, 179–233. URL: <https://www.biodiversitylibrary.org/part/359111>,
1061 doi:10.5962/p.359111.
- 1062 Dasgupta, R., Hirschmann, M.M., 2006. Melting in the Earth's deep upper mantle caused by carbon dioxide. *Nature* 440,
1063 659–662. doi:10.1038/nature04612.
- 1064 Dasgupta, R., Hirschmann, M.M., Smith, N.D., 2007. Partial melting experiments of peridotite + CO₂ at 3 GPa and
1065 genesis of alkalic ocean island basalts. *Journal of Petrology* 48, 2093–2124. doi:10.1093/petrology/egm053.

- David, T.W.E., Anderson, W., 1889. The Leucite-basalts of N. S. Wales. *Records of the Geological Survey of New South Wales* 1, 153–172. 1066
1067
- Davies, D.R., Rawlinson, N., Iaffaldano, G., Campbell, I.H., 2015. Lithospheric controls on magma composition along Earth's longest continental hotspot track. *Nature* 525, 511–514. URL: <http://www.nature.com/articles/nature14903>, doi:10.1038/nature14903. 1068
1069
1070
- Davies, R.M., O'Reilly, S.Y., Griffin, W.L., 2002. Multiple Origins of Alluvial Diamonds from New South Wales, Australia. *Economic Geology* 97, 109–123. 1071
1072
- Dawson, J.B., 1984. Contrasting types of upper-mantle metasomatism. *Kimberlites II: The Mantle and Crust-Mantle Relationships*, 289–294doi:10.1016/b978-0-444-42274-3.50030-5. 1073
1074
- Dawson, J.B., Smith, J.V., 1973. Alkalic pyroxenite xenoliths from the lashaine volcano, Northern Tanzania. *Journal of Petrology* 14, 113–131. doi:10.1093/petrology/14.1.113. 1075
1076
- Dickinson, W.R., 1975. Potash-Depth (K-h) relations in continental margin and intra-oceanic magmatic arcs. *Geology* 3, 53–56. doi:10.1130/0091-7613(1975)3<53:PKRICM>2.0.CO;2. 1077
1078
- Domanik, K.J., Holloway, J.R., 2000. Experimental synthesis and phase relations of phengitic muscovite from 6.5 to 11 GPa in a calcareous metapelite from the Dabie Mountains, China. *Lithos* 52, 51–77. doi:10.1016/S0024-4937(99)00084-5. 1079
1080
- Doublier, M.P., Purdy, D.J., Hegarty, R., Nicoll, M.G., Zwingmann, H., 2018. Structural elements of the southern Thomson Orogen (Australian Tasmanides): a tale of megafolds. *Australian Journal of Earth Sciences* 65, 943–966. URL: <https://doi.org/10.1080/08120099.2018.1526213>, doi:10.1080/08120099.2018.1526213. 1081
1082
1083
- Duvernay, T., Davies, D.R., Mathews, C.R., Gibson, A.H., Kramer, S.C., 2021. Linking Intraplate Volcanism to Lithospheric Structure and Asthenospheric Flow. *Geochemistry, Geophysics, Geosystems* 22, 1–29. doi:10.1029/2021GC009953. 1084
1085
1086
- Duvernay, T., Davies, D.R., Mathews, C.R., Gibson, A.H., Kramer, S.C., 2022. Continental Magmatism: The Surface Manifestation of Dynamic Interactions Between Cratonic Lithosphere, Mantle Plumes and Edge-Driven Convection. *Geochemistry, Geophysics, Geosystems* 23. doi:10.1029/2022GC010363. 1087
1088
1089
- Ebinger, C.J., Yemane, T., Harding, D.J., Tesfaye, S., Kelley, S., Rex, D.C., 2000. Rift deflection, migration, and propagation: Linkage of the Ethiopian and Eastern rifts, Africa. *Bulletin of the Geological Society of America* 112, 163–176. doi:10.1130/0016-7606(2000)112<163:RDMAPL>2.0.CO;2. 1090
1091
1092
- Edgar, A.D., Lloyd, F.E., Vukadinovic, D., 1994. The role of fluorine in the evolution of ultrapotassic magmas. *Mineralogy and Petrology* 51, 173–193. doi:10.1007/BF01159726. 1093
1094
- Edgar, A.D., Mitchell, R.H., 1997. Ultra high pressure-temperature melting experiments on an SiO₂-rich lamproite from Smoky Butte, Montana: Derivation of siliceous lamproite magmas from enriched sources deep in the Continental Mantle. *Journal of Petrology* 38, 457–477. doi:10.1093/petroj/38.4.457. 1095
1096
1097
- Elkins-Tanton, L.T., Grove, T.L., 2003. Evidence for deep melting of hydrous metasomatized mantle: Pliocene high-potassium magmas from the Sierra Nevadas. *Journal of Geophysical Research: Solid Earth* 108. doi:10.1029/2002jb002168. 1098
1099
1100

- 1101 Elliott, T., Plank, T., Zindler, A., White, W., Bourdon, B., 1997. Element transport from slab to volcanic front at the
1102 Mariana arc. *Journal of Geophysical Research: Solid Earth* 102, 14991–15019. URL: <https://agupubs.onlinelibrary.wiley.com/doi/10.1029/97JB00788>, doi:10.1029/97JB00788.
- 1103
1104 Erlank, A.J., Waters, F.G., Hawkesworth, C.J., Haggerty, S.E., Allsopp, H.L., Rickard, R.S., Menzies, M.A.,
1105 1987. Evidence for mantle metasomatism in peridotite nodules from the Kimberley pipes, South Africa. *Mantle
1106 Metasomatism*, 221–311 URL: [https://www.scopus.com/inward/record.uri?eid=2-s2.0-0023469399&partnerID=40&
1107 md5=8e5113147b2ca27467fa10bea5cf4bd1](https://www.scopus.com/inward/record.uri?eid=2-s2.0-0023469399&partnerID=40&md5=8e5113147b2ca27467fa10bea5cf4bd1).
- 1108 Ersoy, Y.E., Palmer, M.R., Uysal, I., Gündoğan, I., 2014. Geochemistry and petrology of the Early Miocene lamproites
1109 and related volcanic rocks in the Thrace Basin, NW Anatolia. *Journal of Volcanology and Geothermal Research* 283,
1110 143–158. doi:10.1016/j.jvolgeores.2014.06.016.
- 1111 Ewart, A., Chappell, B.W., Menzies, M.A., 1988. An overview of the geochemical and isotopic characteristics of the eastern
1112 Australian Cretaceous volcanic provinces. *Journal of Petrology Special_Vo*, 225–273. doi:10.1093/petrology/Special_
1113 Volume.1.225.
- 1114 Ezad, I.S., Blanks, D.E., Foley, S.F., Holwell, D.A., Bennett, J., Fiorentini, M.L., 2024. Lithospheric hydrous pyroxenites
1115 control localisation and Ni endowment of magmatic sulfide deposits. *Mineralium Deposita* 59, 227–236. URL: <https://doi.org/10.1007/s00126-023-01238-z>, doi:10.1007/s00126-023-01238-z.
- 1116
1117 Ezad, I.S., Foley, S.F., 2022. Experimental partitioning of fluorine and barium in lamproites. *American Mineralogist* 107,
1118 2008–2019. doi:10.2138/am-2022-8289.
- 1119 Falloon, T.J., Green, D.H., 1988. Anhydrous partial melting of peridotite from 8 to 35 kb and the petrogenesis of morb.
1120 *Journal of Petrology Special_Vo*, 379–414. doi:10.1093/petrology/Special_Volume.1.379.
- 1121 Falloon, T.J., Green, D.H., O'Neill, H.S.C., Hibberson, W.O., 1997. Experimental tests of low degree peridotite partial
1122 melt compositions: Implications for the nature of anhydrous near-solidus peridotite melts at 1 GPa. *Earth and Planetary
1123 Science Letters* 152, 149–162. doi:10.1016/s0012-821x(97)00155-6.
- 1124 Farmer, G.L., Glazner, A.F., Manley, C.R., 2002. Did lithospheric delamination trigger late Cenozoic potassic volcanism
1125 in the southern Sierra Nevada, California? *Bulletin of the Geological Society of America* 114, 754–768. doi:10.1130/
1126 0016-7606(2002)114<0754:DLTLC>2.0.CO;2.
- 1127 Farsang, S., Louvel, M., Zhao, C., Mezouar, M., Rosa, A.D., Widmer, R.N., Feng, X., Liu, J., Redfern, S.A., 2021. Deep
1128 carbon cycle constrained by carbonate solubility. *Nature Communications* 12, 1–9. URL: [http://dx.doi.org/10.1038/
1129 s41467-021-24533-7](http://dx.doi.org/10.1038/s41467-021-24533-7), doi:10.1038/s41467-021-24533-7.
- 1130 Fergusson, C.L., Henderson, R.A., 2015. Early Palaeozoic continental growth in the Tasmanides of northeast Gondwana
1131 and its implications for Rodinia assembly and rifting. *Gondwana Research* 28, 933–953. URL: [http://dx.doi.org/10.
1132 1016/j.gr.2015.04.001](http://dx.doi.org/10.1016/j.gr.2015.04.001), doi:10.1016/j.gr.2015.04.001.
- 1133 Foley, S., 1989. The genesis of lamproitic magmas in a reduced fluorine-rich mantle, in: Ross, J., Jaques, A.L., Ferguson,
1134 J., Green, D.H., O'Reilly, S.Y., Danchin, R.V., Janse, A.J.A. (Eds.), *Kimberlites and related rocks, volume 1: their
1135 composition, occurrence, origin and emplacement*. Carlton, Vic, pp. 616–631.

- Foley, S., 1991. High-pressure stability of the fluor- and hydroxy-endmembers of pargasite and K-richterite. *Geochimica et Cosmochimica Acta* 55, 2689–2694. doi:10.1016/0016-7037(91)90386-J. 1136
- Foley, S., 1992a. Petrological characterization of the source components of potassic magmas: geochemical and experimental constraints. *Lithos* 28, 187–204. URL: <https://linkinghub.elsevier.com/retrieve/pii/002449379290006K>, doi:10.1016/0024-4937(92)90006-K. 1138
- Foley, S., 1992b. Vein-plus-wall-rock melting mechanisms in the lithosphere and the origin of potassic alkaline magmas. *Lithos* 28, 435–453. doi:10.1016/0024-4937(92)90018-T. 1141
- Foley, S., Peccerillo, A., 1992. Potassic and ultrapotassic magmas and their origin. *Lithos* 28, 181–185. URL: <https://linkinghub.elsevier.com/retrieve/pii/002449379290005J>, doi:10.1016/0024-4937(92)90005-J. 1143
- Foley, S., Venturelli, G., Green, D., Toscani, L., 1987. The ultrapotassic rocks: Characteristics, classification, and constraints for petrogenetic models. *Earth-Science Reviews* 24, 81–134. URL: <https://linkinghub.elsevier.com/retrieve/pii/0012825287900018>, doi:10.1016/0012-8252(87)90001-8. 1145
- Foley, S.F., 1993. An experimental study of olivine lamproite: First results from the diamond stability field. *Geochimica et Cosmochimica Acta* 57, 483–489. doi:10.1016/0016-7037(93)90448-6. 1148
- Foley, S.F., 2008. Rejuvenation and erosion of the cratonic lithosphere. *Nature Geoscience* 1, 503–510. doi:10.1038/ngeo261. 1150
- Foley, S.F., 2011. A reappraisal of redox melting in the earth's mantle as a function of tectonic setting and time. *Journal of Petrology* 52, 1363–1391. doi:10.1093/petrology/egq061. 1151
- Foley, S.F., Chen, C., Jacob, D.E., 2024. The effects of local variations in conditions on carbon storage and release in the continental mantle. *National Science Review* 11. URL: <https://doi.org/10.1093/nsr/nwae098>, doi:10.1093/nsr/nwae098. 1153
- Foley, S.F., Ezad, I.S., 2024. Melting of hydrous pyroxenites with alkali amphiboles in the continental mantle: 2. Trace element compositions of melts and minerals. *Geoscience Frontiers* 15, 101692. URL: <https://doi.org/10.1016/j.gsf.2023.101692>, doi:10.1016/j.gsf.2023.101692. 1154
- Foley, S.F., Ezad, I.S., van der Laan, S.R., Pertermann, M., 2022. Melting of hydrous pyroxenites with alkali amphiboles in the continental mantle: 1. Melting relations and major element compositions of melts. *Geoscience Frontiers* 13, 101380. URL: <https://doi.org/10.1016/j.gsf.2022.101380>, doi:10.1016/j.gsf.2022.101380. 1155
- Foley, S.F., Ezad, I.S., Shu, C., Förster, M.W., 2025. Melting of amphibole-apatite-rich metasomes in the continental mantle and comparison of melt compositions with natural igneous rocks. *Lithos* , 107976 URL: <https://doi.org/10.1016/j.lithos.2025.107976><https://linkinghub.elsevier.com/retrieve/pii/S0024493725000350>, doi:10.1016/j.lithos.2025.107976. 1156
- Foley, S.F., Fischer, T.P., 2017. An essential role for continental rifts and lithosphere in the deep carbon cycle. *Nature Geoscience* 10, 897–902. URL: <http://dx.doi.org/10.1038/s41561-017-0002-7>, doi:10.1038/s41561-017-0002-7. 1157
- Foley, S.F., Pertermann, M., 2021. Dynamic metasomatism experiments investigating the interaction between migrating potassic melt and garnet peridotite. *Geosciences (Switzerland)* 11. doi:10.3390/geosciences11100432. 1158
- Foley, S.F., Pintér, Z., 2018. Primary Melt Compositions in the Earth's Mantle, in: Kono, Y., Sanloup, C. (Eds.), *Magmas Under Pressure*. Elsevier, Amsterdam. chapter 1, pp. 3–42. doi:10.1016/B978-0-12-811301-1.00001-0. 1159

- 1172 Foley, S.F., Yaxley, G.M., Rosenthal, A., Buhre, S., Kiseeva, E.S., Rapp, R.P., Jacob, D.E., 2009. The composition of
1173 near-solidus melts of peridotite in the presence of CO₂ and H₂O between 40 and 60 kbar. *Lithos* 112, 274–283. URL:
1174 <http://dx.doi.org/10.1016/j.lithos.2009.03.020>, doi:10.1016/j.lithos.2009.03.020.
- 1175 Förster, M.W., Bussweiler, Y., Prelević, D., Daczko, N.R., Buhre, S., Mertz-Kraus, R., Foley, S.F., 2021. Sediment-
1176 Peridotite Reaction Controls Fore-Arc Metasomatism and Arc Magma Geochemical Signatures. *Geosciences* 11, 372.
1177 URL: <https://www.mdpi.com/2076-3263/11/9/372>, doi:10.3390/geosciences11090372.
- 1178 Förster, M.W., Prelević, D., Buhre, S., Mertz-Kraus, R., Foley, S.F., 2019. An experimental study of the role of partial
1179 melts of sediments versus mantle melts in the sources of potassic magmatism. *Journal of Asian Earth Sciences* 177, 76–88.
1180 URL: <https://linkinghub.elsevier.com/retrieve/pii/S1367912019301270>, doi:10.1016/j.jseaes.2019.03.014.
- 1181 Frey, F.A., Green, D.H., 1974. The mineralogy, geochemistry and origin of Iherzolite inclusions in Victorian basanites.
1182 *Geochimica et Cosmochimica Acta* 38, 1023–1059. doi:10.1016/0016-7037(74)90003-9.
- 1183 Frey, F.A., Green, D.H., Roy, S.D., 1978. Integrated models of basalt petrogenesis: A study of quartz tholeiites to olivine
1184 melilitites from South Eastern Australia utilizing geochemical and experimental petrological data. *Journal of Petrology*
1185 19, 463–513. doi:10.1093/petrology/19.3.463.
- 1186 Fritschle, T., Prelević, D., Foley, S.F., Jacob, D.E., 2013. Petrological characterization of the mantle source of Mediterranean
1187 lamproites: Indications from major and trace elements of phlogopite. *Chemical Geology* 353, 267–279. doi:10.1016/j.
1188 *chemgeo*.2012.09.006.
- 1189 Funk, S.P., Luth, R.W., 2013. Melting phase relations of a mica-clinopyroxenite from the Milk River area, southern Alberta,
1190 Canada. *Contributions to Mineralogy and Petrology* 166, 393–409. doi:10.1007/s00410-013-0881-6.
- 1191 Gale, A., Dalton, C.A., Langmuir, C.H., Su, Y., Schilling, J.G., 2013. The mean composition of ocean ridge basalts.
1192 *Geochemistry, Geophysics, Geosystems* 14, 489–518. doi:10.1029/2012GC004334.
- 1193 Gaul, O.F., Griffin, W.L., O'Reilly, S.Y., Pearson, N.J., 2000. Mapping olivine composition in the lithospheric mantle.
1194 *Earth and Planetary Science Letters* 182, 223–235. URL: [http://www.sciencedirect.com/science/article/pii/](http://www.sciencedirect.com/science/article/pii/S0012821X00002430)
1195 [S0012821X00002430](http://dx.doi.org/10.1016/S0012-821X(00)00243-0), doi:[http://dx.doi.org/10.1016/S0012-821X\(00\)00243-0](http://dx.doi.org/10.1016/S0012-821X(00)00243-0).
- 1196 Gaul, O.F., O'Reilly, S.Y., Griffin, W.L., 2003. Lithosphere structure and evolution in southeastern Australia. *Special*
1197 *Paper of the Geological Society of America* 372, 185–202. doi:10.1130/0-8137-2372-8.185.
- 1198 Ghent, E.D., Edwards, B.R., Russell, J.K., 2019. Pargasite-bearing vein in spinel Iherzolite from the mantlelithosphere of
1199 the North America cordillera. *Canadian Journal of Earth Sciences* 56, 870–885. doi:10.1139/cjes-2018-0239.
- 1200 Gibson, S.A., Thompson, R.N., Leat, P.T., Morrison, M.A., Hendry, G.L., Dickin, A.P., Mitchell, J.G., 1993. Ultrapotassic
1201 magmas along the flanks of the oligo-miocene rio grande rift, USA: Monitors of the zone of lithospheric mantle extension
1202 and thinning beneath a continental rift. *Journal of Petrology* 34, 187–228. doi:10.1093/petrology/34.1.187.
- 1203 Glen, R.A., 2005. The Tasmanides of eastern Australia. Geological Society, London, Special Publications 246, 23–96. URL:
1204 <http://sp.lyellcollection.org/lookup/doi/10.1144/GSL.SP.2005.246.01.02>, doi:10.1144/GSL.SP.2005.246.01.02.
- 1205 Glen, R.A., Belousova, E., Griffin, W.L., 2016. Different styles of modern and ancient non-collisional Orogens and
1206 implications for crustal growth: A Gondwanaland perspective. *Canadian Journal of Earth Sciences* 53, 1372–1415.
1207 doi:10.1139/cjes-2015-0229.

- Glen, R.A., Korsch, R.J., Hegarty, R., Saeed, A., Djomani, Y.P., Costelloe, R.D., Belousova, E., 2013. Geodynamic significance of the boundary between the Thomson Orogen and the Lachlan Orogen, northwestern New South Wales and implications for Tasmanide tectonics. *Australian Journal of Earth Sciences* 60, 371–412. doi:10.1080/08120099.2013.782899.
- Green, D.H., 2015. Experimental petrology of peridotites, including effects of water and carbon on melting in the Earth's upper mantle. *Physics and Chemistry of Minerals* 42, 95–122. URL: <https://doi.org/10.1007/s00269-014-0729-2>, doi:10.1007/s00269-014-0729-2.
- Green, D.H., Hibberson, W.O., Rosenthal, A., Kovács, I., Yaxley, G.M., Falloon, T., Brink, F., 2014. Experimental study of the influence of water on melting and phase assemblages in the upper mantle. *Journal of Petrology* 55, 2067–2096. doi:10.1093/petrology/egu050.
- Griffin, W.L., O'Reilly, S.Y., Davies, R.M., 1998. Subduction-Related Diamond Deposits? Constraints, Possibilities, and New Data from Eastern Australia, in: Vokes, F.M., Marshall, B., Spry, P.G. (Eds.), *Metamorphic and Metamorphogenic Ore Deposits*. Society of Economic Geologists. January, pp. 1–20. URL: <http://pubs.geoscienceworld.org/books/book/1221/chapter/107021009/SubductionRelated-Diamond-Deposits-Constraints>, doi:10.5382/Rev.11.13.
- Griffin, W.L., Sutherland, F.L., Hollis, J.D., 1987. Geothermal profile and crust-mantle transition beneath east-central Queensland: Volcanology, xenolith petrology and seismic data. *Journal of Volcanology and Geothermal Research* 31, 177–203. doi:10.1016/0377-0273(87)90067-9.
- Griffin, W.L., Wass, S.Y., Hollis, J.D., 1984. Ultramafic Xenoliths from Bullenmerri and Gnotuk Maars, Victoria, Australia: Petrology of a Sub-Continental Crust-Mantle Transition. *Journal of Petrology* 25, 53–87. URL: <http://petrology.oxfordjournals.org/>, doi:10.1093/petrology/25.1.53.
- Gupta, A.K., Fyfe, W.S., 1975. Leucite survival; the alteration to analcime. *The Canadian Mineralogist* 13, 361–363.
- Harlow, G.E., 2003. Diopside + F-rich phlogopite at high P and T: Systematics, crystal chemistry and the stability of KMgF₃, clinohumite and chondrodite. *American Mineralogist* 88, 1625.
- Harlow, G.E., Davies, R., 2004. Status report on stability of K-rich phases at mantle conditions. *Lithos* 77, 647–653. doi:10.1016/j.lithos.2004.04.010.
- Harte, B., 1983. Mantle peridotites and processes - the kimberlite sample. *Continental Basalts and Mantle Xenoliths*, 46–91.
- Harvey, M.H., Joplin, G.A., 1940. A note on some leucite bearing rocks from New South Wales with special reference to an ultrabasic occurrence at Murrumburrah. *Journal and proceedings of the Royal Society of New South Wales* 74, 419–441. URL: <https://www.biodiversitylibrary.org/pdf4/100904400174258.pdf>.
- Hauri, E.H., Maclennan, J., McKenzie, D., Gronvold, K., Oskarsson, N., Shimizu, N., 2018. CO₂ content beneath northern Iceland and the variability of mantle carbon. *Geology* 46, 55–58. doi:10.1130/G39413.1.
- Heath, M., Phillips, D., Matchan, E.L., 2018. An evidence-based approach to accurate interpretation of ⁴⁰Ar/³⁹Ar ages from basaltic rocks. *Earth and Planetary Science Letters* 498, 65–76. doi:10.1016/j.epsl.2018.06.024.
- Heath, M., Phillips, D., Matchan, E.L., 2020. Basalt lava flows of the intraplate Newer Volcanic Province in south-east Australia (Melbourne region): ⁴⁰Ar/³⁹Ar geochronology reveals ~8 Ma of episodic activity. *Journal of Volcanology and*

- 1244 Geothermal Research 389. doi:10.1016/j.jvolgeores.2019.106730.
- 1245 Herzberg, C., 2011. Identification of source lithology in the Hawaiian and Canary Islands: Implications for origins. *Journal*
1246 *of Petrology* 52, 113–146. doi:10.1093/petrology/egq075.
- 1247 Herzberg, C., Asimow, P.D., 2008. Petrology of some oceanic island basalts: PRIMELT2.XLS software for primary magma
1248 calculation. *Geochemistry, Geophysics, Geosystems* 9. doi:10.1029/2008GC002057.
- 1249 Hirose, K., 1997. Partial melt compositions of carbonated peridotite at 3 GPa and role of CO₂ in alkali-basalt magma
1250 generation. *Geophysical Research Letters* 24, 2837–2840. doi:10.1029/97GL02956.
- 1251 Hirose, K., Kushiro, I., 1993. Partial melting of dry peridotites at high pressures: Determination of compositions of
1252 melts segregated from peridotite using aggregates of diamond. *Earth and Planetary Science Letters* 114, 477–489.
1253 doi:10.1016/0012-821X(93)90077-M.
- 1254 Hirschmann, M.M., Kogiso, T., Baker, M.B., Stolper, E.M., 2003. Alkalic magmas generated by partial melting of garnet
1255 pyroxenite. *Geology* 31, 481–484. doi:10.1130/0091-7613(2003)031<0481:AMGBPM>2.0.CO;2.
- 1256 Hofmann, A.W., Jochum, K.P., Seufert, M., White, W.M., 1986. Nb and Pb in oceanic basalts: new constraints on mantle
1257 evolution. *Earth and Planetary Science Letters* 79, 33–45. doi:10.1016/0012-821X(86)90038-5.
- 1258 Hoggard, M.J., Czarnota, K., Richards, F.D., Huston, D.L., Jaques, A.L., Ghelichkhan, S., 2020. Global distribution of
1259 sediment-hosted metals controlled by craton edge stability. *Nature Geoscience* 13, 504–510. URL: [http://dx.doi.org/](http://dx.doi.org/10.1038/s41561-020-0593-2)
1260 [10.1038/s41561-020-0593-2](http://dx.doi.org/10.1038/s41561-020-0593-2), doi:10.1038/s41561-020-0593-2.
- 1261 Hough, F.E., 1972. The petrogenesis of strongly alkaline mafic lavas and associated nodule suites from the West Eifel and
1262 south west Uganda. Ph.D. thesis. University of Reading.
- 1263 Innocenzi, F., Ronca, S., Agostini, S., Benedetti, F., Lustrino, M., 2024. On the occurrence of kalsilite in melilite-
1264 bearing ultrapotassic lavas from the Roman Province (Vulsini Mts., central Italy). *Lithos* 482-483, 107704. URL:
1265 <https://doi.org/10.1016/j.lithos.2024.107704>, doi:10.1016/j.lithos.2024.107704.
- 1266 Irving, A.J., 1974. Geochemical and high pressure experimental studies of garnet pyroxenite and pyroxene granulite
1267 xenoliths from the delegate basaltic pipes, Australia. *Journal of Petrology* 15, 1–40. doi:10.1093/petrology/15.1.1.
- 1268 Irving, A.J., Frey, F.A., 1984. Trace element abundances in megacrysts and their host basalts: Constraints on partition
1269 coefficients and megacryst genesis. *Geochimica et Cosmochimica Acta* 48, 1201–1221. doi:10.1016/0016-7037(84)
1270 90056-5.
- 1271 Ishimaru, S., Arai, S., 2008. Calcic amphiboles in peridotite xenoliths from Avacha volcano, Kamchatka, and their
1272 implications for metasomatic conditions in the mantle wedge. *Geological Society Special Publication* 293, 35–55. doi:10.
1273 1144/SP293.3.
- 1274 Ito, M., 1986. Kimberlites and their ultramafic xenoliths from western Kenya. *TMPM Tschermaks Mineralogische und*
1275 *Petrographische Mitteilungen* 35, 193–216. doi:10.1007/BF01082085.
- 1276 Jacob, D., 2004. Nature and origin of eclogite xenoliths from kimberlites. *Lithos* 77, 295–316. URL: [https://linkinghub.](https://linkinghub.elsevier.com/retrieve/pii/S0024493704001045)
1277 [elsevier.com/retrieve/pii/S0024493704001045](https://linkinghub.elsevier.com/retrieve/pii/S0024493704001045), doi:10.1016/j.lithos.2004.03.038.
- 1278 Jacob, D.E., Viljoen, K.S., Grassineau, N.V., 2009. Eclogite xenoliths from Kimberley, South Africa - A case study of
1279 mantle metasomatism in eclogites. *Lithos* 112, 1002–1013. URL: <http://dx.doi.org/10.1016/j.lithos.2009.03.034>,

- doi:10.1016/j.lithos.2009.03.034. 1280
- Jaques, A.L., 2002. Australian diamond deposits, kimberlites, and related rocks. 1: 5 000 000 scale map. URL: <https://www.ga.gov.au/pdf/RR0114.pdf>. 1281
- Jia, Y., Kerrich, R., Gupta, A.K., Fyfe, W.S., 2003. 15N-enriched Gondwana lamproites, eastern India: Crustal N in the 1283
mantle source. *Earth and Planetary Science Letters* 215, 43–56. doi:10.1016/S0012-821X(03)00426-6. 1284
- Jochum, K.P., Nohl, U., Herwig, K., Lammel, E., Stoll, B., Hofmann, A.W., 2005. GeoReM: A new geochemical database 1285
for reference materials and isotopic standards. *Geostandards and Geoanalytical Research* 29, 333–338. doi:10.1111/j. 1286
1751-908x.2005.tb00904.x. 1287
- Johnson, B., Goldblatt, C., 2015. The nitrogen budget of Earth. *Earth-Science Reviews* 148, 150–173. URL: <http://dx.doi.org/10.1016/j.earscirev.2015.05.006>, doi:10.1016/j.earscirev.2015.05.006, arXiv:1505.03813. 1288
1289
- Judd, J.W., 1887. On the Discovery of Leucite in Australia. *Mineralogical Magazine and Journal of the Mineralogical* 1290
Society 7, 194–195. URL: <https://www.cambridge.org/core/product/AD6A8061FFF8A3882C0B31DD671B657B>, doi:DOI: 1291
10.1180/minmag.1887.007.35.06. 1292
- Katz, R.F., Spiegelman, M., Langmuir, C.H., 2003. A new parameterization of hydrous mantle melting. *Geochemistry,* 1293
Geophysics, Geosystems 4, 1–19. doi:10.1029/2002GC000433. 1294
- Kennett, B., Saygin, E., Fomin, T., Blewett, R.S., 2013. Deep crustal seismic reflection profiling, Australia: 1976-2011. 2nd 1295
ed., Australian National University Press, Acton. 1296
- Kirkby, A.L., Musgrave, R.J., Czarnota, K., Doublier, M.P., Duan, J., Cayley, R.A., Kyi, D., 2020. Lithospheric architecture 1297
of a Phanerozoic orogen from magnetotellurics: AusLAMP in the Tasmanides, southeast Australia. *Tectonophysics* 793, 1298
228560. URL: <https://doi.org/10.1016/j.tecto.2020.228560>, doi:10.1016/j.tecto.2020.228560. 1299
- Klemme, S., van der Laan, S., Foley, S., Günther, D., 1995. Experimentally determined trace and minor element partitioning 1300
between clinopyroxene and carbonatite melt under upper mantle conditions. *Earth and Planetary Science Letters* 1301
133, 439–448. URL: <https://linkinghub.elsevier.com/retrieve/pii/0012821X9500098W>, doi:10.1016/0012-821X(95) 1302
00098-W. 1303
- Klöcking, M., White, N.J., Maclennan, J., McKenzie, D., Fitton, J.G., 2018. Quantitative Relationships Between Basalt 1304
Geochemistry, Shear Wave Velocity, and Asthenospheric Temperature Beneath Western North America. *Geochemistry,* 1305
Geophysics, Geosystems 19, 3376–3404. doi:10.1029/2018GC007559. 1306
- Kogiso, T., Hirschmann, M.M., Frost, D.J., 2003. High-pressure partial melting of garnet pyroxenite: Possible mafic 1307
lithologies in the source of ocean island basalts. *Earth and Planetary Science Letters* 216, 603–617. doi:10.1016/ 1308
S0012-821X(03)00538-7. 1309
- Konzett, J., 1997. Phase relations and chemistry of Ti-rich K-richterite-bearing mantle assemblages: an experimental 1310
study to 8.0 GPa in a Ti-KNCMASH system. *Contributions to Mineralogy and Petrology* 128, 385–404. doi:10.1007/ 1311
s004100050316. 1312
- Konzett, J., Fei, Y., 2000. Transport and storage of potassium in the earth's upper mantle and transition zone: An 1313
experimental study to 23 GPa in simplified and natural bulk compositions. *Journal of Petrology* 41, 583–603. doi:10. 1314
1093/petrology/41.4.583. 1315

- 1316 Konzett, J., Sweeney, R.J., Thompson, A.B., Ulmer, P., 1997. Potassium amphibole stability in the upper mantle: An
1317 experimental study in a peralkaline KNCMASH system to 8.5 GPa. *Journal of Petrology* 38, 537–568. doi:10.1093/
1318 *petroj/38.5.537*.
- 1319 Konzett, J., Ulmer, P., 1999. The stability of hydrous potassic phases in lherzolitic mantle—An experimental study to 9.5
1320 GPa in simplified and natural bulk compositions. *Journal of Petrology* 40, 629–652. doi:10.1093/*petroj/40.4.629*.
- 1321 de Laat, J.I., Lebedev, S., Celli, N.L., Bonadio, R., Chagas de Melo, B., Rawlinson, N., 2023. Structure and evolution
1322 of the Australian plate and underlying upper mantle from waveform tomography with massive data sets. *Geophysical*
1323 *Journal International* 234, 153–189. URL: <https://doi.org/10.1093/gji/ggad062>, doi:10.1093/gji/ggad062.
- 1324 Lambart, S., Laporte, D., Provost, A., Schiano, P., 2012. Fate of pyroxenite-derived melts in the peridotitic mantle:
1325 Thermodynamic and experimental constraints. *Journal of Petrology* 53, 451–476. doi:10.1093/*petrology/egr068*.
- 1326 Lambart, S., Laporte, D., Schiano, P., 2009. An experimental study of pyroxenite partial melts at 1 and 1.5 GPa:
1327 Implications for the major-element composition of Mid-Ocean Ridge Basalts. *Earth and Planetary Science Letters* 288,
1328 335–347. URL: <http://dx.doi.org/10.1016/j.epsl.2009.09.038>, doi:10.1016/j.epsl.2009.09.038.
- 1329 Lambart, S., Laporte, D., Schiano, P., 2013. Markers of the pyroxenite contribution in the major-element compositions of
1330 oceanic basalts: Review of the experimental constraints. *Lithos* 160–161, 14–36. URL: <http://dx.doi.org/10.1016/j.lithos.2012.11.018>,
1331 doi:10.1016/j.lithos.2012.11.018.
- 1332 Lanati, A.W., Shea, J.J., 2022. Chemical analyses of the Eastern Australian Potassic Suite: Whole-rock major and trace
1333 element geochemistry including loss on ignition. URL: <https://doi.org/10.25625/AB5PLG>, doi:10.25625/AB5PLG.
- 1334 Lanati, A.W., Shea, J.J., 2025. Chemical analyses of the Eastern Australian Potassic Suite: Whole-rock major, trace, and
1335 volatile element geochemistry. doi:<https://doi.org/10.5880/digis.2025.005>.
- 1336 Lanati, A.W., Shea, J.J., Foley, S.F., Klöcking, M.S., Rohrbach, A., Gerdes-Berndt, J., Klemme, S., in prep. The petrology,
1337 geochemistry, & origin of the east australian potassic suite: The minerals.
- 1338 Le Bas, M.J., 1989. Nephelinitic and basanitic rocks. *Journal of Petrology* 30, 1299–1312. doi:10.1093/*petrology/30.5*.
1339 1299.
- 1340 Le Bas, M.J., Streckeisen, A.L., 1991. The IUGS systematics of igneous rocks. *Journal of the Geological Society*
1341 148, 825–833. URL: <http://jgs.lyellcollection.org/content/148/5/825.short>[http://jgs.lyellcollection.org/
1342 cgi/doi/10.1144/gsjgs.148.5.0825](http://jgs.lyellcollection.org/cgi/doi/10.1144/gsjgs.148.5.0825), doi:10.1144/gsjgs.148.5.0825.
- 1343 Le Maitre, R.W., Streckeisen, A., Zanettin, B., Le Bas, M.J., Bonin, B., Bateman, P. (Eds.), 2002. *Igneous Rocks: A*
1344 *Classification and Glossary of Terms: Recommendations of the International Union of Geological Sciences Subcommission*
1345 *on the Systematics of Igneous Rocks*. 2 ed., Cambridge University Press, Cambridge. URL: [https://www.cambridge.
1346 org/core/product/7F458E82BF81BF6A011CEA0D41DE9311](https://www.cambridge.org/core/product/7F458E82BF81BF6A011CEA0D41DE9311), doi:DOI:10.1017/CB09780511535581.
- 1347 Lee, C.T.A., Cheng, X., Horodyskyj, U., 2006. The development and refinement of continental arcs by primary basaltic
1348 magmatism, garnet pyroxenite accumulation, basaltic recharge and delamination: Insights from the Sierra Nevada,
1349 California. *Contributions to Mineralogy and Petrology* 151, 222–242. URL: [https://link.springer.com/article/10.
1350 1007/s00410-005-0056-1](https://link.springer.com/article/10.1007/s00410-005-0056-1), doi:10.1007/s00410-005-0056-1.

- Lee, C.T.A., Luffi, P., Plank, T., Dalton, H., Leeman, W.P., 2009. Constraints on the depths and temperatures of basaltic magma generation on Earth and other terrestrial planets using new thermobarometers for mafic magmas. *Earth and Planetary Science Letters* 279, 20–33. doi:10.1016/j.epsl.2008.12.020.
- Libon, L., Spiekermann, G., Blanchard, I., Kaa, J.M., Dominijanni, S., Sieber, M.J., Förster, M., Albers, C., Morgenroth, W., McCammon, C., Schreiber, A., Roddatis, V., Glazyrin, K., Husband, R.J., Hennet, L., Appel, K., Wilke, M., 2024. Reevaluating the fate of subducted magnesite in the Earth's lower mantle. *Physics of the Earth and Planetary Interiors* 355. doi:10.1016/j.pepi.2024.107238.
- Liu, Z., Shea, J.J., Foley, S.F., Bussweiler, Y., Rohrbach, A., Klemme, S., Berndt, J., 2021. Clarifying source assemblages and metasomatic agents for basaltic rocks in eastern Australia using olivine phenocryst compositions. *Lithos* 390-391, 106122. URL: <https://doi.org/10.1016/j.lithos.2021.106122>, doi:10.1016/j.lithos.2021.106122.
- Lloyd, F.E., Arima, M., Edgar, A.D., 1985. Partial melting of a phlogopite-clinopyroxenite nodule from south-west Uganda: an experimental study bearing on the origin of highly potassic continental rift volcanics. *Contributions to Mineralogy and Petrology* 91, 321–329. doi:10.1007/BF00374688.
- Lloyd, F.E., Bailey, D.K., 1975. Light element metasomatism of the continental mantle: The evidence and the consequences. *Physics and Chemistry of the Earth* 9, 389–416. doi:10.1016/0079-1946(75)90030-0.
- Lustrino, M., Fedele, L., Agostini, S., Prelević, D., Salari, G., 2019. Leucitites within and around the Mediterranean area. *Lithos* 324-325, 216–233. doi:10.1016/j.lithos.2018.11.007.
- Lustrino, M., Wilson, M., 2007. The circum-Mediterranean anorogenic Cenozoic igneous province. *Earth-Science Reviews* 81, 1–65. doi:10.1016/j.earscirev.2006.09.002.
- Luth, R.W., 1997. Experimental study of the system phlogopite-diopside from 3.5 to 17 GPa. *American Mineralogist* 82, 1198–1209. doi:10.2138/am-1997-11-1216.
- Mallik, A., Dasgupta, R., Tsuno, K., Nelson, J., 2016. Effects of water, depth and temperature on partial melting of mantle-wedge fluxed by hydrous sediment-melt in subduction zones. *Geochimica et Cosmochimica Acta* 195, 226–243. URL: <http://dx.doi.org/10.1016/j.gca.2016.08.018>, doi:10.1016/j.gca.2016.08.018.
- Mallik, A., Nelson, J., Dasgupta, R., 2015. Partial melting of fertile peridotite fluxed by hydrous rhyolitic melt at 2–3 GPa: implications for mantle wedge hybridization by sediment melt and generation of ultrapotassic magmas in convergent margins. *Contributions to Mineralogy and Petrology* 169. doi:10.1007/s00410-015-1139-2.
- Manassero, M.C., Özaydın, S., Afonso, J.C., Shea, J.J., Ezad, I.S., Kirkby, A., Thiel, S., Fomin, I., Czarnota, K., 2024. Lithospheric Structure and Melting Processes in Southeast Australia: New Constraints From Joint Probabilistic Inversions of 3D Magnetotelluric and Seismic Data. *Journal of Geophysical Research: Solid Earth* 129, 1–30. doi:10.1029/2023JB028257.
- Mandler, B.E., Grove, T.L., 2016. Controls on the stability and composition of amphibole in the Earth's mantle. *Contributions to Mineralogy and Petrology* 171, 1–20. doi:10.1007/s00410-016-1281-5.
- Mather, B.R., Dietmar Müller, R., Seton, M., Ruttor, S., Nebel, O., Mortimer, N., 2020. Intraplate volcanism triggered by bursts in slab flux. *Science Advances* 6, 1–8. doi:10.1126/sciadv.abd0953.

- 1386 Matthews, S., Shorttle, O., MacLennan, J., Rudge, J.F., 2021. The global melt inclusion C/Ba array: Mantle variability,
1387 melting process, or degassing? *Geochimica et Cosmochimica Acta* 293, 525–543. URL: <https://doi.org/10.1016/j.gca.2020.09.030>, doi:10.1016/j.gca.2020.09.030.
- 1388
- 1389 Matthews, S., Shorttle, O., Rudge, J.F., MacLennan, J., 2017. Constraining mantle carbon: CO₂-trace element systematics
1390 in basalts and the roles of magma mixing and degassing. *Earth and Planetary Science Letters* 480, 1–14. URL:
1391 <https://doi.org/10.1016/j.epsl.2017.09.047>, doi:10.1016/j.epsl.2017.09.047.
- 1392 McDonough, W.F., 1990. Constraints on the composition of the continental lithospheric mantle. *Earth and Planetary*
1393 *Science Letters* 101, 1–18. doi:10.1016/0012-821X(90)90119-I.
- 1394 McDougall, I., Wellman, P., 1976. Potassium-argon ages for some australian mesozoic igneous rocks. *Journal of the*
1395 *Geological Society of Australia* 23, 1–9. doi:10.1080/00167617608728916.
- 1396 McQueen, K.G., Gonzalez, O.R., Roach, I.C., Pillans, B.J., Dunlap, W.J., Smith, M.L., 2007. Landscape and regolith
1397 features related to Miocene leucitite lava flows, El Capitan northeast of Cobar, New South Wales. *Australian Journal of*
1398 *Earth Sciences* 54, 1–17. doi:10.1080/08120090600923311.
- 1399 Menzies, M.A., Wass, S.Y., 1983. CO₂-and LREE-rich mantle below eastern Australia: a REE and isotopic study of alkaline
1400 magmas and apatite-rich mantle xenoliths from the Southern Highlands Province, Australia. *Earth and Planetary Science*
1401 *Letters* 65, 387–302.
- 1402 Mitchell, R.H., 1995. Melting experiments on a sanidine phlogopite lamproite at 4-7 gpa and their bearing on the sources
1403 of lamproitic magmas. *Journal of Petrology* 36, 1455–1474. doi:10.1093/petrology/36.5.1455.
- 1404 Mitchell, R.H., 2020. Igneous Rock Associations 26. Lamproites, Exotic Potassic Alkaline Rocks: A Review of their
1405 Nomenclature, Characterization and Origins. *Geoscience Canada* 47, 119–142. URL: <https://journals.lib.unb.ca/index.php/GC/article/view/31174>, doi:10.12789/geocanj.2020.47.162.
- 1406
- 1407 Mitchell, R.H., 2021. Potassic Alkaline Rocks: Leucitites, Lamproites, and Kimberlites, in: Alderton, D., Elias, S.A.
1408 (Eds.), *Encyclopedia of Geology*. 2 ed.. Elsevier, pp. 215–239. URL: <https://linkinghub.elsevier.com/retrieve/pii/B9780124095489124820>, doi:10.1016/B978-0-12-409548-9.12482-0.
- 1409
- 1410 Mitchell, R.H., Bergman, S.C., 1991. *Petrology of Lamproites*. 1 ed., Springer New York, New York. doi:10.1007/
1411 978-1-4615-3788-5.
- 1412 Müller, D., Groves, D.I., 1993. Direct and indirect associations between potassic igneous rocks, shoshonites and gold-
1413 copper deposits. *Ore Geology Reviews* 8, 383–406. URL: <https://www.sciencedirect.com/science/article/pii/S016913689390035W>, doi:10.1016/0169-1368(93)90035-W.
- 1414
- 1415 Müller, D., Rock, N.M., Groves, D.I., 1992. Geochemical discrimination between shoshonitic and potassic volcanic rocks
1416 in different tectonic settings: A pilot study. *Mineralogy and Petrology* 46, 259–289. URL: <http://link.springer.com/10.1007/BF01173568>, doi:10.1007/BF01173568.
- 1417
- 1418 Nelson, D.R., 1992. Isotopic characteristics of potassic rocks: evidence for the involvement of subducted sediments in
1419 magma genesis. *Lithos* 28, 403–420. doi:10.1016/0024-4937(92)90016-R.
- 1420 Nelson, D.R., McCulloch, M.T., Sun, S.S., 1986. The origins of ultrapotassic rocks as inferred from Sr, Nd and Pb isotopes.
1421 *Geochimica et Cosmochimica Acta* 50, 231–245. doi:10.1016/0016-7037(86)90172-9.

- Novella, D., Frost, D.J., 2014. The composition of hydrous partial melts of garnet peridotite at 6GPa: Implications for the origin of group II Kimberlites. *Journal of Petrology* 55, 2097–2124. doi:10.1093/petrology/egu051.
- O'Reilly, S.Y., 1987. Volatile-rich mantle beneath eastern Australia, in: Nixon, P.H. (Ed.), *Mantle Xenoliths*. John Wiley & Sons, Chichester, UK, pp. 661–670.
- O'Reilly, S.Y., Griffin, W., 1988. Mantle metasomatism beneath western Victoria, Australia: I. Metasomatic processes in Cr-diopside lherzolites. *Geochimica et Cosmochimica Acta* 52, 433–447. URL: <https://linkinghub.elsevier.com/retrieve/pii/0016703788900993>, doi:10.1016/0016-7037(88)90099-3.
- O'Reilly, S.Y., Griffin, W.L., 1984. Sr isotopic heterogeneity in primitive basaltic rocks, southeastern Australia: correlation with mantle metasomatism. *Contributions to Mineralogy and Petrology* 87, 220–230. URL: <http://link.springer.com/10.1007/BF00373055>, doi:10.1007/BF00373055.
- O'Reilly, S.Y., Griffin, W.L., 1985. A xenolith-derived geotherm for southeastern Australia and its geophysical implications. *Tectonophysics* 111, 41–63. doi:10.1016/0040-1951(85)90065-4.
- O'Reilly, S.Y., Griffin, W.L., 2000. Apatite in the mantle: Implications for metasomatic processes and high heat production in Phanerozoic mantle. *Lithos* 53, 217–232. doi:10.1016/S0024-4937(00)00026-8.
- O'Reilly, S.Y., Griffin, W.L., 2013. Mantle metasomatism, in: Harlov, D.E., Austrheim, H. (Eds.), *Metasomatism and the Chemical Transformation of Rock*. Lecture Notes in Earth System Sciences. 1 ed.. Springer Berlin Heidelberg. 9783642283932. chapter 12, pp. 471–533. doi:10.1007/978-3-642-28394-9_12.
- O'Reilly, S.Y., Griffin, W.L., Pearson, N.J., Jackson, S.E., Belousova, E.A., Alard, O., Saeed, A., 2008. Taking the pulse of the Earth: Linking crustal and mantle events. *Australian Journal of Earth Sciences* 55, 983–995. doi:10.1080/08120090802097450.
- Palme, H., O'Neill, H., 2013. Cosmochemical Estimates of Mantle Composition, in: *Treatise on Geochemistry: Second Edition*. Elsevier. volume 3, pp. 1–39. URL: <https://www.sciencedirect.com/science/article/pii/B9780080959757002011?via%3Dihub>, doi:10.1016/B978-0-08-095975-7.00201-1.
- Paul, B., Hergt, J.M., Woodhead, J.D., 2005. Mantle heterogeneity beneath the Cenozoic volcanic provinces of central Victoria inferred from trace-element and Sr, Nd, Pb and Hf isotope data. *Australian Journal of Earth Sciences* 52, 243–260. URL: <http://www.tandfonline.com/doi/abs/10.1080/08120090500139448>, doi:10.1080/08120090500139448.
- Pe-Piper, G., Piper, D.J., 1992. Geochemical variation with time in the Cenozoic high-k volcanic rocks of the island of Lesbos, Greece: significance for shoshonite petrogenesis. *Journal of Volcanology and Geothermal Research* 53, 371–387. URL: <https://www.sciencedirect.com/science/article/pii/037702739290092R>, doi:10.1016/0377-0273(92)90092-R.
- Pe-Piper, G., Zhang, Y., Piper, D.J., Prelević, D., 2014. Relationship of Mediterranean type lamproites to large shoshonite volcanoes, Miocene of Lesbos, NE Aegean Sea. *Lithos* 184–187, 281–299. doi:10.1016/j.lithos.2013.11.004.
- Pearce, J.A., 1983. Role of the sub-continental lithosphere in magma genesis at active continental margins. *Continental Basalts and Mantle Xenoliths*, 230–249.
- Pearson, N.J., Griffin, W.L., Alard, O., O'Reilly, S.Y., 2006. The isotopic composition of magnesium in mantle olivine: Records of depletion and metasomatism. *Chemical Geology* 226, 115–133. doi:10.1016/j.chemgeo.2005.09.029.

- 1457 Pertermann, M., Hirschmann, M.M., 2003. Partial melting experiments on a MORB-like pyroxenite between 2 and 3 GPa:
1458 Constraints on the presence of pyroxenite in basalt source regions from solidus location and melting rate. *Journal of*
1459 *Geophysical Research: Solid Earth* 108, 1–17. doi:10.1029/2000jb000118.
- 1460 Pintér, Z., Foley, S.F., Yaxley, G.M., 2022. Diamonds, dunites, and metasomatic rocks formed by melt/rock reaction in
1461 craton roots. *Communications Earth and Environment* 3, 1–8. doi:10.1038/s43247-022-00630-3.
- 1462 Pintér, Z., Foley, S.F., Yaxley, G.M., Rosenthal, A., Rapp, R.P., Lanati, A.W., Rushmer, T., 2021. Experimental
1463 investigation of the composition of incipient melts in upper mantle peridotites in the presence of CO₂ and H₂O. *Lithos*
1464 396–397, 106224. doi:10.1016/j.lithos.2021.106224.
- 1465 Plank, T., 2005. Constraints from Thorium/Lanthanum on sediment recycling at subduction zones and the evolution of
1466 the continents. *Journal of Petrology* 46, 921–944. doi:10.1093/petrology/egi005.
- 1467 Plank, T., Langmuir, C.H., 1998. The chemical composition of subducting sediment and its consequences for the crust and
1468 mantle. *Chemical Geology* 145, 325–394. doi:10.1016/S0009-2541(97)00150-2.
- 1469 Powell, W., O'Reilly, S., 2007. Metasomatism and sulfide mobility in lithospheric mantle beneath eastern Australia:
1470 Implications for mantle Re-Os chronology. *Lithos* 94, 132–147. doi:10.1016/j.lithos.2006.06.010.
- 1471 Powell, W., Zhang, M., O'Reilly, S.Y., Tiepolo, M., 2004. Mantle amphibole trace-element and isotopic signatures trace
1472 multiple metasomatic episodes in lithospheric mantle, western Victoria, Australia. *Lithos* 75, 141–171. doi:10.1016/j.
1473 *lithos*.2003.12.017.
- 1474 Prelević, D., Akal, C., Foley, S.F., 2008a. Orogenic vs anorogenic lamproites in a single volcanic province: Mediterranean-
1475 type lamproites from Turkey. *IOP Conference Series: Earth and Environmental Science* 2, 012024. doi:10.1088/
1476 1755-1307/2/1/012024.
- 1477 Prelević, D., Akal, C., Foley, S.F., Romer, R.L., Stracke, A., Van den Bogaard, P., 2012. Ultrapotassic mafic rocks as
1478 geochemical proxies for post-collisional dynamics of orogenic lithospheric mantle: The case of southwestern Anatolia,
1479 Turkey. *Journal of Petrology* 53, 1019–1055. doi:10.1093/petrology/egs008.
- 1480 Prelević, D., Foley, S.F., 2007. Accretion of arc-oceanic lithospheric mantle in the Mediterranean: Evidence from extremely
1481 high-Mg olivines and Cr-rich spinel inclusions in lamproites. *Earth and Planetary Science Letters* 256, 120–135. doi:10.
1482 1016/j.epsl.2007.01.018.
- 1483 Prelević, D., Foley, S.F., Cvetković, V., 2007. A review of petrogenesis of Mediterranean Tertiary lamproites: A perspective
1484 from the Serbian ultrapotassic province. *Special Paper of the Geological Society of America* 418, 113–129. doi:10.1130/
1485 2007.2418(06).
- 1486 Prelević, D., Foley, S.F., Cvetković, V., L. Romer, R., 2004. The analcime problem and its impact on the geochemistry of
1487 ultrapotassic rocks from Serbia. *Mineralogical Magazine* 68, 633–648. doi:10.1180/0026461046840209.
- 1488 Prelević, D., Foley, S.F., Romer, R., Conticelli, S., 2008b. Mediterranean tertiary lamproites derived from multiple source
1489 components in postcollisional geodynamics. *Geochimica et Cosmochimica Acta* 72, 2125–2156. doi:10.1016/j.gca.2008.
1490 01.029.
- 1491 Prelević, D., Foley, S.F., Romer, R.L., Cvetković, V., Downes, H., 2005. Tertiary ultrapotassic volcanism in Serbia:
1492 Constraints on petrogenesis and mantle source characteristics. *Journal of Petrology* 46, 1443–1487. doi:10.1093/

- petrology/egi022. 1493
- Prelević, D., Jacob, D.E., Foley, S.F., 2013a. Recycling plus: A new recipe for the formation of Alpine-Himalayan orogenic mantle lithosphere. *Earth and Planetary Science Letters* 362, 187–197. URL: <https://www.sciencedirect.com/science/article/pii/S0012821X1200653X#ep-keywords-id18>, doi:10.1016/j.epsl.2012.11.035. 1494
1495
1496
- Prelević, D., Jacob, D.E., Foley, S.F., 2013b. Recycling plus: A new recipe for the formation of Alpine-Himalayan orogenic mantle lithosphere. *Earth and Planetary Science Letters* 362, 187–197. doi:10.1016/j.epsl.2012.11.035. 1497
1498
- Prelević, D., Stracke, A., Foley, S.F., Romer, R.L., Conticelli, S., 2010. Hf isotope compositions of Mediterranean lamproites: Mixing of melts from asthenosphere and crustally contaminated mantle lithosphere. *Lithos* 119, 297–312. doi:10.1016/j.lithos.2010.07.007. 1499
1500
1501
- Prider, R.T., 1939. Some minerals from the leucite-rich rocks of the West Kimberley area, Western Australia. *Mineralogical Magazine and Journal of the Mineralogical Society* 25, 373–387. URL: <https://www.cambridge.org/core/article/some-minerals-from-the-leucite-rich-rocks-of-the-west-kimberley-area-western-australia/79BE347327D000D424521C6508C4B851>, doi:DOI:10.1180/minmag.1939.025.166.01. 1502
1503
1504
1505
- Putirka, K., Jean, M., Cousens, B., Sharma, R., Torrez, G., Carlson, C., 2012. Cenozoic volcanism in the Sierra Nevada and Walker Lane, California, and a new model for lithosphere degradation. *Geosphere* 8, 265–291. doi:10.1130/GES00728.1. 1506
1507
- Putirka, K.D., 2008. Thermometers and barometers for volcanic systems. *Reviews in Mineralogy and Geochemistry* 69, 61–120. doi:10.2138/rmg.2008.69.3. 1508
1509
- Putnis, C.V., Geisler, T., Schmid-Beurmann, P., Stephan, T., Giampaolo, C., 2007. An experimental study of the replacement of leucite by analcime. *American Mineralogist* 92, 19–26. doi:10.2138/am.2007.2249. 1510
1511
- Rawlinson, N., Davies, D.R., Pilia, S., 2017. The mechanisms underpinning Cenozoic intraplate volcanism in eastern Australia: Insights from seismic tomography and geodynamic modeling. *Geophysical Research Letters* 44, 9681–9690. URL: <https://onlinelibrary.wiley.com/doi/abs/10.1002/2017GL074911>, doi:10.1002/2017GL074911. 1512
1513
1514
- Rawlinson, N., Pilia, S., Young, M., Salmon, M., Yang, Y., 2016. Crust and upper mantle structure beneath southeast Australia from ambient noise and teleseismic tomography. *Tectonophysics* 689, 143–156. doi:10.1016/j.tecto.2015.11.034. 1515
1516
1517
- Rehfeldt, T., Foley, S.F., Jacob, D.E., Carlson, R.W., Lowry, D., 2008. Contrasting types of metasomatism in dunite, wehrlite and websterite xenoliths from Kimberley, South Africa. *Geochimica et Cosmochimica Acta* 72, 5722–5756. URL: <http://dx.doi.org/10.1016/j.gca.2008.08.020>, doi:10.1016/j.gca.2008.08.020. 1518
1519
1520
- Robertson, A.D., Sutherland, F.L., Hollis, J.D., 1985. Upper mantle xenoliths and megacrysts and the origin of the Brigooda Basalt and Breccia, near Proston, Queensland. *Papers (University of Queensland. Dept. of Geology)* 11, 58 – 71. URL: <https://espace.library.uq.edu.au/view/UQ:734631>. 1521
1522
1523
- Robinson, J.A., Wood, B.J., 1998. The depth of the spinel to garnet transition at the peridotite solidus. *Earth and Planetary Science Letters* 164, 277–284. doi:10.1016/S0012-821X(98)00213-1. 1524
1525
- Robinson, J.A., Wood, B.J., Blundy, J.D., 1998. The beginning of melting of fertile and depleted peridotite at 1.5 GPa. *Earth and Planetary Science Letters* 155, 97–111. doi:10.1016/S0012-821X(97)00162-3. 1526
1527
- Rock, N.M.S., 1991. *Lamprophyres*. 1 ed., Springer, New York. doi:10.1007/978-1-4757-0929-2. 1528

- 1529 Rohrbach, A., Schmidt, M.W., 2011. Redox freezing and melting in the Earth's deep mantle resulting from carbon-iron
1530 redox coupling. *Nature* 472, 209–214. doi:10.1038/nature09899.
- 1531 Rosenthal, A., Foley, S.F., Pearson, D.G., Nowell, G.M., Tappe, S., 2009. Petrogenesis of strongly alkaline primitive
1532 volcanic rocks at the propagating tip of the western branch of the East African Rift. *Earth and Planetary Science Letters*
1533 284, 236–248. doi:10.1016/j.epsl.2009.04.036.
- 1534 Roux, J., Hamilton, D.L., 1976. Primary igneous analcite—an experimental study. *Journal of Petrology* 17, 244–257.
1535 doi:10.1093/petrology/17.2.244.
- 1536 Rudnick, R.L., Gao, S., 2013. Composition of the Continental Crust. volume 4. 2 ed., Elsevier Ltd. URL: <http://dx.doi.org/10.1016/B978-0-08-095975-7.00301-6>, doi:10.1016/B978-0-08-095975-7.00301-6.
- 1537 //dx.doi.org/10.1016/B978-0-08-095975-7.00301-6, doi:10.1016/B978-0-08-095975-7.00301-6.
- 1538 Rudnick, R.L., McDonough, W.F., Chappell, B.W., 1993. Carbonatite metasomatism in the northern Tanzanian mantle:
1539 petrographic and geochemical characteristics. *Earth and Planetary Science Letters* 114, 463–475. doi:10.1016/
1540 0012-821X(93)90076-L.
- 1541 Schmidt, M.W., 1996. Experimental constraints on recycling of potassium from subducted oceanic crust. *Science* 272, 1927.
1542 doi:10.1126/science.272.5270.1927.
- 1543 Schmidt, M.W., Poli, S., 2003. Generation of Mobile Components during Subduction of Oceanic Crust. *Treatise on*
1544 *Geochemistry* 3-9, 567–591. doi:10.1016/B0-08-043751-6/03034-6.
- 1545 Seton, M., Williams, S., Mortimer, N., Meffre, S., Micklethwaite, S., Zahirovic, S., 2019. Magma production along the Lord
1546 Howe Seamount Chain, northern Zealandia. *Geological Magazine* 156, 1605–1617. doi:10.1017/S0016756818000912.
- 1547 Shea, J., Foley, S., Dalton, H., Lanati, A., Phillips, D., 2024. Mid-Jurassic volcanism at Bokhara River and insights
1548 into metasomatism in the lithospheric mantle of the Thomson Orogen, eastern Australia. *Australian Journal of Earth*
1549 *Sciences* 0, 1–13. URL: <https://doi.org/10.1080/08120099.2024.2302360>, doi:10.1080/08120099.2024.2302360.
- 1550 Shea, J.J., Ezad, I.S., Foley, S.F., Lanati, A.W., 2022. The Eastern Australian Volcanic Province, its primitive melts,
1551 constraints on melt sources and the influence of mantle metasomatism. *Earth-Science Reviews* 233, 104168. URL:
1552 <https://doi.org/10.1016/j.earscirev.2022.104168>, doi:10.1016/j.earscirev.2022.104168.
- 1553 Shea, J.J., Foley, S.F., 2019. Evidence for a carbonatite-influenced source assemblage for intraplate basalts from the
1554 Buckland Volcanic Province, Queensland, Australia. *Minerals* 9. doi:10.3390/min9090546.
- 1555 Shu, C., Foley, S.F., Ezad, I.S., Daczko, N.R., Shcheka, S.S., 2024. Experimental Melting of Phlogopite Websterite in
1556 the Upper Mantle between 1.5 and 4.5 GPa. *Journal of Petrology* 65. URL: [https://academic.oup.com/petrology/](https://academic.oup.com/petrology/article/doi/10.1093/petrology/egae030/7631318)
1557 [article/doi/10.1093/petrology/egae030/7631318](https://academic.oup.com/petrology/article/doi/10.1093/petrology/egae030/7631318), doi:10.1093/petrology/egae030.
- 1558 Shu, C., Foley, S.F., Shea, J.J., Lanati, A.W., Daczko, N.R., Shcheka, S.S., in revision. Short timeframe between formation
1559 and remelting of the phlogopite websterite source for leucitites along earth's longest continental hotspot track.
- 1560 Smith, B.W., Prescott, J.R., 1987. Thermoluminescence dating of the eruption at Mt Schank, South Australia. *Australian*
1561 *Journal of Earth Sciences* 34, 335–342. doi:10.1080/08120098708729415.
- 1562 Stonier, G.A., 1893. On the Occurrence of Leucite-Basalt at Lake Cudgellico (Cargelligo). *Records of the Geological Survey*
1563 of New South Wales 3, 71–74.

- Stracke, A., Bourdon, B., 2009. The importance of melt extraction for tracing mantle heterogeneity. *Geochimica et Cosmochimica Acta* 73, 218–238. URL: <http://dx.doi.org/10.1016/j.gca.2008.10.015>, doi:10.1016/j.gca.2008.10.015. 1564–1566
- Sudholz, Z.J., Reddicliffe, T.H., Jaques, A.L., Yaxley, G.M., Haynes, M., Gorbatov, A., Czarnota, K., Frigo, C., Maas, R., Knowles, B., 2023. Petrology, Age, and Rift Origin of Ultramafic Lamprophyres (Aillikites) at Mount Webb, a New Alkaline Province in Central Australia. *Geochemistry, Geophysics, Geosystems* 24, 1–29. doi:10.1029/2023GC011120. 1567–1569
- Sudo, A., Tatsumi, Y., 1990. Phlogopite and K-amphibole in the upper mantle: Implication for magma genesis in subduction zones. *Geophysical Research Letters* 17, 29–32. URL: <https://agupubs.onlinelibrary.wiley.com/doi/10.1029/GL017i001p00029>, doi:10.1029/GL017i001p00029. 1570–1572
- Sutherland, F.L., 1983. Timing, trace and origin of basaltic migration in eastern Australia. *Nature* 305, 123–126. URL: <https://doi.org/10.1038/305123a0>, doi:10.1038/305123a0. 1573–1574
- Sutherland, F.L., 1996. Alkaline rocks and gemstones, Australia: A review and synthesis. *Australian Journal of Earth Sciences* 43, 323–343. doi:10.1080/08120099608728259. 1575–1576
- Sutherland, F.L., 2003. 'Boomerang' migratory intraplate Cenozoic volcanism, eastern Australian rift margins and the Indian-Pacific mantle boundary. *Special Paper of the Geological Society of America* 372, 203–221. doi:10.1130/0-8137-2372-8.203. 1577–1579
- Sutherland, F.L., Barron, L.M., 2003. Diamonds of multiple origins from New South Wales: Further data and discussion. *Australian Journal of Earth Sciences* 50, 975–981. doi:10.1111/j.1400-0952.2003.01038.x. 1580–1581
- Sweeney, R.J., Thompson, A.B., Ulmer, P., 1993. Phase relations of a natural MARID composition and implications for MARID genesis, lithospheric melting and mantle metasomatism. *Contributions to Mineralogy and Petrology* 115, 225–241. doi:10.1007/BF00321222. 1582–1584
- Takahashi, E., 1986. Melting of a dry peridotite KLB-1 up to 14 GPa: Implications on the Origin of peridotitic upper mantle. *Journal of Geophysical Research* 91, 9367. doi:10.1029/jb091i1b09p09367. 1585–1586
- Tappe, S., Foley, S.F., Jenner, G.A., Kjarsgaard, B.A., 2005. Integrating ultramafic lamprophyres into the IUGS classification of igneous rocks: Rationale and implications. *Journal of Petrology* 46, 1893–1900. doi:10.1093/petrology/egi039. 1587–1589
- Tappe, S., Romer, R.L., Stracke, A., Steinfeld, A., Smart, K.A., Muehlenbachs, K., Torsvik, T.H., 2017. Sources and mobility of carbonate melts beneath cratons, with implications for deep carbon cycling, metasomatism and rift initiation. *Earth and Planetary Science Letters* 466, 152–167. URL: <http://dx.doi.org/10.1016/j.epsl.2017.03.011>, doi:10.1016/j.epsl.2017.03.011. 1590–1593
- Tapu, A.T., Ubide, T., Vasconcelos, P.M., 2023. Increasing complexity in magmatic architecture of volcanoes along a waning hotspot. *Nature Geoscience* 16, 371–379. doi:10.1038/s41561-023-01156-9. 1594–1595
- Thomson, A.R., Walter, M.J., Kohn, S.C., Brooker, R.A., 2016. Slab melting as a barrier to deep carbon subduction. *Nature* 529, 76–79. doi:10.1038/nature16174. 1596–1597
- Thomson, A.R., Walter, M.J., Lord, O.T., Kohn, S.C., 2014. Chemistry and mineralogy of earth's mantle. Experimental determination of melting in the systems enstatite-magnesite and magnesite-calcite from 15 to 80 GPa. *American* 1598–1599

- 1600 Mineralogist 99, 1544–1554. doi:10.2138/am.2014.4735.
- 1601 Toyokuni, G., Zhao, D., 2024. Slab-Plume Interactions Beneath Australia and New Zealand: New Insight From Whole-
1602 Mantle Tomography. *Geochemistry, Geophysics, Geosystems* 25. doi:10.1029/2024GC011739.
- 1603 Trønnes, R.G., 2002. Stability range and decomposition of potassic richterite and phlogopite end members at 5-15 GPa.
1604 *Mineralogy and Petrology* 74, 129–148. doi:10.1007/s007100200001.
- 1605 Turner, S., Foden, J., George, R., Evans, P., Varne, R., Elburg, M., Jenner, G., 2003. Rates and processes of potassic
1606 magma evolution beneath Sangeang Api Volcano, East Sunda Arc, Indonesia. *Journal of Petrology* 44, 491–516. doi:10.
1607 1093/petrology/44.3.491.
- 1608 Van Keken, P.E., Hacker, B.R., Syracuse, E.M., Abers, G.A., 2011. Subduction factory: 4. Depth-dependent flux of H₂O
1609 from subducting slabs worldwide. *Journal of Geophysical Research: Solid Earth* 116. doi:10.1029/2010JB007922.
- 1610 Vetter, M., Foley, S.F., Mertz-Kraus, R., Groschopf, N., 2017. Trace elements in olivine of ultramafic lamprophyres controlled
1611 by phlogopite-rich mineral assemblages in the mantle source. *Lithos* 292–293, 81–95. doi:10.1016/j.lithos.2017.08.020.
- 1612 Wade, A., Prider, R.T., 1940. The leucite-bearing rocks of the West Kimberley area, Western Australia. *Quarterly Journal*
1613 *of the Geological Society of London* 96, 39. URL: [https://www.lyellcollection.org/doi/10.1144/GSL.JGS.1940.096.](https://www.lyellcollection.org/doi/10.1144/GSL.JGS.1940.096.01-04.04)
1614 [01-04.04](https://www.lyellcollection.org/doi/10.1144/GSL.JGS.1940.096.01-04.04), doi:10.1144/GSL.JGS.1940.096.01-04.04.
- 1615 Walter, M., 1998. Melting of Garnet Peridotite and the Origin of Komatiite and Depleted Lithosphere. *Journal of Petrology*
1616 39, 29–60. doi:10.1093/petrology/39.1.29.
- 1617 Wang, K., Plank, T., Walker, J.D., Smith, E.I., 2002. A mantle melting profile across the Basin and Range, SW USA.
1618 *Journal of Geophysical Research: Solid Earth* 107. doi:10.1029/2001jb000209.
- 1619 Wang, Q., Wyman, D.A., Xu, J.F., Zhao, Z.H., Jian, P., Xiong, X.L., Bao, Z.W., Li, C.F., Bai, Z.H., 2006. Petrogenesis of
1620 Cretaceous adakitic and shoshonitic igneous rocks in the Luzong area, Anhui Province (eastern China): Implications for
1621 geodynamics and Cu-Au mineralization. *Lithos* 89, 424–446. URL: [https://www.sciencedirect.com/science/article/
1622 pii/S0024493706000302#aep-acknowledgment-id44](https://www.sciencedirect.com/science/article/pii/S0024493706000302#aep-acknowledgment-id44), doi:10.1016/j.lithos.2005.12.010.
- 1623 Wang, X., Wang, Z., Cheng, H., Zong, K., Wang, C.Y., Ma, L., Cai, Y.C., Foley, S., Hu, Z., 2022. Gold endowment
1624 of the metasomatized lithospheric mantle for giant gold deposits: Insights from lamprophyre dykes. *Geochimica et*
1625 *Cosmochimica Acta* 316, 21–40. URL: <https://doi.org/10.1016/j.gca.2021.10.006>, doi:10.1016/j.gca.2021.10.006.
- 1626 Wang, Y., Foley, S.F., 2018. Hybridization Melting Between Continent-Derived Sediment and Depleted Peridotite in
1627 Subduction Zones. *Journal of Geophysical Research: Solid Earth* 123, 3414–3429. doi:10.1029/2018JB015507.
- 1628 Wang, Y., Foley, S.F., Buhre, S., Soldner, J., Xu, Y., 2021. Origin of potassic postcollisional volcanic rocks in young,
1629 shallow, blueschist-rich lithosphere. *Science Advances* 7. doi:10.1126/sciadv.abc0291.
- 1630 Wang, Y., Prelević, D., Buhre, S., Foley, S.F., 2017. Constraints on the sources of post-collisional K-rich magmatism:
1631 The roles of continental clastic sediments and terrigenous blueschists. *Chemical Geology* 455, 192–207. doi:10.1016/j.
1632 chemgeo.2016.10.006.
- 1633 Wang, Z.N., Wang, Y., Sossi, P., He, Y., Peng, Y., Lu, W.N., Wu, H., 2024. Calcium isotopic composition of the bulk silicate
1634 Earth: A komatiite perspective. *Lithos* 480–481, 107638. URL: <https://doi.org/10.1016/j.lithos.2024.107638>,
1635 doi:10.1016/j.lithos.2024.107638.

- Wass, S.Y., 1979a. Fractional crystallization in the mantle of late-stage kimberlitic liquids—evidence in xenoliths from the Kiama Area, N.S.W., Australia, in: *The Mantle Sample: Inclusion in Kimberlites and Other Volcanics*. American Geophysical Union, Washington, D. C.. volume 16, pp. 366–373. URL: <http://doi.wiley.com/10.1029/SP016p0366>, doi:10.1029/SP016p0366.
- Wass, S.Y., 1979b. Multiple origins of clinopyroxenes in alkali basaltic rocks. *Lithos* 12, 115–132.
- Wass, S.Y., Henderson, P., Elliot, C.J., 1980. Chemical heterogeneity and metasomatism in the upper mantle: evidence from rare earth and other elements in apatite-rich xenoliths in basaltic rocks from eastern Australia. *Philosophical Transactions of the Royal Society of London. Series A, Mathematical and Physical Sciences* 297, 333–346. URL: <https://royalsocietypublishing.org/doi/10.1098/rsta.1980.0219>, doi:10.1098/rsta.1980.0219.
- Wass, S.Y., Rogers, N.W., 1980. Mantle metasomatism-precursor to continental alkaline volcanism. *Geochimica et Cosmochimica Acta* 44, 1811–1823.
- Wellman, P., Cundari, A., McDougall, I., 1970. Potassium – argon ages for leucite-bearing rocks from New South Wales, Australia. *Journal and Proceedings of the Royal Society of New South Wales* 103, 103–107.
- Wellman, P., McDougall, I., 1974. Potassium-argon ages on the Cainozoic volcanic rocks of New South Wales. *Journal of the Geological Society of Australia* 21, 247–272. doi:10.1080/00167617408728849.
- Wilkinson, J.F., 1975. Ultramafic inclusions and high pressure megacrysts from a nephelinite sill, Nandewar Mountains, north-eastern New South Wales, and their bearing on the origin of certain ultramafic inclusions in alkaline volcanic rocks. *Contributions to Mineralogy and Petrology* 51, 235–262. doi:10.1007/BF00372144.
- Wilkinson, J.F.G., Hensel, H.D., 1991. An analcime mugearite-megacryst association from north-eastern New South Wales: implications for high-pressure amphibole-dominated fractionation of alkaline magmas. *Contributions to Mineralogy and Petrology* 109, 240–251. URL: <http://link.springer.com/10.1007/BF00306482>, doi:10.1007/BF00306482.
- Willbold, M., Stracke, A., 2006. Trace element composition of mantle end-members: Implications for recycling of oceanic and upper and lower continental crust. *Geochemistry, Geophysics, Geosystems* 7, 1–30. doi:10.1029/2005GC001005.
- Williams, L.A.J., 1982. Physical aspects of magmatism in continental rifts, in: Pálmason, G. (Ed.), *Continental and Oceanic Rifts*. volume 8, pp. 193–222. URL: <http://www.agu.org/books/gd/v008/GD008p0193/GD008p0193.shtml>, doi:10.1029/GD008p0193.
- Winterburn, P.A., Harte, B., Gurney, J.J., 1990. Peridotite xenoliths from the Jagersfontein kimberlite pipe: I. Primary and primary-metasomatic mineralogy. *Geochimica et Cosmochimica Acta* 54, 329–341. doi:10.1016/0016-7037(90)90322-C.
- Woolley, A.R., Bergman, S.C., Edgar, A.D., Le Bas, M.J., Mitchell, R.H., Rock, N.M., Scott Smith, B.H., 1996. Classification of lamprophyres, lamproites, kimberlites, and the kalsilitic, melilitic, and leucitic rocks. *Canadian Mineralogist* 34, 175–186.
- Yang, J.H., Sun, J.F., Chen, F., Wilde, S.A., Wu, F.Y., 2007. Sources and petrogenesis of late triassic dolerite dikes in the Liaodong Peninsula: Implications for post-collisional lithosphere thinning of the eastern North China Craton. *Journal of Petrology* 48, 1973–1997. doi:10.1093/petrology/egm046.
- Yaxley, G.M., Crawford, A.J., Green, D.H., 1991. Evidence for carbonatite metasomatism in spinel peridotite xenoliths from western Victoria, Australia. *Earth and Planetary Science Letters* 107, 305–317. doi:10.1016/0012-821X(91)90078-V.

-
- 1672 Yaxley, G.M., Kamenetsky, V., Green, D.H., Falloon, T.J., 1997. Glasses in mantle xenoliths from western Victoria,
1673 Australia, and their relevance to mantle processes. *Earth and Planetary Science Letters* 148, 433–446. doi:10.1016/
1674 s0012-821x(97)00058-7.
- 1675 Zhang, M., O'Reilly, S.Y., 1997. Multiple sources for basaltic rocks from Dubbo, eastern Australia: Geochemical evidence
1676 for plume-lithospheric mantle interaction. *Chemical Geology* 136, 33–54. doi:10.1016/S0009-2541(96)00130-1.
- 1677 Zhang, M., O'Reilly, S.Y., Chen, D., 1999. Location of Pacific and Indian mid-ocean ridge-type mantle in two time slices:
1678 Evidence from Pb, Sr, and Nd isotopes for Cenozoic Australian basalts. *Geology* 27, 39–42. doi:10.1130/0091-7613(1999)
1679 027<0039:L0PAIM>2.3.CO;2.
- 1680 Zhang, M., Stephenson, P.J., O'Reilly, S.Y., McCulloch, M.T., Norman, M., 2001. Petrogenesis and geodynamic
1681 implications of late Cenozoic basalts in North Queensland, Australia: Trace-element and Sr-Nd-Pb Isotope Evidence.
1682 *Journal of Petrology* 42, 685–719. doi:10.1093/petrology/42.4.685.
- 1683 Zinngrebe, E., Foley, S.F., 1995. Metasomatism in mantle xenoliths from Gees, West Eifel, Germany: Evidence for the
1684 genesis of calc-alkaline glasses and metasomatic Ca-enrichment. *Contributions to Mineralogy and Petrology* 122, 79–96.
1685 doi:10.1007/s004100050114.